ECON INCORPORATED

THE FIRST SEASAT-A INDUSTRIAL USERS WORKSHOP

HELD AT

PRINCETON, NEW JERSEY

NOVEMBER 29 AND 30, 1977

ECON INCORPORATED

NINE HUNDRED STATE ROAD
PRINCETON, NEW JERSEY 08540
609-924-8778

THE FIRST SEASAT-A INDUSTRIAL USERS WORKSHOP

HELD AT

PRINCETON, NEW JERSEY

NOVEMBER 29 AND 30, 1977

Prepared for

National Aeronautics and Space Administration

Prepared by

ECON, Inc.
900 State Road
Princeton, NJ 08540

Contract No. NASW-3047

February 10, 1978

TABLE OF CONTENTS

NOTE OF TRANSMITTAL

This report of the First SEASAT-A Industrial Users Workshop was prepared for the National Aeronautics and Space Administration, Office of Space and Terrestrial Applications, under Contract NASW-3047. This workshop was sponsored by the SEASAT-A Program Office, NASA Headquarters. Technical Officer for this task was Mr. Donald Montgomery of the Jet Propulsion Laboratory. The authors of this report are Mr. Kenneth W. Hicks and Mr. B. P. Miller. The authors wish to thank the speakers and participants in this workshop for their cooperation in providing the material contained in this report.

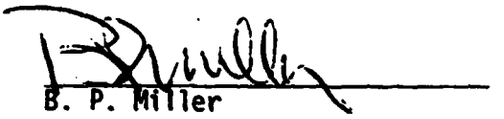

B. P. Miller

INTRODUCTION

There were some 50 attendees at a SEASAT-A Industrial User's Workshop held at Prospect Hall, Princeton University, Princeton, New Jersey, on 29 and 30 November 1977. The purpose of this workshop was to begin the process of definition and development of the SEASAT-A Industry Demonstration Program, leading to the implementation of a set of experiments which would begin during the later part of 1978 following the launch of SEASAT-A (now scheduled for May 1978). The workshop brought together various representatives associated under NASA with the production of geophysical data and information from SEASAT-A and representatives of industry and government agencies who will individually and independently evaluate this geophysical data and information, for NASA and for themselves, in cooperative experiments. The representation also included a foreign participant (Canada) and a foreign observer (ESA).

Studies of the economic potential of an operational satellite system to provide improved forecasts of weather and ocean conditions for ocean regions indicate that the benefits that could be derived from the use of these data and forecasts will come about as a result of their use by industries that operate in these environments.[1] These studies have shown that the major areas of expected benefit from the improved data and forecasts are marine transportation, offshore resource exploration and development, Arctic operations and ocean fishing. An initial step in the exploration of the technical and economic feasibility of the use of satellite systems to

---

[1] SEASAT Economic Assessment, ECON, Inc., 31 August 1976.

provide improved weather and ocean condition data and forecasts for ocean regions will be taken with the launch of SEASAT-A. NASA, through the SEASAT-A program, has encouraged the planning of cooperative experiments by industries and government agencies that operate in areas of ocean activity that could benefit from improved measurements and forecasts of weather and ocean conditions.[2,3] The objectives of these experiments are to:

- Evaluate the significance of SEASAT-A data to commercial user organizations
- Assist in identifying those characteristics of follow-on systems that are important to industrial users
- Obtain experimental evidence that could be used to refine estimates of the economic potential of an operational system
- Begin the technology transfer process to the industrial users.

Since the workshop occurred subsequent to NASA approval of funding for the cooperative experiments, it was the first meeting of the SEASAT-A industrial users having an approved explicit objective of defining the requirements of the cooperative experiments involving SEASAT-A data. It is expected that there will be one or two additional workshops before SEASAT-A derived geographical data and information are ready for dissemination.

Through presentation and discussion, six major topics were addressed throughout the workshop as follows:

1. The current status of the SEASAT-A program.

---

[2] An Evaluation of SEASAT-A Candidate Ocean Industry Economic Verification Experiments, ECON, Inc., 1 April 1977.

[3] SEASAT-A Industry Demonstration Program (ASVT Program), Volumes I and II, NASA Headquarters, 1 June 1977.

2. A detailed presentation of the SEASAT-A instrumentation; the various physical interactions involved and the translation of these interactions to geophysical data; the confidence determined for these translations and the data accuracies expected.

3. The involvement of Fleet Numeric Weather Central (FNWC) as a source of oceanographic and meteorological information and the mechanics of data and information dissemination that will be available to the industrial users, as provided by NASA.

4. Preliminary written definitions of the requirements of the cooperative experiments as determined by the experimenters after consultation with resource personnel at the workshop.

5. The goals of the experiments for NASA and the users.

6. Initial comments, by the users, on a preliminary draft of the cooperative agreement that will exist between each of them and NASA for the accomplishment of the experiments and the subsequent independent reporting of their results.

The workshop was clearly successful and effective in producing the initial momentum necessary to the planning and implementation of the cooperative experiments, a momentum that must be sustained if the experiments are to be successfully concluded. It is the intent of this report to sustain that momentum and the spirit of cooperation brought about by the workshop toward a successful experiment program.

WORKSHOP STRUCTURE

The workshop was structured under an agenda. Certain logistical and scheduling difficulties led to deviation from the agenda during the workshop. While in actuality some presentations were curtailed or deleted during the workshop, the order in this report will be the more logical and complete one of the agenda.

The workshop opened with an introduction, a statement of the workshop objectives and an overview of the SEASAT system. These were followed by technical discussions and presentations of the major SEASAT instruments; the SEASAT-A Scatterometer, the Scanning Microwave Radiometer, the Radio Altimeter and the Synthetic Aperture Radar. The remaining instrument, the Visible and Infrared Radiometer, was not discussed in detail. Following the discussion of the instruments, SEASAT-A data and information sources availability and dissemination were presented as JPL Data Systems, FNWC Data Processing and Products, and the Data Distribution Facility. These laid the groundwork for the discussion of the industrial user experiments. The first day concluded with a presentation of the proposed Canadian experiments and the assignment of the workshop groupings, the group coordinators and the specialized resource personnel.

During the second day the conferees were divided into five working groups. The experimenters, with the assistance of data processing, sensor and spacecraft specialists, prepared written formulations of their experiments. The entire workshop then reconvened and the experimenters reviewed all of the proposed experiments. The meeting adjourned with a summary of the workshop.

THE WORKSHOP OPENING

Welcoming and introductory remarks were provided by Mr. B. P. Miller of ECON, Inc., the workshop chairman. He stressed the new status of the cooperative experiments as a funded element of the NASA program and the urgent need to formalize the requirements of these experiments so that they could be responded to within the proposed budget allocation. This theme was expanded and elaborated by Mr. S. Walter McCandless and Mr. Donald Montgomery of the SEASAT-A Program Office at NASA Headquarters as they outlined the Workshop Objectives presented in the introduction. Mr. McCandless, in his System Overview, described the SEASAT-A satellite, the instrumentation packages, their locations and footprints and emphasized the space uniqueness of the SEASAT-A active instruments. Although the SEASAT-A program has been in progress for about four years, he said, the program is within about one week of schedule, all the subsystem tests have been completed successfully and there is no impediment to a May 1978 launch. A critical system test remains to be done, the RFI test. If RFI proves to be an unexpected problem, it could necessitate a modification to the instrumentation programming, and hence to the coverage provided. All instruments, except for the SAR, will be operated continuously with data being recorded on board until it is read out to a ground station. The SAR, on the other hand, is switched on and read out only when the spacecraft is within line-of-sight of a ground station. He illustrated that approximately full earth coverage by the instrumentation, except the SAR, occurs once every 36 hours.

THE SEASAT-A INSTRUMENTATION

Technical discussions of the principal SEASAT-A instrumentation were presented either by those involved in the development and evaluation of the instruments or by their representatives. The instruments, their presentors and their affiliations are tabulated below.

Instrument	Presentor	Affiliation
Windfield Scatterometer (SCAT or SASS)	Dr. W. Linwood Jones	NASA-Langley Hampton, VA
Scanning Multichannel Microwave Radiometer (SMMR)	Mr. Edwin Pounder	JPL Pasadena, CA
Radar Altimeter (ALT)	Dr. Byron D. Tapley	University of Texas Houston, TX
Synthetic Aperture Radar (SAR)	Dr. Omar H. Shemdin	JPL Pasadena, CA

No presentation of the Visible and Infrared Radiometer (VIR) was given since the instrument is an existing design and its operating characteristics are well established.

THE WINDFIELD SCATTEROMETER (SCAT OR SASS)

Introduction

This instrument is an active pulsed radar whose returns from the ocean surface contain information from which surface wind vectors can be inferred, quantitatively, after appropriate processing of the return signals.

The procedures for scatterometer operation and for appropriate processing of the return signals have resulted from evaluation and verification of considerable experimental flight data. These procedures require corrections obtained from the Visible Infrared Radiometer and the Scanning Microwave Radiometer, two other SEASAT instruments.

Currently three processing algorithms are under consideration for transforming the sensor data records to the geophysical data records of surface wind and direction and the final choice of algorithm is expected to be made during the proving-in period of operation of SEASAT-A. Normally the wind vectors identified are those at the sea surface, but the measurements can be translated to winds at altitude using appropriate atmospheric modeling.

The SEASAT-A instrument characteristics, its coverage and its performance coincide with requirements established by a SEASAT user working panel.

Research is continuing to define the influence on observed measurements of fetch and nonlinear wave interactions.

The presentation actually given at the workshop by Dr. W. Linwood Jones is not provided in this report. Instead, at Dr. Jones' suggestion, two of

his recent papers on the instrument are introduced because of their greater completeness. These papers are provided in Appendix A. JPL provided the SASS IGDR Flow Chart which is included in this section.

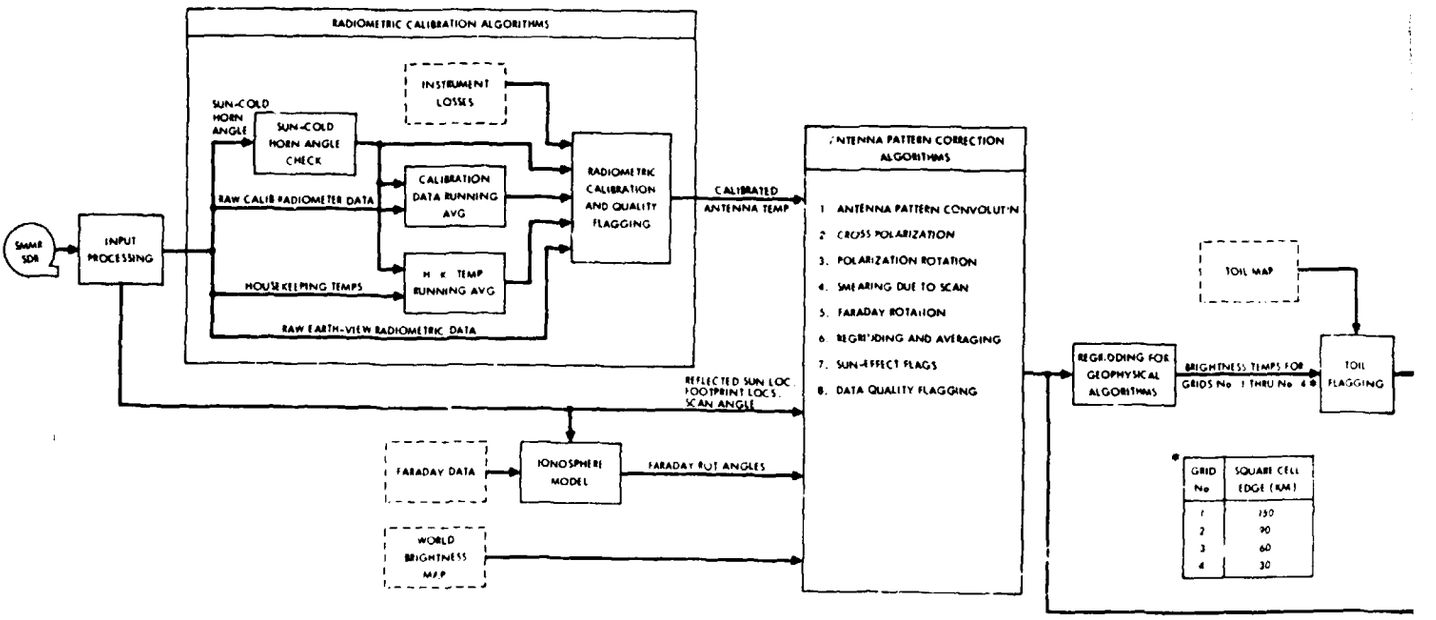

FOLDOUT FRAME

2

MR IGDR FLOW CHART

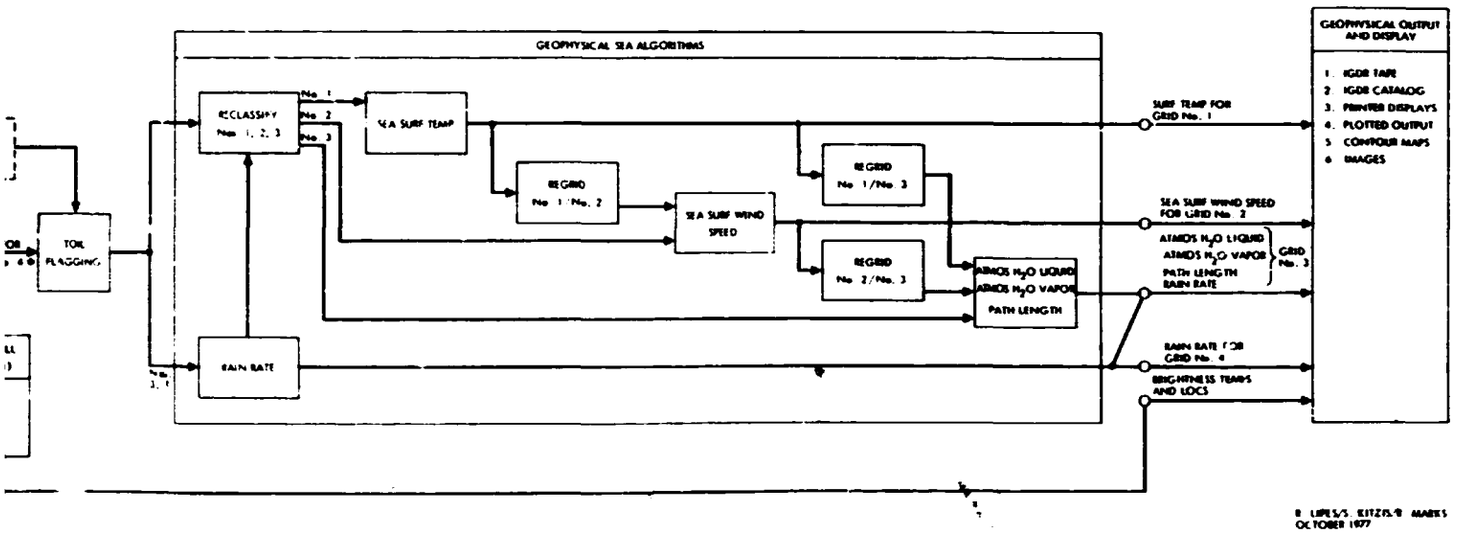

OCTOBER 1977

THE SCANNING MULTICHANNEL MICROWAVE RADIOMETER (SMMR)

Introduction

This instrument operates passively at five different microwave frequencies and is conically scanned over a cone angle of 48.8° to provide radiometric brightness components as ten channels of data, when polarization diversity is included as well as frequency diversity. Radiometric brightnesses are then converted to microwave brightness using well developed techniques.

Subsequently, employing reasonable theoretical and experimental assumptions about the atmosphere and the surface emissivity of the ocean, the microwave brightness can be converted to an estimate of the sea surface temperature.

Because microwave brightness has been experimentally demonstrated to vary with sea surface wind, the wind speed can also be inferred from the collected data.

Nimbus 5 and 6 have further demonstrated the applicability of the SMMR to sea ice coverage. Potentially, also, certain descriptive parameters of the terrain can be extracted from SMMR data.

On SEASAT-A, the SMMR coverage overlaps that of the SAR and the scatterometer to provide correction data to these instruments.

The presentation that follows was given by Mr. Edwin Pounder of JPL.

SMMR OBJECTIVES

MAP:

- SEA ICE COVERAGE
- WIND SPEED
- WATER VAPOR
- ATMOSPHERIC PATH LENGTH
- CLOUD LIQUID WATER
- RAIN AREAS / RAIN RATE
- SEA SURFACE TEMP

TOP VERTICAL

Flow diagram for retrieval technique

Flow Diagram for Application of the Data Inversion Methodology to Parameter Estimation for a Radiometric Experiment. (The $\underline{p}$ and $\underline{d}$ data sets may be simulated for study purposes, as shown by dashed lines.)

Conceptual flow diagram for SMMR interpretation

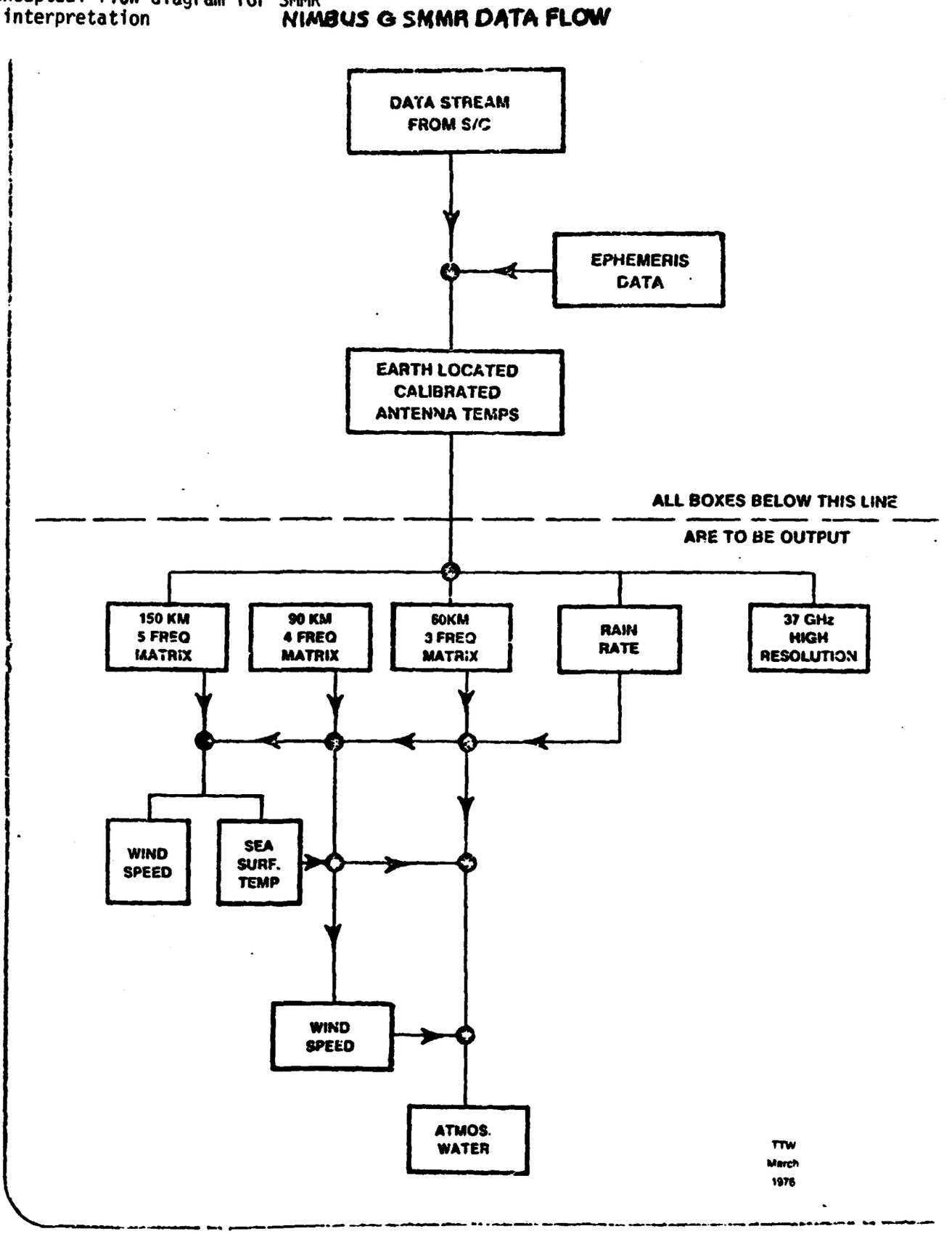

SMMR

ANTICIPATED RESULTS

(Simulations Tempered by Experimental Judgment)

Parameter	Resolution	Accuracy
Sea Surface Temperature	150 km	1.5°C
Wind Speed	90 km	1 m/x
Water Vapor	60 km	0.15 gm/cm^2
Liquid Water	60 km	3 mg/cm^2
Path Length Correction	60 km	2 cm
Rain Rate	60 km	Factor of 2
Sea Ice	60 km	$\lesssim$ 5%
	30 km	$\lesssim$ 25%

GROUND PROCESSING WILL REDUCE DATA TO FOUR CONSISTENT GRIDS

Grid #	1	2	3	4
Resolution	150 km	90 km	60 km	30 km
6.6 GHZ	✓			
10.7 GHZ	✓	✓		
18 GHZ	✓	✓	✓	
21 GHZ	✓	✓	✓	
37 GHZ	✓	✓	✓	✓

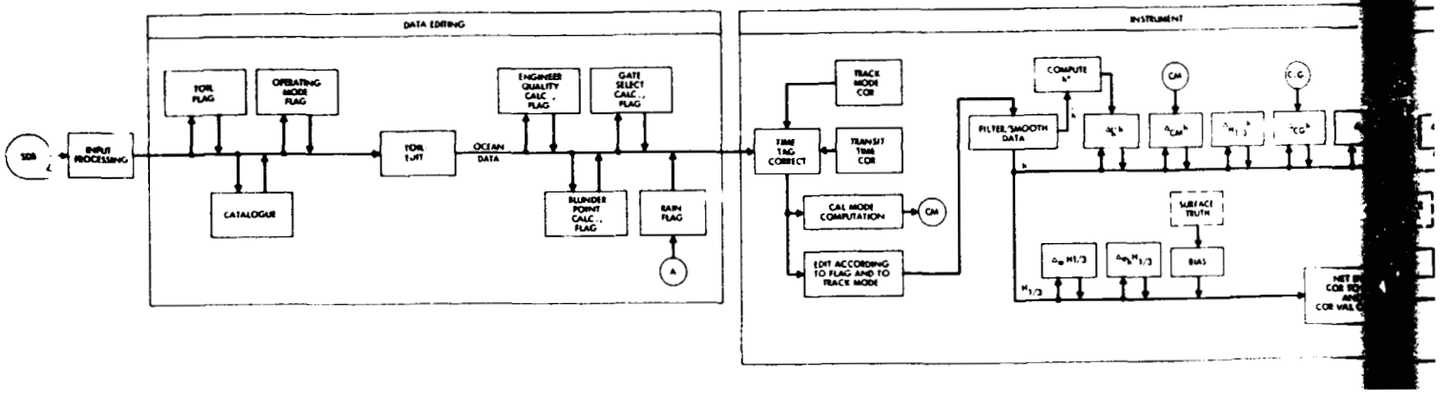

ALTIMETER IGDR PROCESSING ALGORITHMS

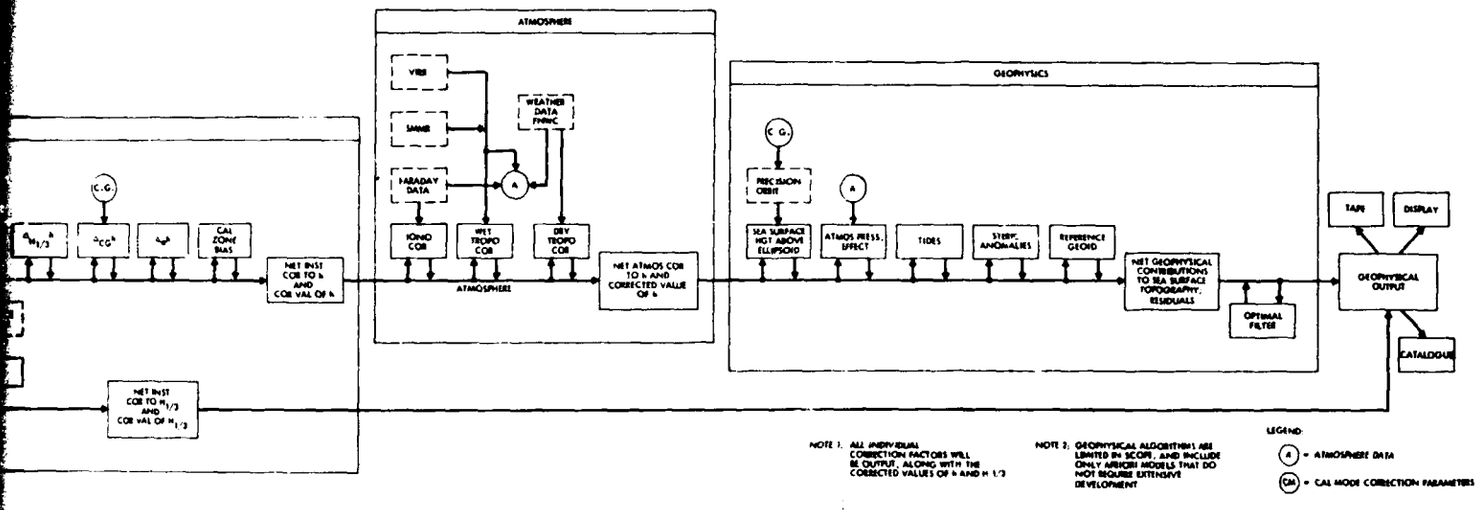

J. LORELL
OCT. 19, 1977

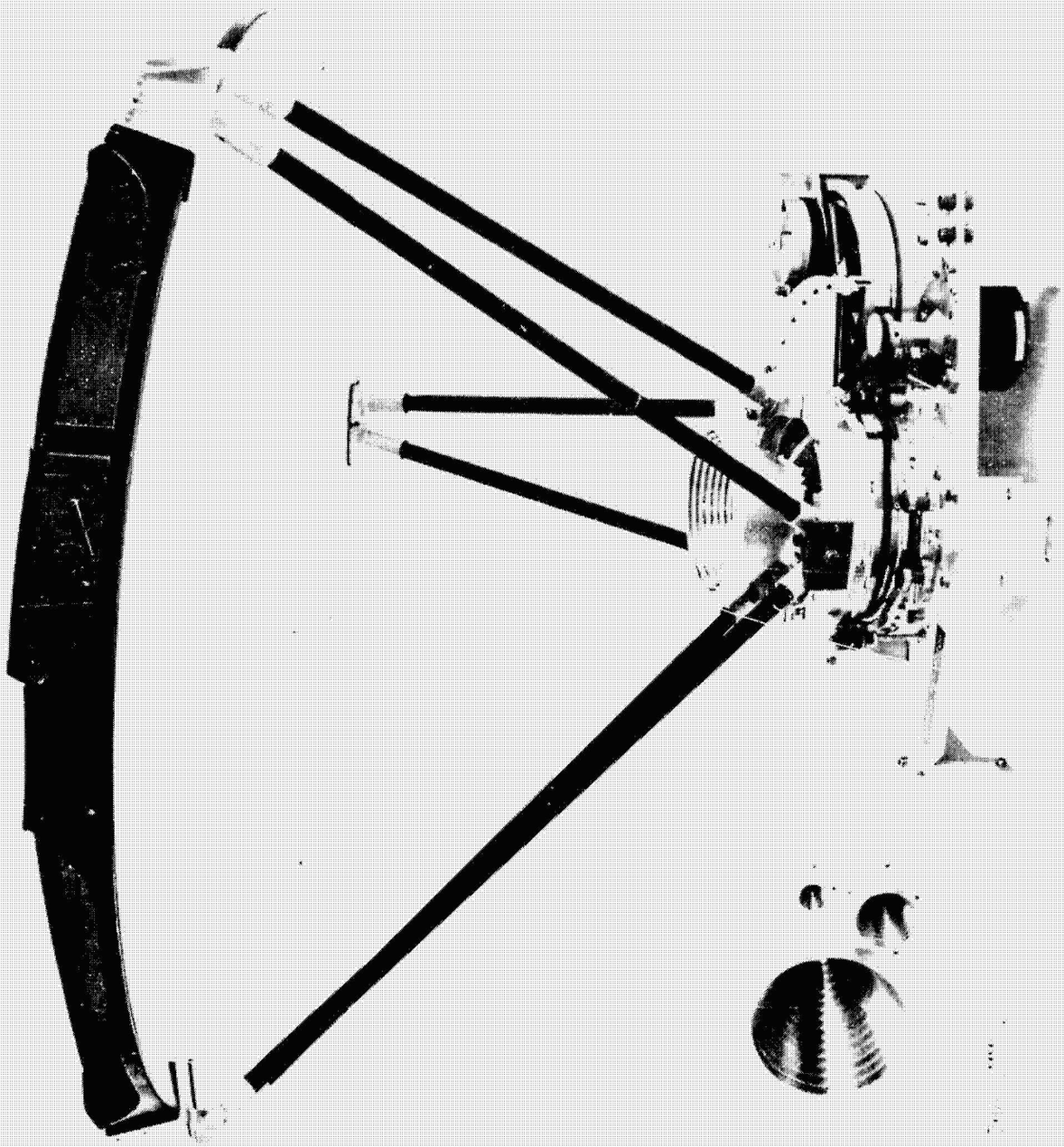

THE RADAR ALTIMETER (ALT)

Introduction

The radar altimeter is an active microwave instrument operating in a pulsewidth limited mode to accurately measure the distance between SEASAT-A and the nadir ocean surface.

The SEASAT-A altimeter is a third generation instrument, expanding on the experience with the Skylab and GEOS-3 experiments, and was originally developed for geodesy.

Satellite altimeter measurements can contribute to the study of ocean surface topography such as currents, tides, storm surges and ocean wave height determination. Since the later satellite altimeters have the ability to operate over land and ice as well, a capability is provided for profiling solid surfaces. This latter effect may provide quite significant information in regard to determining the polar ice cap budgets and their influence on global meteorological and climatological conditions.

The Altimeter Measurement

The altimeter transmits a square pulse toward the ocean surface. The average return, as shown in Figure 1, exhibits a linear rise followed by a plateau of constant pulse amplitude after which an amplitude decay occurs. Small antenna pointing errors have little effect upon the measurement due to the fact that altitude and wave height measurements are obtained by analyzing the leading edge of the pulse. As a consequence, most altimeter designs represent a compromise between the desire:

1. to maximize the gain which would reduce the transmitting power and
2. to minimize the effects of antenna pointing errors on the height, precision and bias.

FIGURE 1 PULSEWIDTH LIMITED WAVE FORM CHARACTER

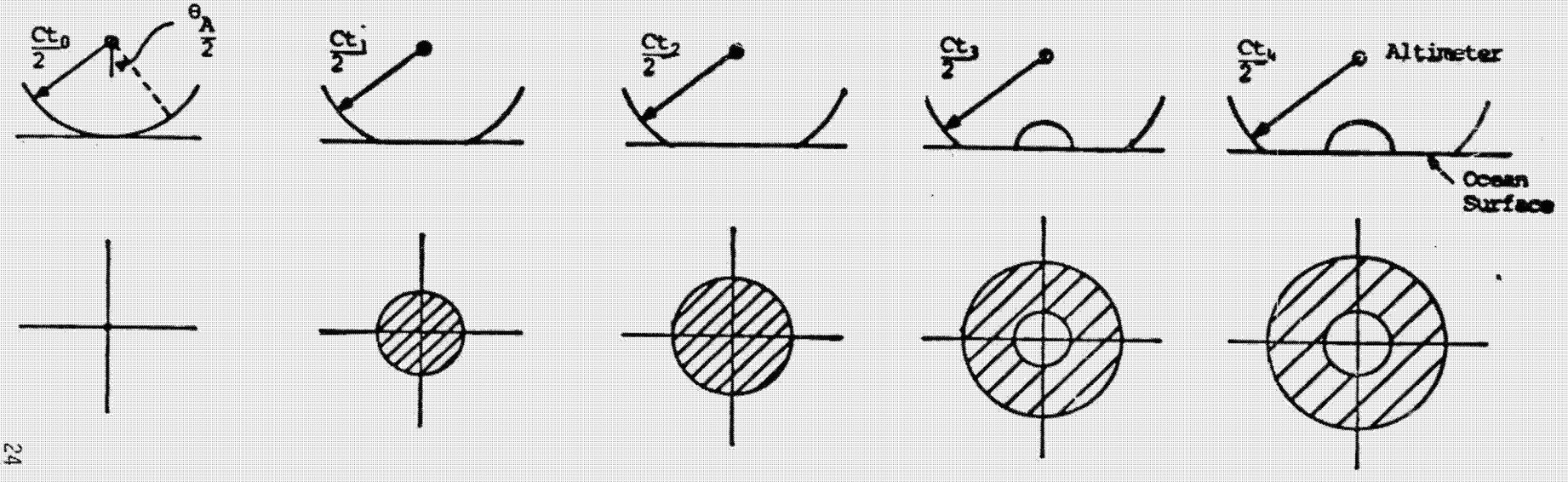

ILLUMINATED AREA

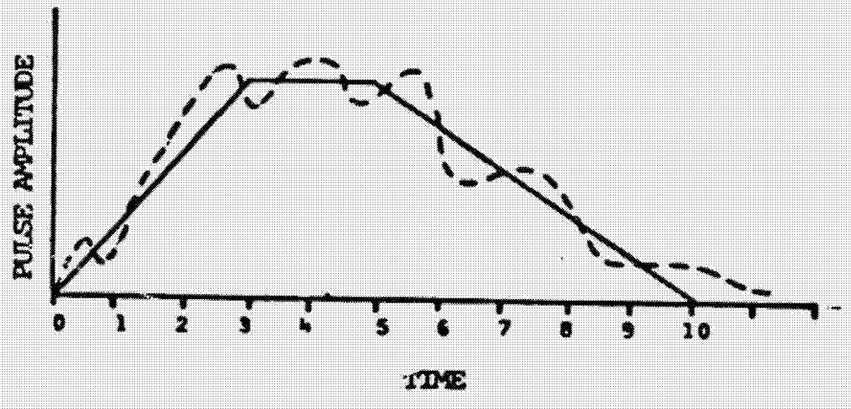

WAVE - FORM RETURN

The basic measurement obtained from the satellite altimeter is the height to the mean sea surface, which is, in turn, related to the time between the transmission of the pulse and the reception of the return pulse at the satellite. The specific formula is $h = \frac{c(\Delta t)}{2}$ where Δt is the total transit time between the pulse transmission and reception at the satellite, c is the speed of light and h is the altitude of the satellite. The time of reception is normally identified as the point which is approximately midway up the initial slope. Further details on this topic can be found in the referenced report.[4] In addition to the height measurement, the ocean wave height will tend to spread out the pulse so that the significant wave height can be correlated directly with the slope of the leading edge of the return signal. By measuring the initial slope, a direct correlation with the significant wave height ($h_{1/3}$) can be obtained. Through additional processing techniques, the $h_{1/3}$ measurement can be related to σ_0, the ocean back scatter coefficient.[5]

Satellite Altimeter Design Parameters and Results

In Table 1, entitled Satellite Altimeter Parameters, the design parameters for each of the three successful satellite altimeters are given. Note the significant increase in pulse repetition frequency from 100 Hz on GEOS-3 to 1,020 Hz for SEASAT-A. Note also that this leads to a reduction in the RMS precision from just less than 50 cm for the GEOS-3 satellite altimeter to less than 10 cm for the SEASAT-A satellite altimeter. Current test results indicate that for sea states less than 12 meters the SEASAT-A satellite

[4]MacArthur, John L., "The Design of the SEASAT-A Radar Altimeter", reprint presented at Ocean '76 Conference, September 13-15, 1976.

[5]Higgins, M. S. Longuet, "On the Statistical Distribution of the Height of Sea Waves", Journal of Marine Institute, Volume II, No. 3, 1952, pp. 245-266.

Table 1 Satellite Altimeter Parameters

	Skylab	GEOS-3 (Intensive)	SEASAT-A
Mean Altitude (km)	435	840	800
Antenna Beamwidth (°)	1.5	2.6	1.6
Frequency (GHz)	13.9	13.9	13.5
Peak RF Power (kW)	2	2	2
Average RF Power (W)	0.05	0.24	6.5
Pulsewidth (uncompressed)	100 ns	1 μs	3.2 μs
Pulsewidth (ns) (compressed)	--	12.5	3.125
Repetition Frequency (Hz)	250	100	1020
Footprint Diameter (km)	8	3.6	1.7
Altitude Precision (rms)	< 1 m	< 50 cm	< 10 cm
Status	Mission Complete	In Orbit	1978 Launch

altimeter will have a precision of 3 to 5 cm. The increase in the pulse repetition frequency, in addition to allowing a higher precision in the altitude measurement, also will allow a more precise determination of the initial edge of the returned wave form. This will lead to a better determination of the $h_{1/3}$. In the remaining slides (taken from referenced material listed below),[6,7] typical examples of the results obtained from the GEOS-3 altimeter both with regard to the sea surface topography measurements and to the wave height measurements are given. In particular, Table 2 presents the results of a comparison of wave height measurements determined from GEOS-3 satellite altimetry with the results obtained from a similar aircraft altimeter as well as results obtained using ocean surface buoys. The results given in this table are shown graphically in Figure 2. The results indicate a comparison of the ground truth and aircraft radar significant wave height measurements compared with the GEOS-3 significant wave height measurements. The conclusion from these results are that the GEOS-3 altimeter has the ability to determine the significant wave height quite accurately. It is anticipated that even more dramatic results will be obtained with the more accurate altimeter to be flown on SEASAT-A in combination with the substantially increased ocean coverage which will result from the fact that SEASAT-A altimeter will be on continuously.

In SEASAT-A applications, the goal is to successfully resolve oceanographic topography; wave heights, ocean currents, tides and coastal upwellings.

---

[6]Parsons, C. L. and G. S. Haynes, "An Assessment of GEOS-3 Wave Height Measurements", unpublished preprint, NASA, Wallops Flight Center.

[7]Haynes, G. S., "Initial Development of a Method of Significant Wave Height Estimation for GEOS-3", NASA Contract Report 141425, August 1977.

Table 2 NDBO Buoy Data Summary

Date	ID	Buoy SWH	GEOS-3		SWH
			Orbit	Time	
2/15	EB35	5.5	9588	164346	5.4
2/17	EB19	4.5	9616	161157	5.1
2/20	EB03	4.5	9659	170948	4.6
2/26	EB19	3.5	9744	172000	4.8
2/27	EB16	3.0	9753	085637	3.3
3/9	EB19	4.0	9896	112745	4.1
3/12	EB16	5.5	9738	104550	5.9
3/12	EB19	8.0	9943	185455	7.2
3/20	EB16	1.5	10057	201436	1.3
3/22	EB16	2.0	10080	113949	2.9
3/23	EB19	2.5	10095	130253	2.7
3/24	EB03	2.5	10110	142745	3.4
3/24	EB17	2.5	10110	142928	2.6
3/26	EB19	4.5	10142	202930	4.3
3/29	EB03	2.5	10181	145421	2.9
3/29	EB17	3.0	10181	145607	3.3
3/31	EB16	2.0	10208	124746	1.2
4/2	EB03	3.5	10238	153543	4.1
4/2	EB17	3.5	10238	153741	4.0

FIGURE 2

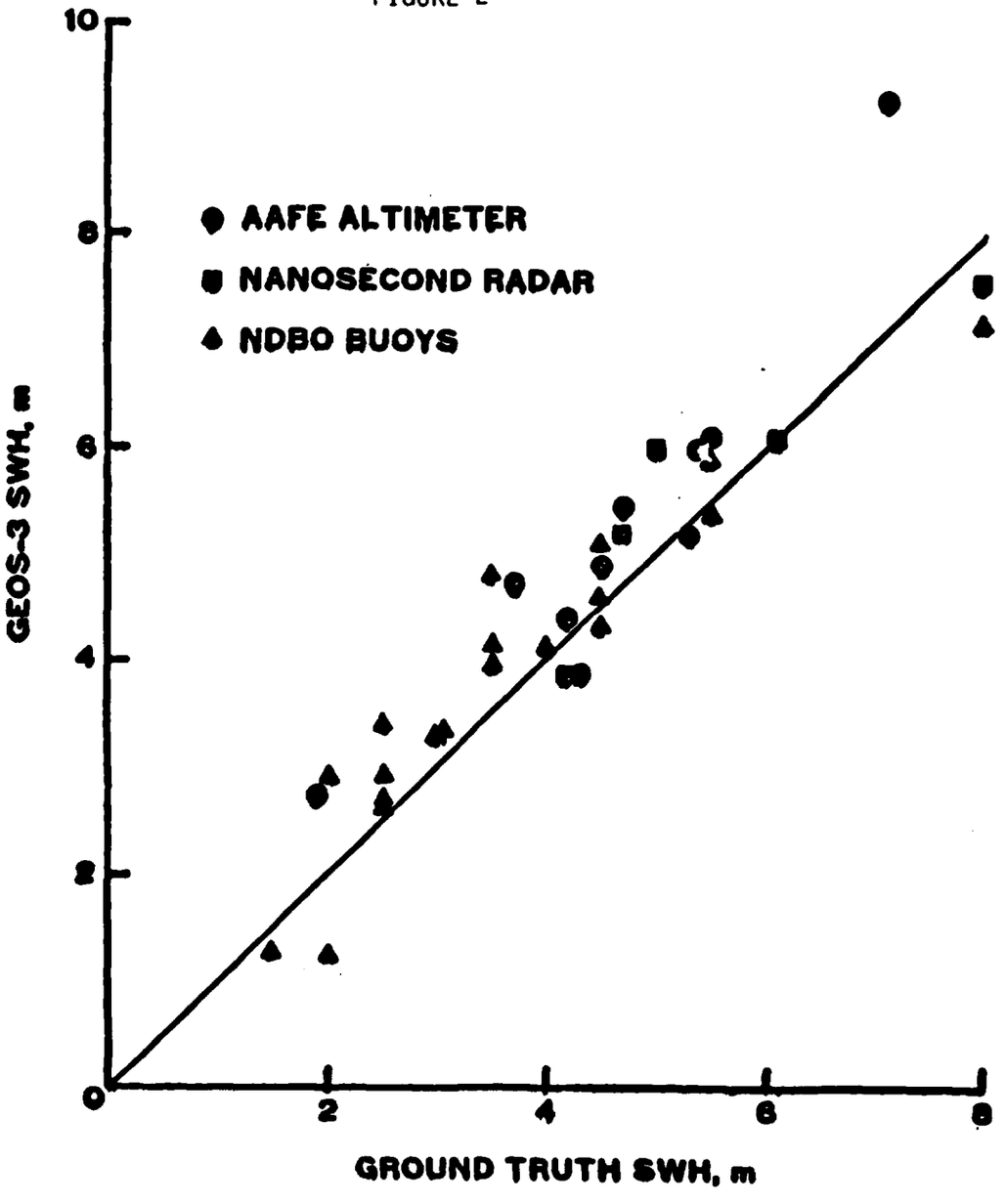
AAFE ALTIMETER
NANOSECOND RADAR
NDBO BUOYS
GEOS-3 SWH, m
GROUND TRUTH SWH, m
0
2
4
6
8
10

Topographic measurements are altitude difference measurements from mean sea level, which in a radar altimeter are essentially time difference measurements characterized by differences in the returned pulse wave form. Processing for optimum wave form analysis requires processing parameter selection which is provided by closed loop adaptive tracking of the wave height of interest to give highly precise measurements. Wave height precision requires precision in the satellite location, and reasonable control of the short-term satellite attitude dynamics.

The Radar Altimeter presentation was given by Professor Byron Tapley. The SEASAT-A Altimeter IGDR Processing Algorithm was provided by JPL.

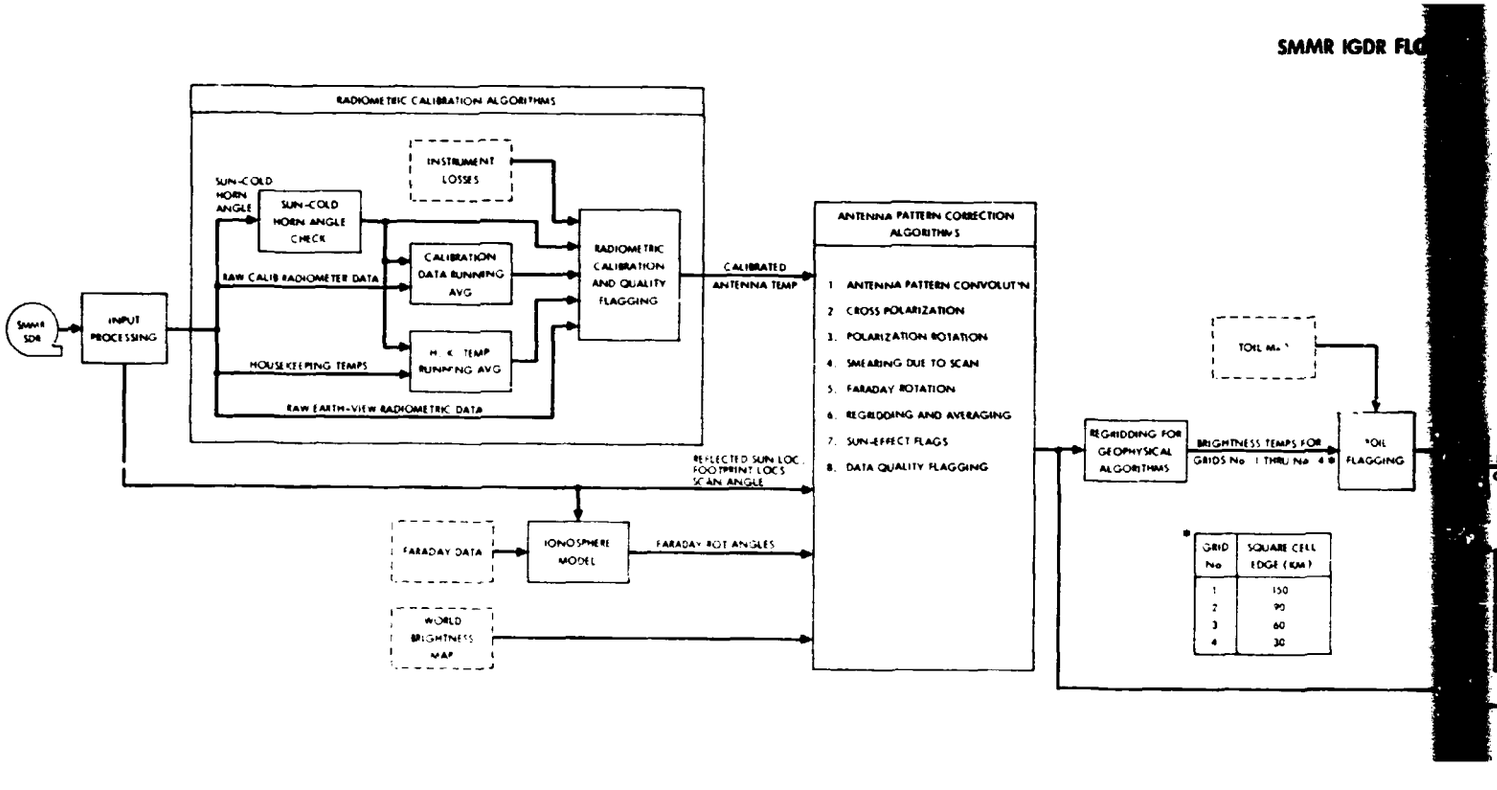

SMMR IGDR FLOW CHART

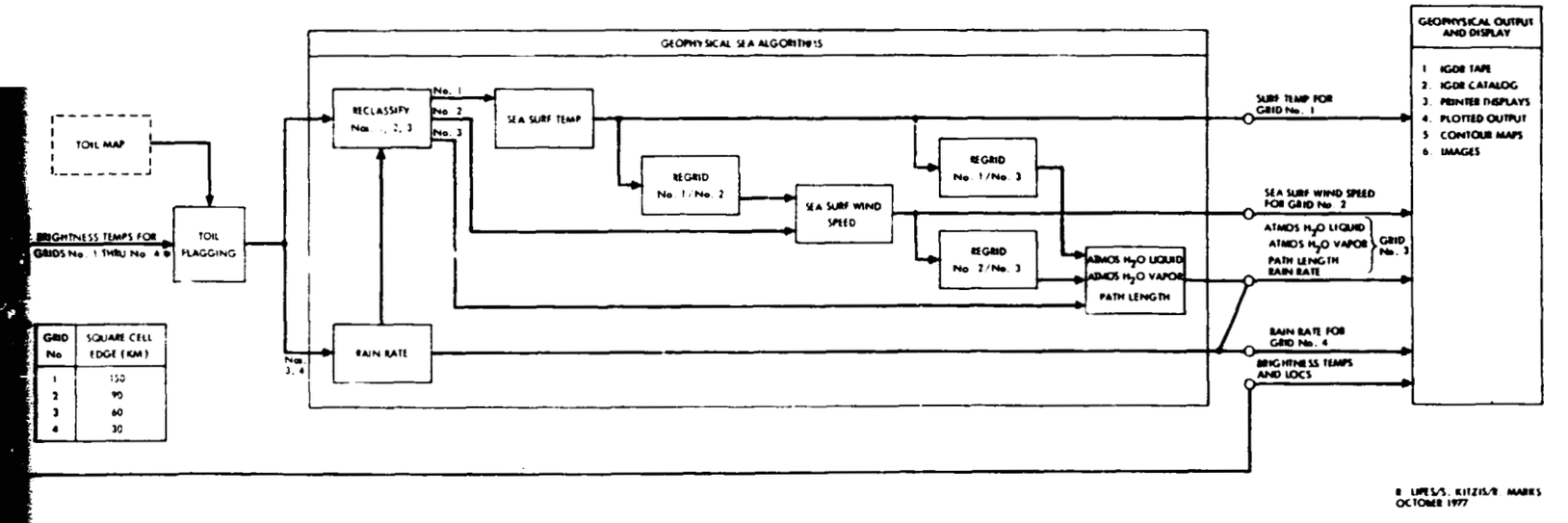

B. LIPES/S. KITZIS/B. MARKS
OCTOBER 1977

THE SYNTHETIC APERTURE RADAR (SAR)

Introduction

The SAR is an experimental active radar instrument which produces data essentially characterizing the radar reflectivity imagery of the illuminated region, in resolution cells identified by their doppler frequency shift. The motion of the antenna allows successive radar illumination of the same "point" up to some maximum repetition defined by the system design. Adequate recognition of the successive point returns allows them to be treated as coherent and summed arithmetically to enhance the definition and contrast of the radar image of the scene. Because of the large quantities of data to be evaluated, the identified returns must be telemetered to the ground to be digitalized and recorded on magnetic tape, later to be processed and converted to film images or digital tapes in concert with orbital and attitude characteristics of the spacecraft.

It is expected that the imagery of the SAR will have pertinancy to deep ocean waves, coastal wave patterns, polar ice characteristics and land forms.

Because of power and data storage constraints aboard the SEASAT-A spacecraft, the SAR will be operated and SAR data transmitted only when the spacecraft is in line of sight of a ground station that is equipped to receive and record the SAR signals. As opposed to data from the scatterometer, the microwave radiometer and the altimeter, the SAR data will not be relayed to FNWC for subsequent processing. A limited quantity of the SAR data will be processed by JPL, but not in real time. It is presently estimated that approximately 15,000 minutes per year of SAR data will be recorded at the ground stations to be operated by NASA. Of this quantity, approximately 2,600 minutes will be processed to imagery by JPL. Additional processing time may be available from JPL on a cost reimbursible basis.

The synthetic aperture presentation was given by Dr. Omar H. Shemdin of JPL, but his actual presentation is not included. Instead two technical papers provided by Dr. Shemdin have been provided in Appendix B. These papers provide source knowledge about the interpretation of SAR imagery for observation of waves and current boundaries that may be of general interest to experimenters.

THE VISIBLE AND IR RADIOMETER

The following VIRR IGDR processing flow chart was provided by JPL.

VIRR IGDR PROCESSING FLOW CHART

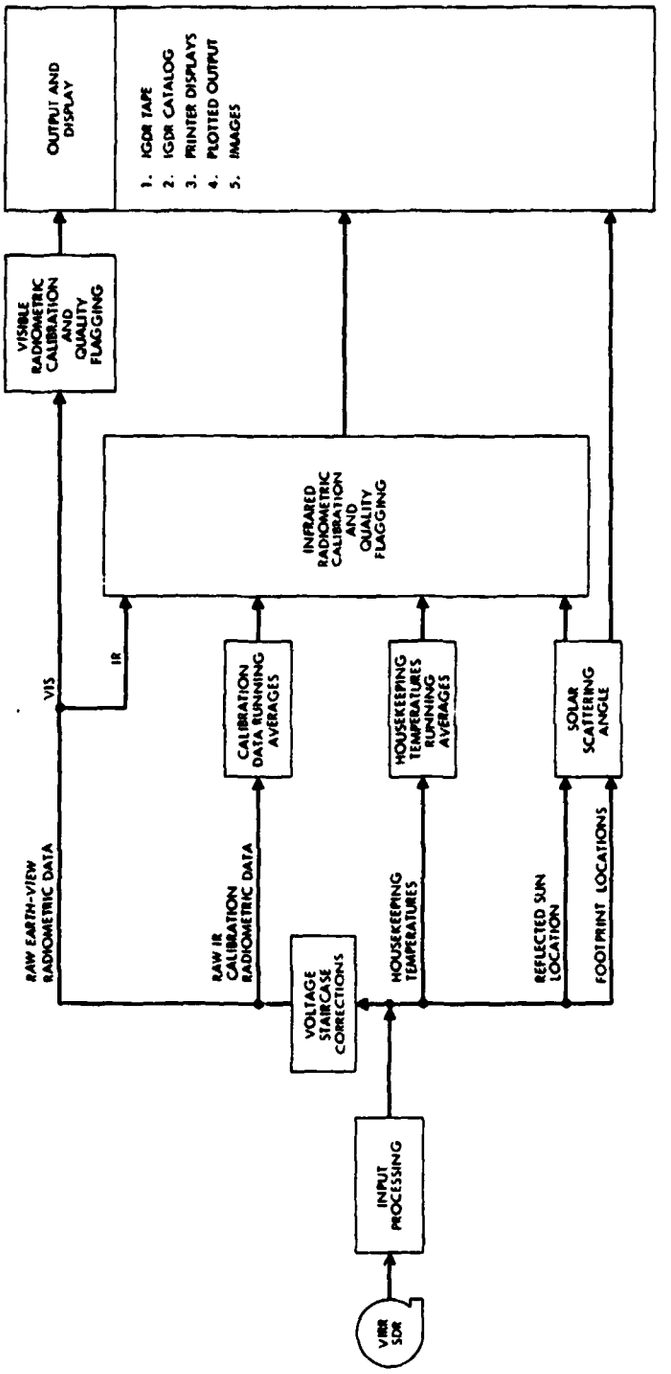

PROCESSING OF SEASAT-A DATA

Introduction

The data received from SEASAT-A onboard sensors is available as recorded signals from the sensors as sensor data records (SDR). To be of application use, the SDRs must be accurately located both in time and geospace and be translated to geophysical data records (GDRs) by transformation algorithms or processes.

The geophysical data so determined can be then introduced, when valid and appropriate, into descriptive, analytic and prognostic computer programs to provide point and synoptic oceanographic and meteorological information.

The oceanographic and meteorological information, both current and prognostic can then be processed and disseminated in a wide variety of formats as required by the applications of the experimentors.

The complete processing of SEASAT-A data, from the sensor data records to the requirements of the experimentors applications is viewed as a three step process in which JPL and FNWC will participate.

Concurrent with the processing procedure is a requirement to accurately locate the satellite center of gravity in orbit and the satellite attitude relative to a vector through its center of gravity and to identify any reservations concerning the data quality.

These processing steps were discussed by three presentors, by Mr. Edwin Pounder for JPL, by Captain Harry Nicholson of FNWC, and by Mr. David Nippert of Battelle for the user.

The data processing provided by JPL is fundamental to the program and has proceeded concurrently with the SEASAT-A program and is in its final stages of development. FNWC provides oceanographic and meteorological information necessary to the operation of the USN and accepts validated data from all sources and modifies its computer programs as required to attain the requirements of USN operations. The data processing and information dissemination for the users associated with SEASAT-A has only recently been initiated and the presentation on this subject is primarily informative for the user; identifying products available, data capacities required and receiving terminals for display and hardcopy that should be selected. As a consequence of the substantive requirements documented by the users, in this workshop, development of an information processing and dissemination system, as appropriate as possible to the user requirements will be necessary.

1. The data presentation of Mr. Edwin Pounder of JPL.

SEASAT-A
DATA TYPES

DATA TYPES

I LOW RATE TELEMETRY
- ENGINEERING
- ALTIMETER
- SCATTEROMETER
- SCANNING MULT RADIOMETER
- V & IR RADIOMETER

II SYNTHETIC APERTURE RADAR

III DATA FOR ORBIT DETERMINATION
- S-BAND
- TRANET
- LASER

SEASAT-A

DATA DEFINITIONS LOW-RATE TELEMETRY

- RAW TELEMETRY DATA
  - DATA WORDS, AS TRANSMITTED BY THE SATELLITE
  - GROUND SYSTEM (STDN) ARTIFACTS REMOVED
  - TIME ORDERED, TIME TAGGED

- SENSOR DATA
  - DATA WORDS IN ENGINEERING UNITS
  - SENSOR INTERNAL CALIBRATIONS CORRECTIONS APPLIED
  - TIME ORDERED, TIME TAGGED
  - EARTH LOCATED (LAT, LONG)

- GEOPHYSICAL DATA
  - SENSOR MEASURED QUANTITIES CONVERTED TO GEOPHYSICAL UNITS
  - INSTRUMENT TRANSFER FUNCTION AND ENVIRONMENTAL EFFECTS REMOVED
  - TIME ORDERED, TIME TAGGED
  - EARTH LOCATED (LAT, LONG)

SEASAT-A

DATA ANALYSIS APPROACH
LOW-RATE

- PROCESS ALL OF THE LOW RATE SENSOR DATA TO ENGINEERING UNITS, EARTH LOCATED

- EVALUATE A SAMPLE SET OF DATA FOR GEOPHYSICAL EVALUATION

SEASAT-A

BLOCK TELEMETRY

SATELLITE DATA STREAM AS SEEN BY S/C RECORDER:

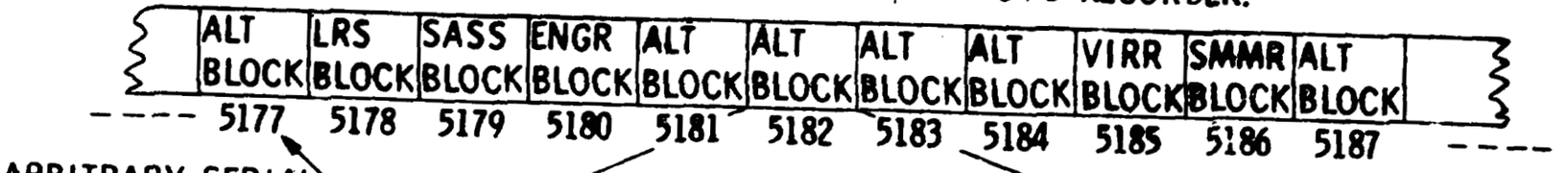

TYPICAL BLOCK COMPOSITION:

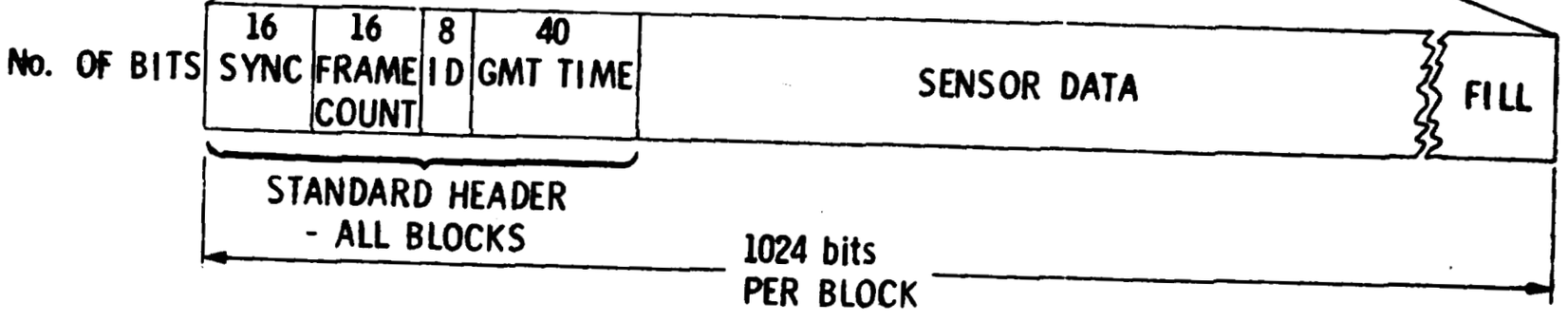

SATELLITE DATA STREAM AS PLAYED BACK BY S/C RECORDER:

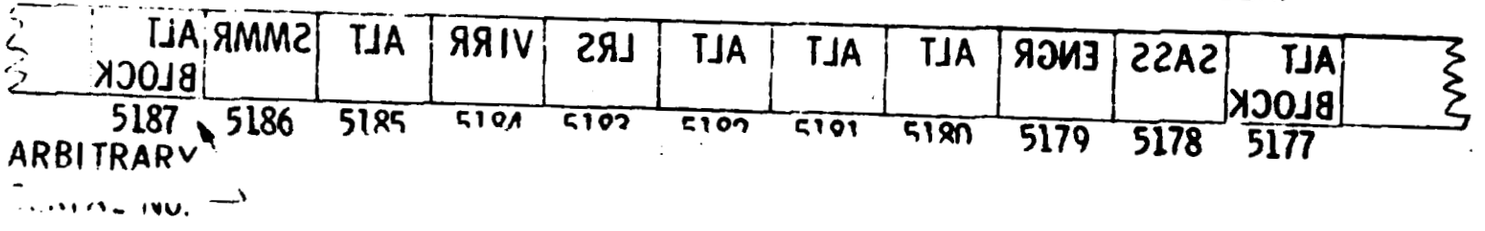

45

ORIGINAL PAGE IS OF POOR QUALITY

SEASAT-A
DATA FLOW

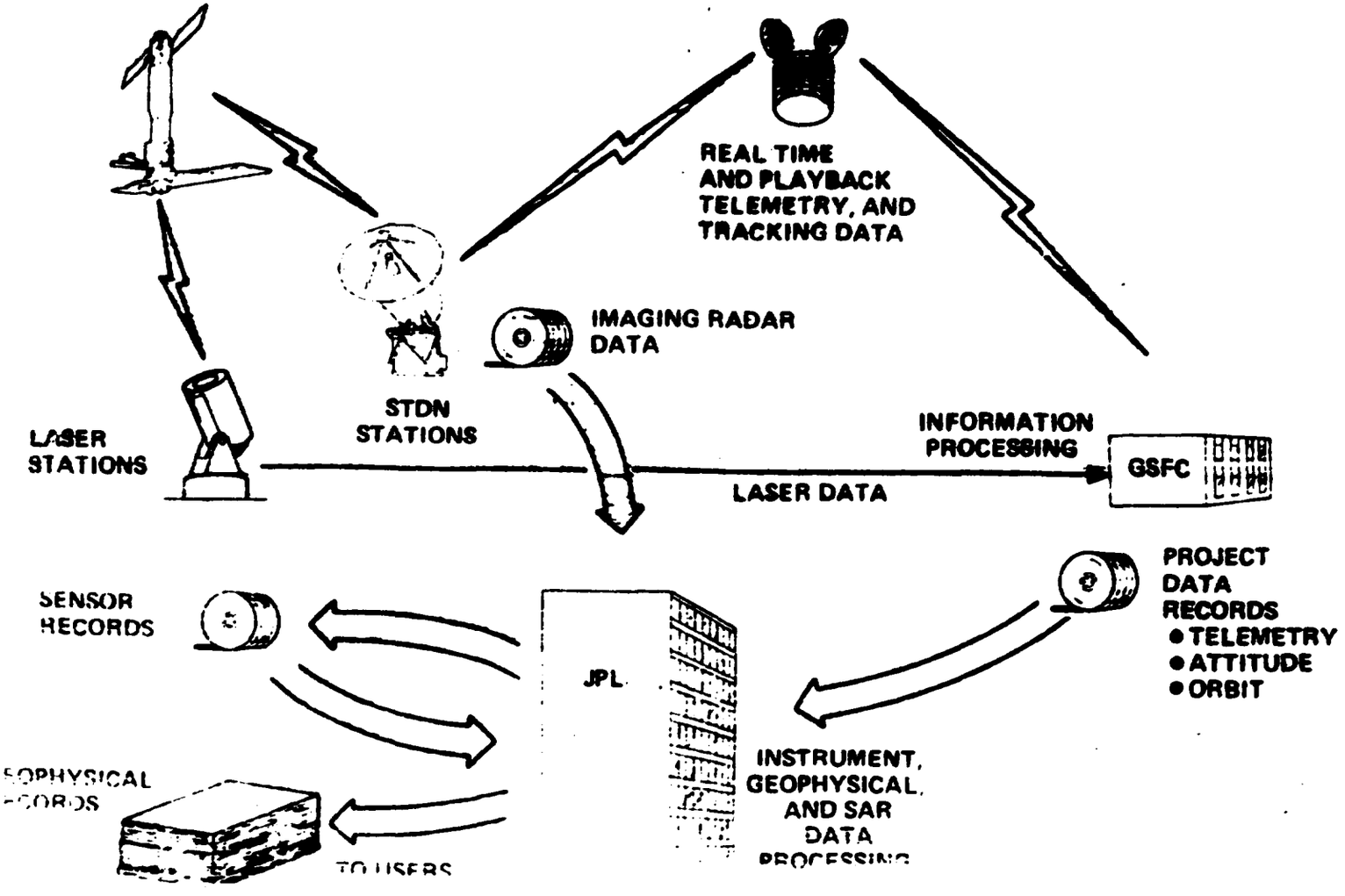

LOW RATE FLOW DIAGRAM

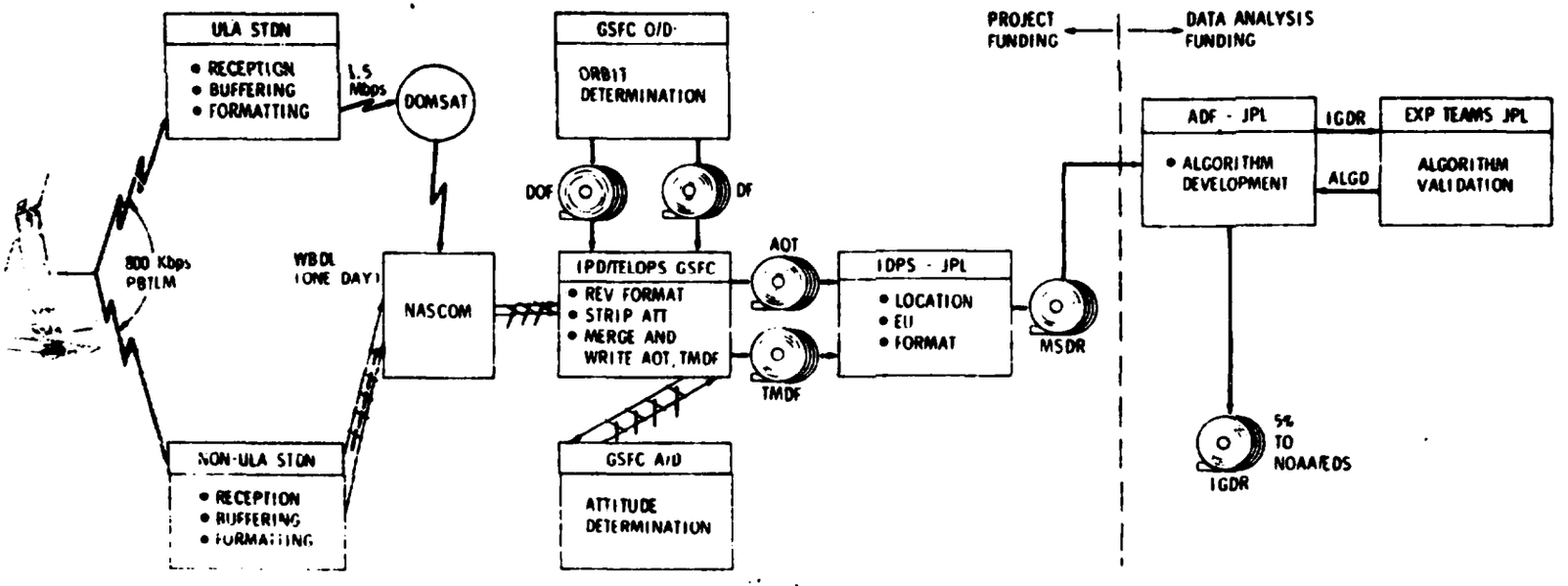

SEASAT-A
DATA DEFINITIONS
SYNTHETIC APERTURE RADAR

- RAW SAR DATA
  - TIME ORDERED STREAM OF ANALOG DATA AS RECEIVED FROM THE SATELLITE
  - SIGNAL DIGITIZED AND FORMATTED ON GROUND INTO RAW DATA WORDS IN REAL TIME

- IMAGE FILM
  - CORRELATED 25 km WIDE STRIP ON 70 mm FILM WITH APPROXIMATE RADIOMETRIC AND GEOMETRIC CORRECTIONS

- DIGITAL IMAGE DATA
  - IMAGE DATA RECORDED IN DIGITAL DATA WORDS ON COMPUTER COMPATIBLE TAPE

DATA ANALYSIS APPROACH (contd)
SAR DATA

- MAINTAIN A COMPLETE SAR SIGNAL TAPE RECORD (15,000 minutes)
- PROCESS REPRESENTATIVE DATA TO IMAGE FILM (2600 minutes)
- EVALUATE FOR GEOPHYSICAL INTERPRETATION (260 minutes)

SEASAT-A
SAR DATA FLOW

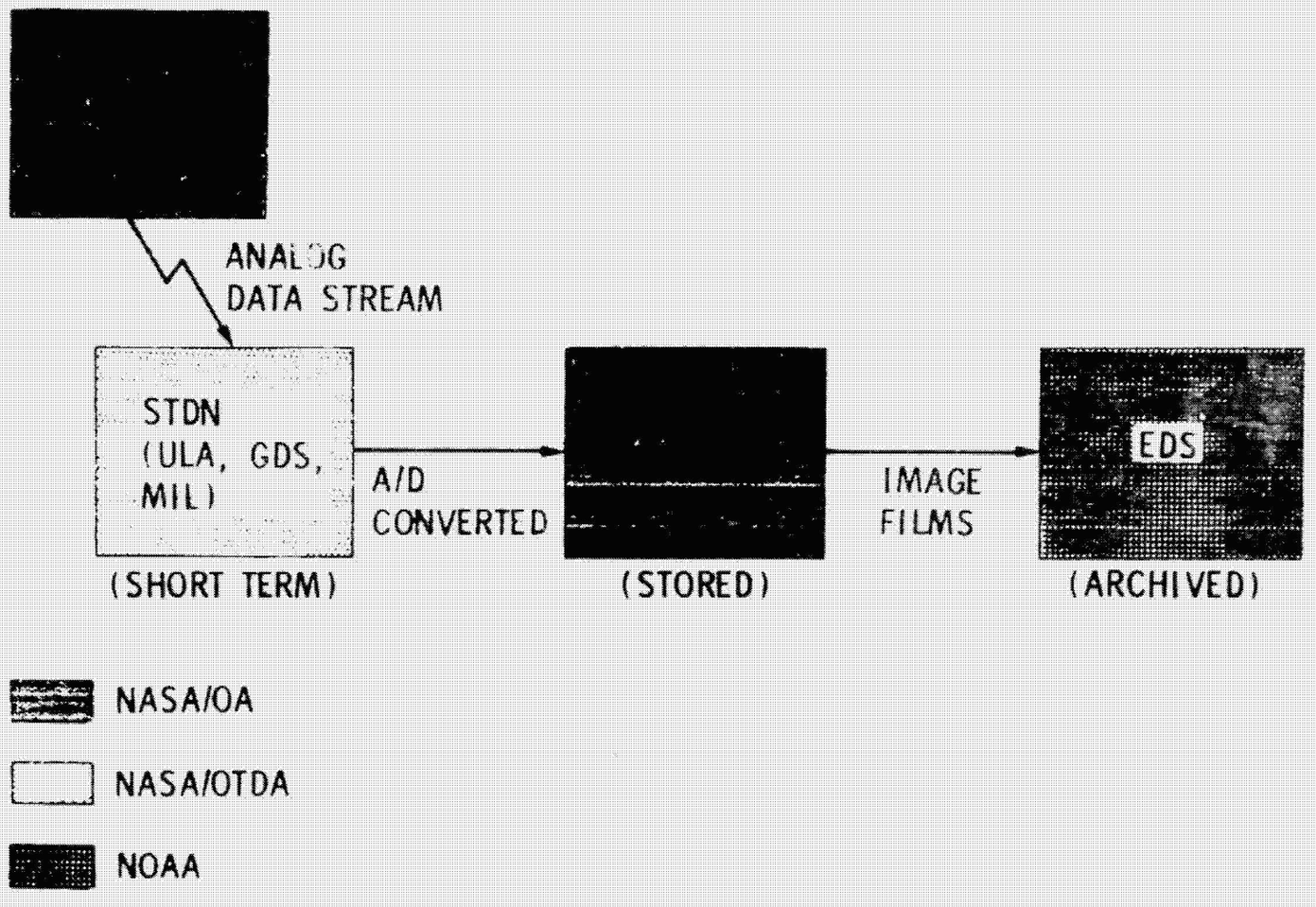

SEASAT-A
SAR DATA FLOW

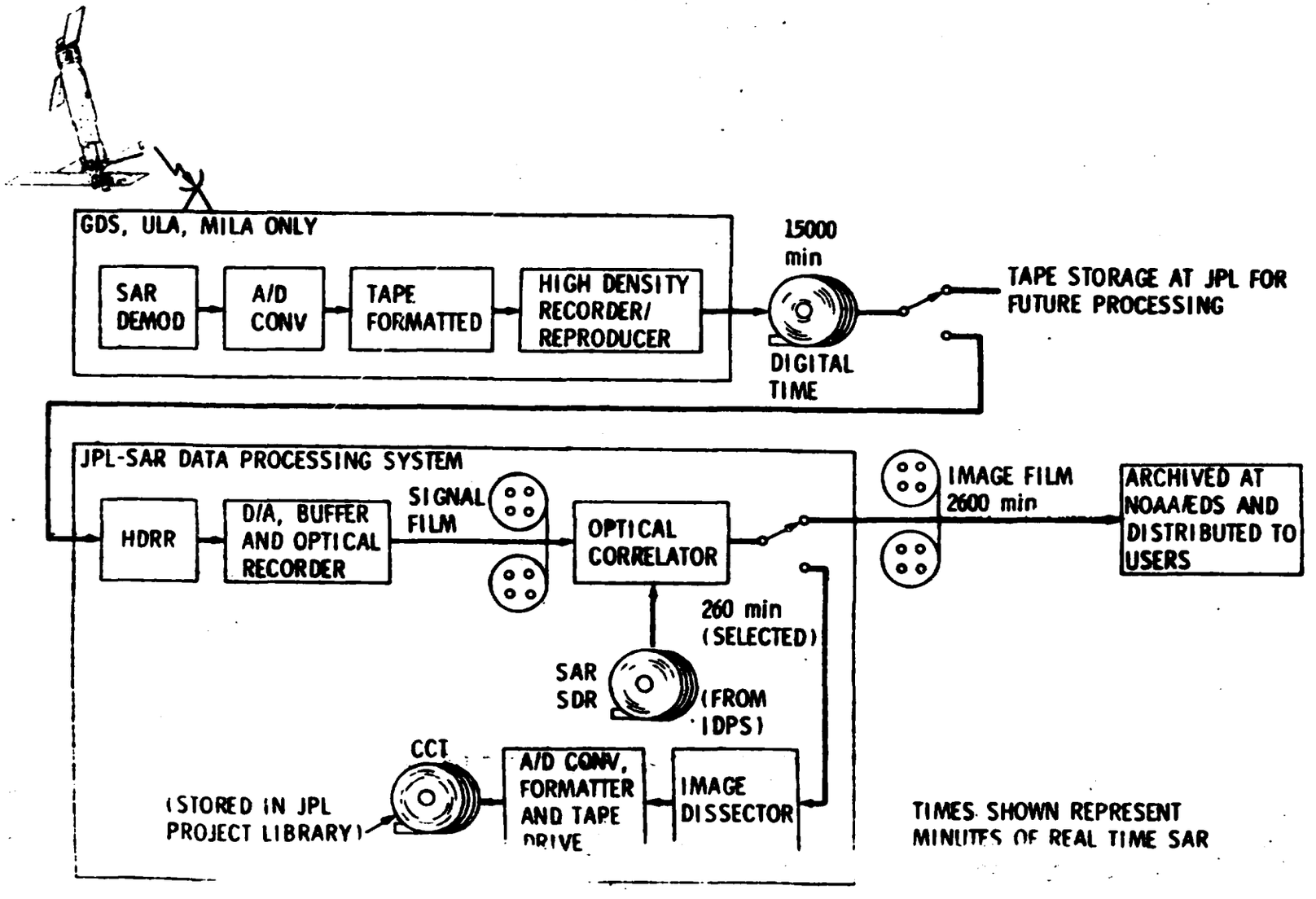

SEASAT-A
FNWC DATA FLOW

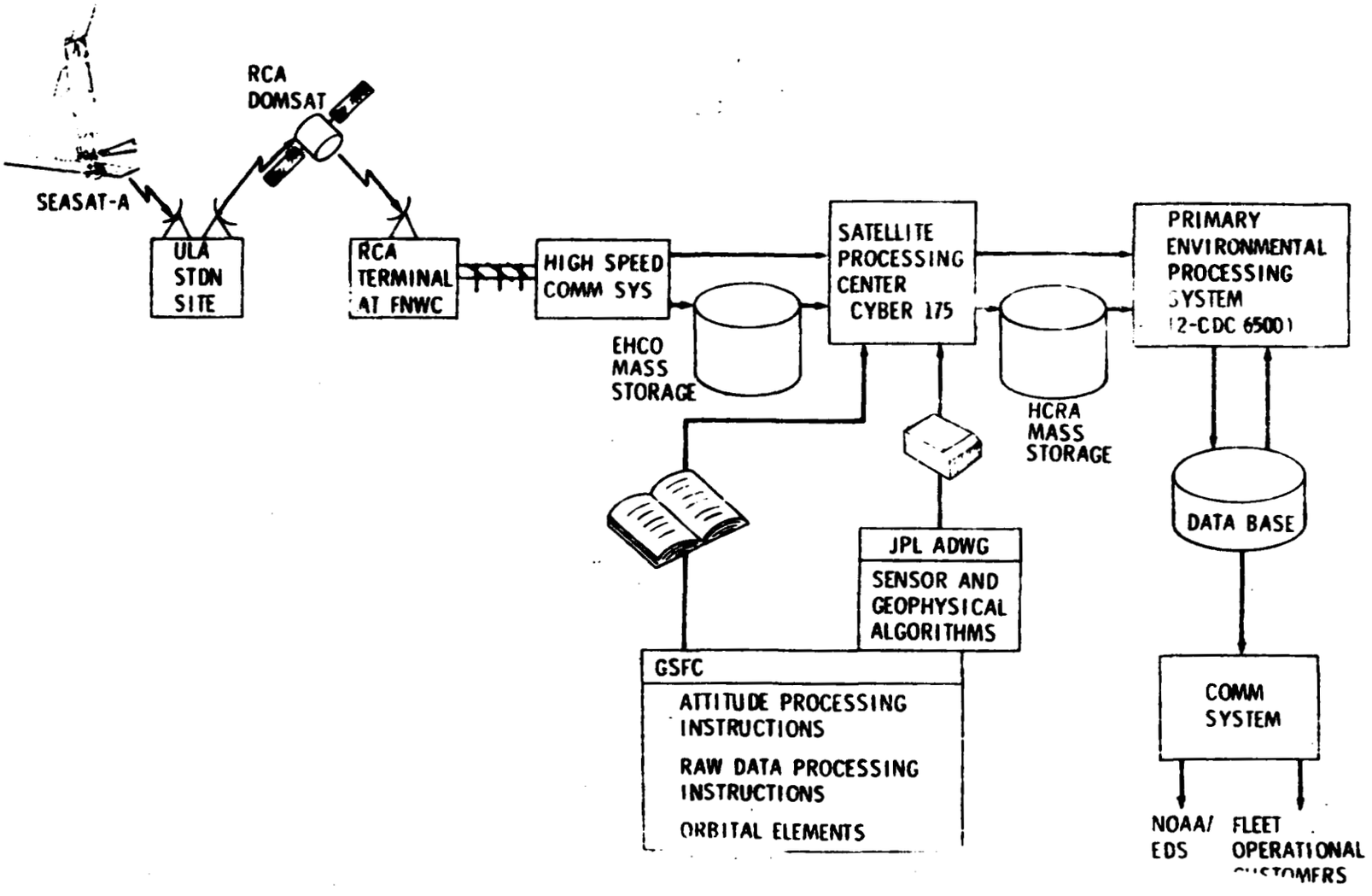

SEASAT-A

SEASAT-A EXPERIMENT DATA ACTIVITY

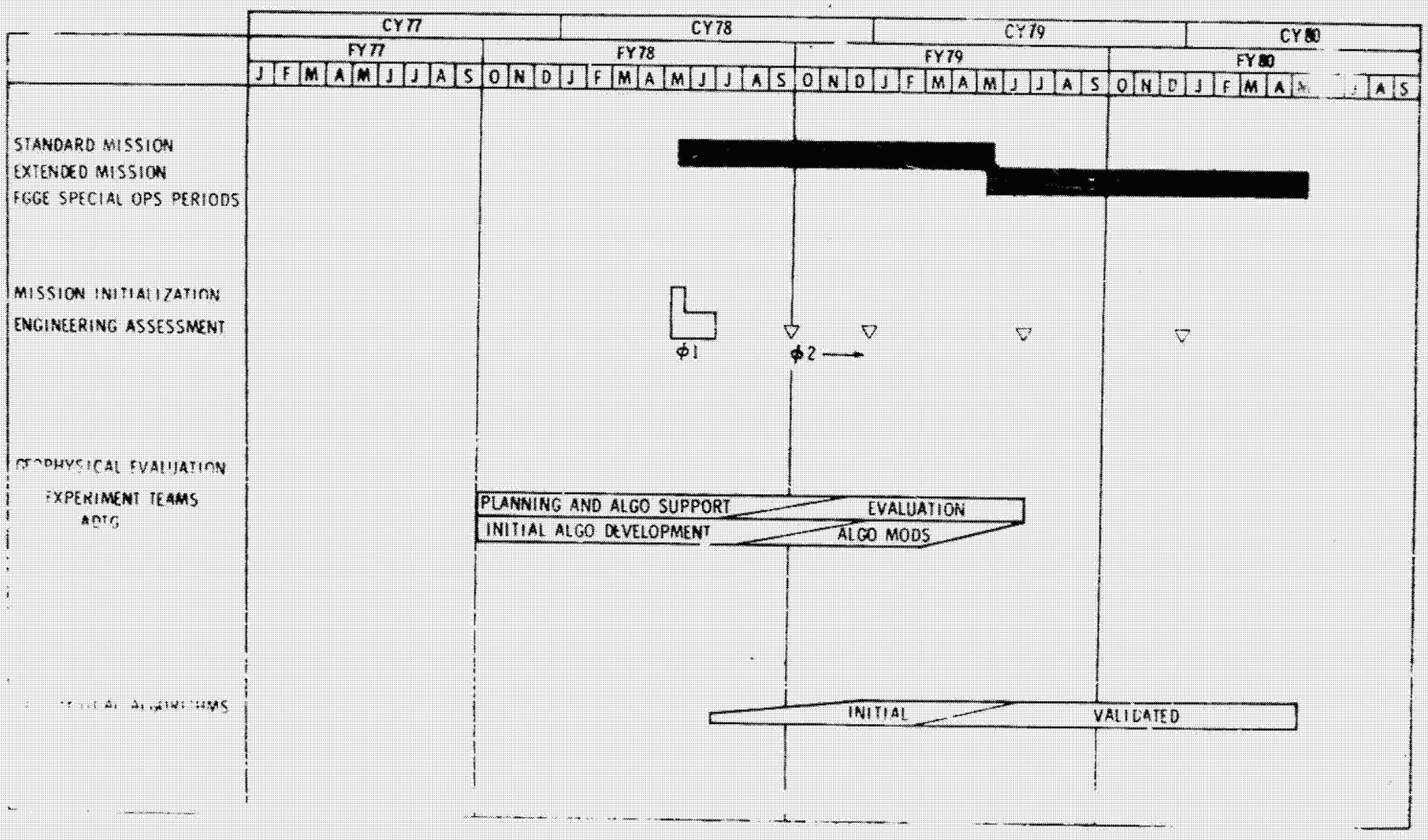

2. The presentation of [illegible] Nicholson of FNWC.

Methods of Display or Use of FNWC Data

Grid Data (Analyses or Forecasts)

Binary Form - a binary value at each grid point.

- Can generally only be used in a computer.
- Computer can use data for local calculations or can format for display as desired.
- The most compact and efficient form for data communications.

Alphanumeric Form -

- Same values as in binary form but converted to coded decimal values.
- Can be displayed directly on a printer or CRT device with the grid represented by columns and lines on the page.

Graphic Form -

- Contours (isopleths) are computed at FNWC from the grid values and formatted for a specific display device.
- Inefficient form for data communications.

SEASAT-A Geophysical Data and Spectral Ocean Wave Data.

- Primary form will be alphanumeric which can be printed as a tale of location, time value.
- A "graphic" form is possible which would allow a value to be displayed at its corresponding geographical location.

General Data Formats at FNWC

Analyses and Predictions (Hemispheric - North and South)

- Values are computed at points on a grid overlain on a Polar Sterographic map projection.
- The most common grid size is 63X63, which gives 31 grid intervals between the equator and pole. Actual distance between grid points varies with latitude but is 381 km at 60°N (or S).
- Some analyses are made at finer resolutions.
- For sea surface temperature analyses, "ZOOM" analyses are made for small areas, using a much finer grid which is a super set of the hemisphere grid.

Analyses (Tropical and mid latitudes)

- Values are computed on a latitude longitude grid of 5° or 2.5° spacing.
- Outside of the tropics values are usually the same as corresponding ones on hemisphere grids.
- Used primarily for wind analyses.
- Usually displayed on a mercator projection.

SEASAT-A Geophysical Data

- Data to be computed is listed on slide 6.
- Data will generally be in the form:

  Latitude, Longitude, Time, Value, Flags

Spectral Ocean Wave Model Data

- Computed at points over the Northern Hemisphere.
- Data can be "degraded" to provide $H_{1/3}$, principal direction and principal period on a Hemispheric grid (see above).
- Values will generally be provided at selected points.

INTRODUCTION

Fleet Numerical Weather Central, usually known as FNWC, is the Navy's primary center for global meteorological and oceanographic forecasting. We use computers to provide forecasts of basic parameters which meteorologists and oceanographers in the field can use to make more specific forecasts for localized operations. We also make direct forecasts of operationally important parameters for specific locations in cases where this is possible. For instance, we provide a global forecast of the sea level pressure pattern but we also provide acoustic propagation loss predictions for specific sensors at specific locations.

The first slide shows the physical configuration of FNWC. I would like to stress three points:

1. The great amount of computer power required to tackle the job we are undertaking;
2. The great amount of communications facilities available to gather all the source data required, and to disseminate the results; and
3. The large historical data base which has been built up.

Fleet Numerical Weather Central
The Navy's Ocean/Atmosphere Data Processing Center

- This is the data flow which processes satellite and conventional data at FNWC.
- Satellite data can be received on either of two domestic communications satellite antennae—RCA and American Satellite.
- The data is collected and written on disk storage.
- From there, it is processed into a geophysically useful form in the Cyber 175 computer and placed in a different set of disks. This processing is generally done as soon as possible after arrival of the data.
- Periodically this data is used as input to analysis and forecast models running in the CDC 6500 computers. These models are generally run 2 to 8 times per day at times based on the major collection of conventional data.
- Outputs from the models and some of the processed satellite data are provided to users on various communications facilities.

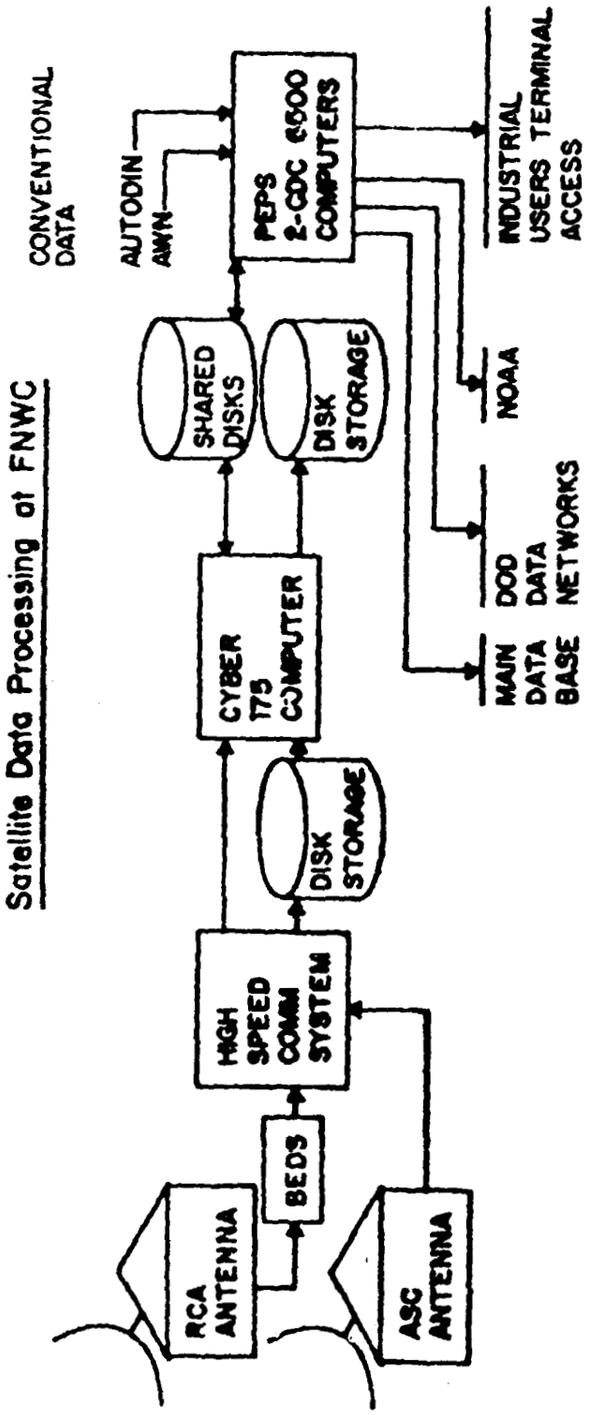

ORIGINAL PAGE IS
OF POOR QUALITY

- The Satellite Data Processing facility at FNWC was originally implemented for processing data from the Defense Meteorological Satellite Program (DMSP). It is expected to be in full operation within a few months.
- There are two general uses for DMSP data:
- First, a global high resolution visual and IR data base will be continuously updated as data arrives.
- Resolution of this data base will be roughly 1.5 NM and the data will be available for extraction of "windows" of virtual imagery to be sent to users in the field.
- An example of this type of use is providing windows to JTWC for the tracking of tropical cyclones over the Indian Ocean.
- The second type data is from the Vertical Temperature Profiling Radiometer on board DMSP. This instrument will provide extremely useful information on the 3-dimensional atmospheric structure--a basic requirement for FNWC models.

Defense Meteorological Satellite Program Processing at FNWC

Global IR and Visual Imagery Data Base
- Continously updated from 2 polar orbiting satellites
- Random area window extraction
- 1.5 NM resolution

Vertical Temperature Profiling Radiometer
- Atmospheric thermal data
- Up to 28,000 profiles per day

The Real-Time Data Demonstration for SEASAT-A is a joint DOD-NASA effort to demonstrate the usefulness of SEASAT data for operational purposes. Initially it was intended to provide data to this system only from the Alaskan readout site, but now it has been decided to bring into FNWC worldwide data from Madrid and Merritt Island also.

- Maximum delay from observation to receipt at FNWC is expected to be 6 hours for data collected at Alaska and 12 hours for the other stations. In practice, it is expected that delays will be about half of these times.

SEASAT-A
REAL TIME DATA PROCESSING DEMONSTRATION

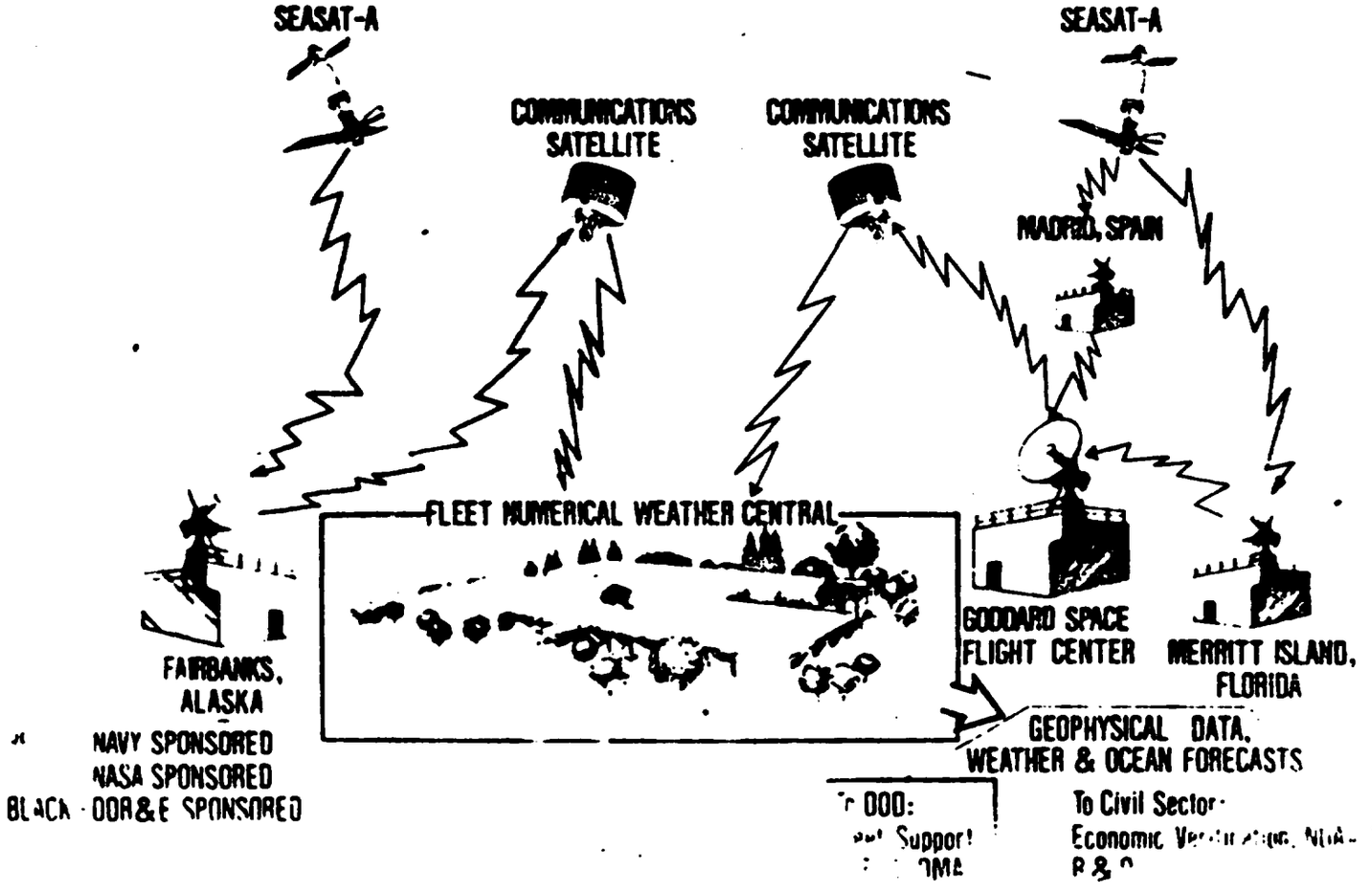

The processing cycle for SEASAT-A at FNWC will be as shown here:

- First, the data will be processed into Sensor Data Records, and then into "Geophysical Data Records." Both of these forms will be stored in temporary disk files for local use.
- The Geophysical Data Records will then be assimilated along with conventional data to provide an analysis of the 3-dimensional mass structure of the atmosphere.
- These analyses become the initial state for sophisticated prediction models.
- Selected data from each of the processing stages will be archived and distributed to users.

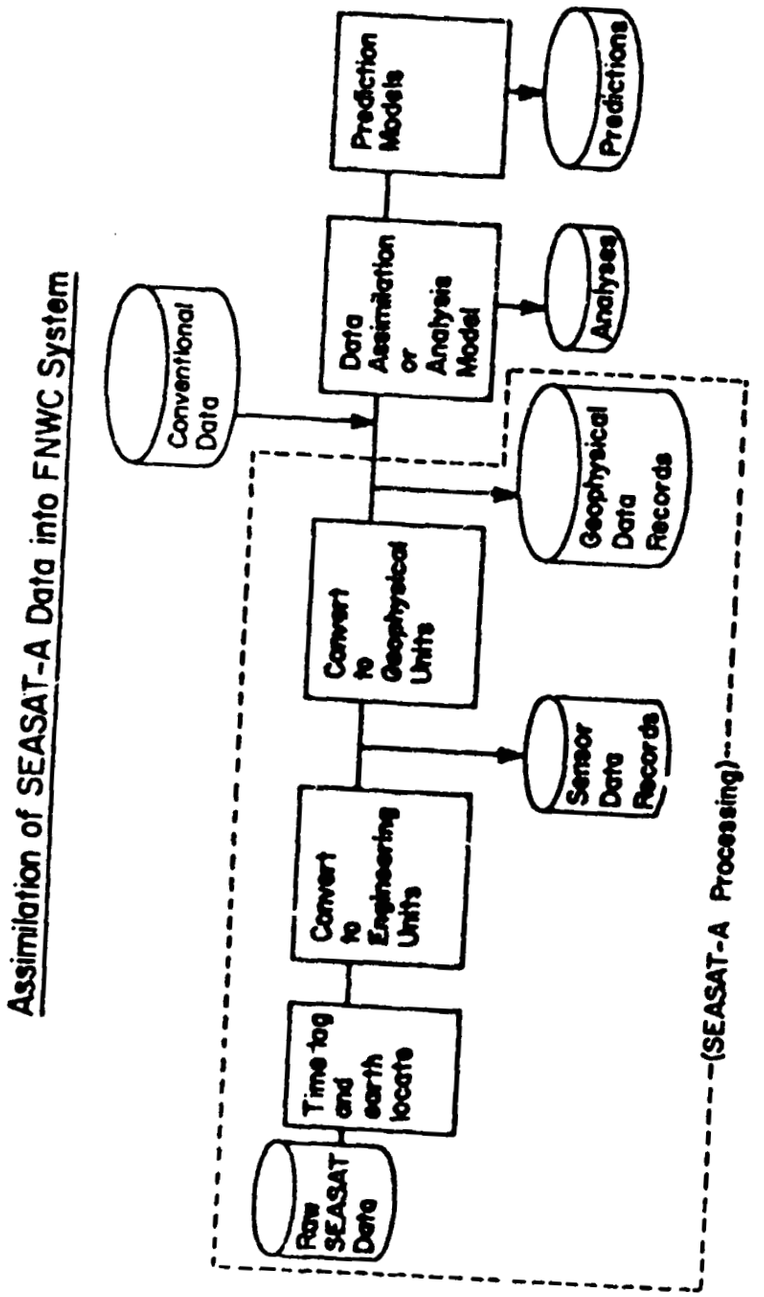

- The geophysical data records planned to be provided from SEASAT-A are as shown.
- Of greatest interest to FNWC initially are the vector winds expected to be available from the scatterometer. These are of primary importance since they offer a major improvement in specifying the initial state of the atmospheric mass structure, and consequently improving performance of prediction models.

GEOPHYSICAL DATA RECORDS TO BE PROCESSED AT FNWC

GEOPHYSICAL PARAMETER	INSTRUMENT
Vector wind (speed, direction)	Scaterometer (SASS)
Wind speed	Scanning Multi-frequency Microwave Radiometer (SMMR)
Sea Surface Temperature	SMMR
Significant Wave Height ($H_{1/3}$)	Altimeter

- I would now like to review and emphasize the importance of both conventional and satellite data to prediction cycle:
- First, combining SEASAT winds with conventional wind and pressure data from ships, buoys and land stations will yield a greatly improved analysis of the surface pressure pattern. I must emphasize that the SEASAT data and the conventional data are very complementary:
- We have good conventional coverage over land but very poor coverage over oceans. Over the ocean the relationship between winds and pressure are reasonably well understood, so we hope to be able to produce an excellent picture of the surface pressure pattern by combining both types of data.
- At FNWC the surface pressure analysis is used as a basis for building up a complete 3-dimensional atmospheric mass structure. Again, conventional data is used and also Vertical Temperature Profile data from DMSP and other satellites. The improvement gained from SEASAT wind data in specifying the surface pressure is thus expected to be felt throughout the entire atmospheric structure.
- Using complex models, and the initial mass structure, a prediction can be made of the mass structure at intervals out to 3 to 5 days. The improvement in specifying the initial state is expected to result in improvement of the predictions throughout the cycle.
- From the predicted mass structure, the operationally important meteorological and oceanographic parameters such as winds and sea conditions can be computed.

The FNWC Raw Data to Forecast Cycle

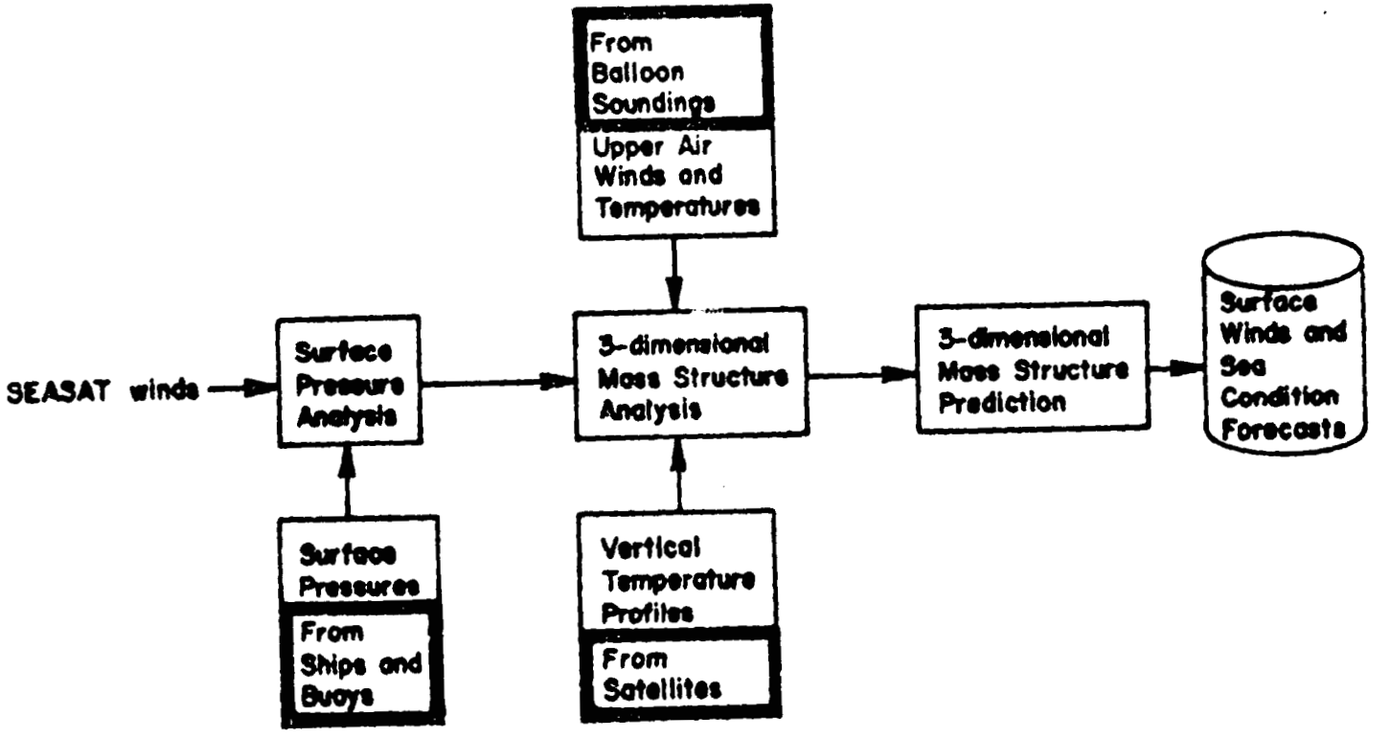

This table emphasizes the variety of observed data required for the atmospheric/ocean models, and the variety of sources, both satellite and conventional, required to obtain this data.

INPUT DATA REQUIRED FOR ATMOSPHERE-OCEAN MODEL

PARAMETER MEASURED	SOURCE
VERTICAL ATMOSPHERIC TEMPERATURE PROFILE	BALLOON OR ROCKET SOUNDING METEOROLOGICAL SATELLITES
UPPER ATMOSPHERE WINDS	BALLOON SOUNDINGS, AIRPLANES
ATMOSPHERIC PRESSURE AT SURFACE	SHIPS, BOUYS, LAND STATIONS
SEA SURFACE WINDS	SHIPS, BOUYS, SEASAT
SEA SURFACE TEMPERATURE	SHIPS, BOUYS, SEASAT
VERTICAL OCEAN TEMPERATURE PROFILE	BATHYTHERMOGRAPHS

I would like to briefly discuss one of the difficulties which will be encountered in utilizing a combination of conventional and satellite data. This relates to data assimilation.

- Conventional data is based on the "synoptic" concept, where everyone takes simultaneous observations at set times. This lends itself well to providing initial state data for prediction models.
- Satellite data is observed continuously and thus is "asynoptic."
- The simplest way of resolving this problem is just to "relable" the satellite data to the nearest synoptic time. This slide attempts to illustrate this process. It is the technique expected to be used initially with SEASAT-A data at FNWC.

REDUCTION OF SATELLITE DATA TO SYNOPTIC TIME

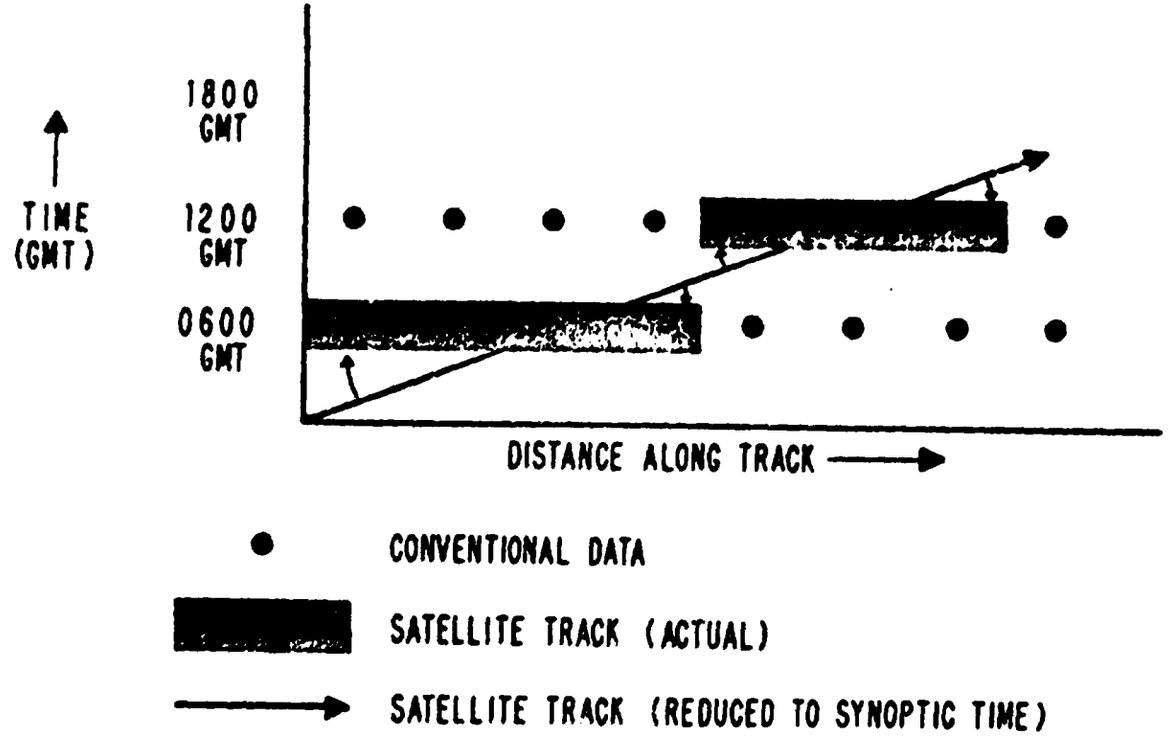

This slide illustrates the conventional way of introducing data into the prediction cycle.

- Starting at zero hundred Greenwich time on the second, a prediction from a previous run is used as a "first guess" and then all data is introduced at a single "synoptic" time and the prediction run is started.
- Twelve hours later, the 12-hour forecast from this run will be used as the first guess for the next cycle.
- These computer runs are now made about 3 to 5 hours after the conventional data is observed.

THE CONVENTIONAL PREDICTION-ANALYSIS CYCLE

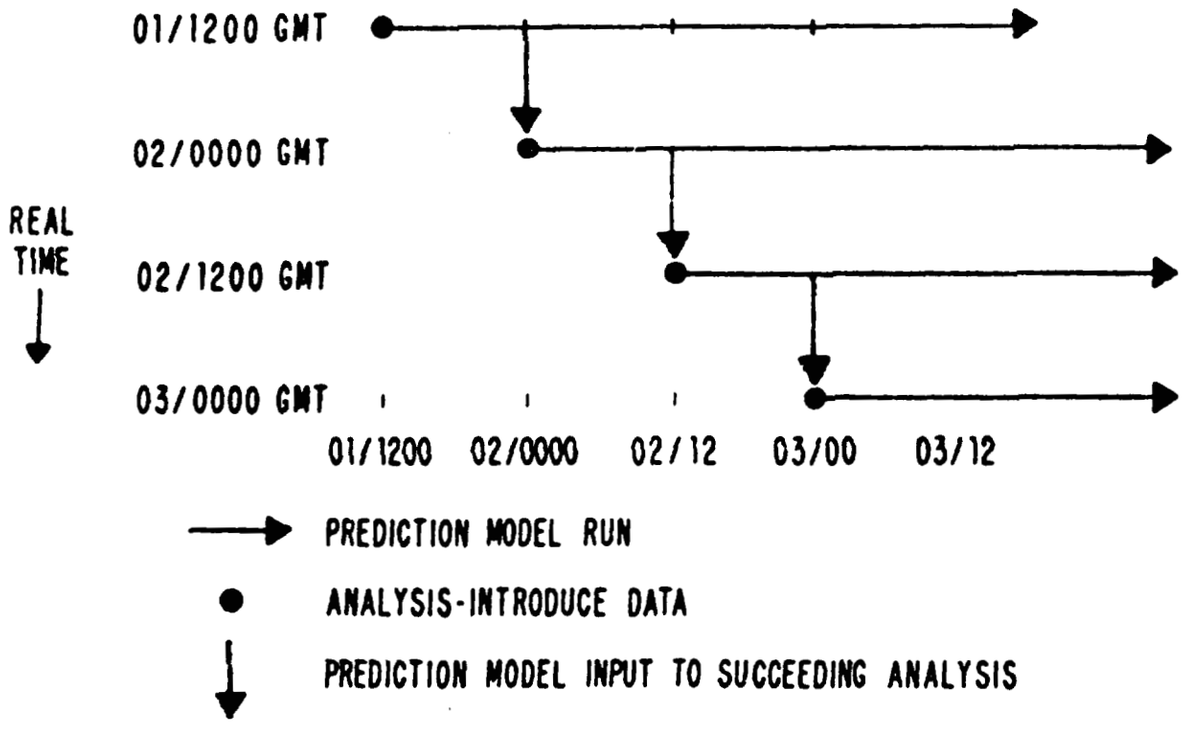

For improved usage of satellite data, a Four Dimensional Data Assimilation Model must be used.

- This model will assimilate data as it integrates forward in time, introducing the data at the point appropriate to its actual observation time and then continuing on through the assimilation and prediction cycle.

This is not as simple as it sounds—a piece of data will rarely exactly fit the model. This causes "model shock" which propagates noise through the model. Considerable research is being done on this problem right now. It is hoped that by late in the SEASAT-A mission we will be able to use this technique operationally.

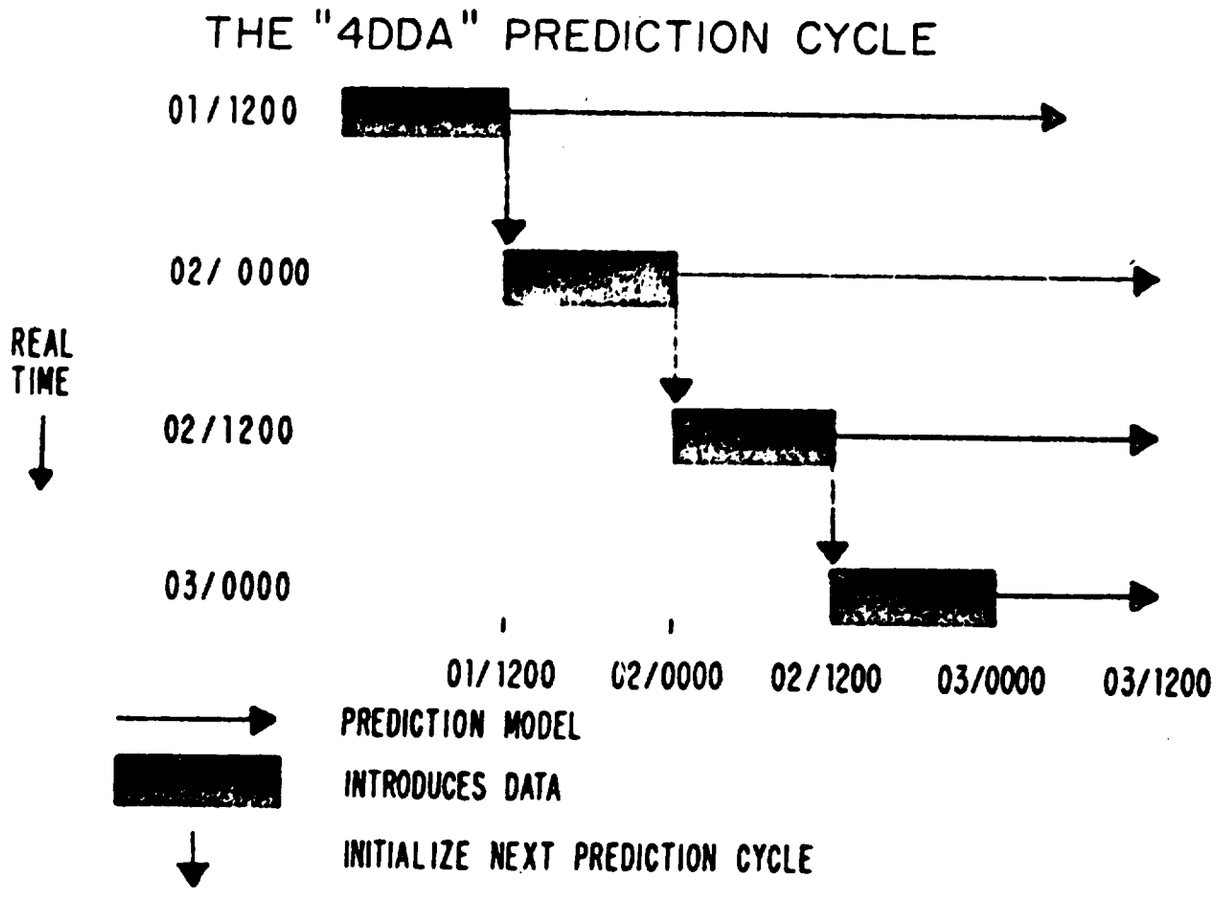

Now a little philosophy:

The operator needs PLATFORM BEHAVIOR information, with maybe supplemental information on equipment performance such as sonar or radar performance.

- Not only that, he doesn't need to be told what is happening now—he can hear, see and feel that.
- He needs information to use as the basis for planning.
- In the purest sense, to plan his operation—set a course or plan for on-deck operations—he needs to know the forces which are going to work on his ship or rig. These forces are reflected in the wave energy spectrum and wind conditions.

WHAT THE AT SEA OPERATOR NEEDS

PLATFORM BEHAVIOR

Platform behavior depends on:

- **Characteristics of platform**
- **Wave energy spectra (direction, frequency)**

This slide speaks for itself.

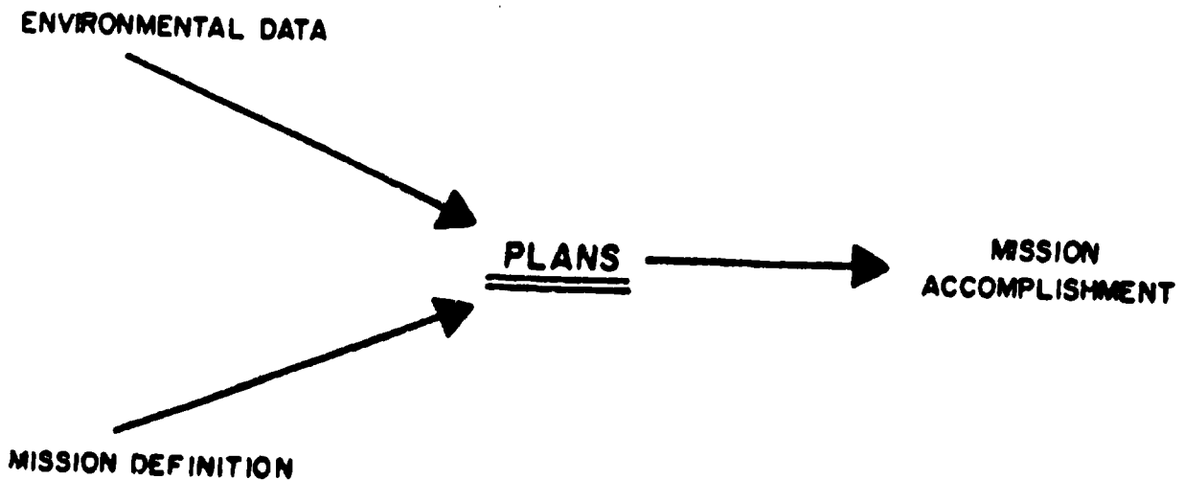
ENVIRONMENTAL DATA
PLANS
MISSION ACCOMPLISHMENT
MISSION DEFINITION

As does this one—please note the word predictions as opposed to observations. But this is not to downgrade observations, because:

PLANNING

REQUIRES

PREDICTIONS

and the point here is that the observations needed may be thousands of miles away from the operator's location. Yesterday's weather off Japan will influence tomorrow's operations in the Gulf of Alaska.

PREDICTIONS REQUIRE OBSERVATIONS

- FROM VARIOUS PLACES
- FROM VARIOUS TIMES

Now let's look at the nature of the "predictions" needed to support a wide range of missions.

- This table first shows a range of mission applications,
- then a rough description of the required validity period;
- then the scope of data required to obtain such validity
- and finally, the type of prediction model suited.

CHARACTERISTICS OF PREDICTIONS IN SUPPORT OF TYPICAL MISSIONS

MISSION SUPPORTED	REQUIRED PERIOD OF PREDICTION VALIDITY	SCOPE OF INPUT DATA		MODEL TYPE
		TIME	AREA	
AIRPLANE FLIGHT PLANNING	MINUTES	IMMEDIATE	LOCAL	EXTRAPOLATION
FAST SHIP ROUTING	HOURS	HOURS	WIDE	PHYSICAL MODEL
TUG WITH TOW ROUTING	DAYS	HOURS	WIDE	PHYSICAL MODEL
VOYAGE PLANNING	WEEKS	WEEKS	WIDE	PHYSICAL STATISTICAL
INSTALLATION PLANNING	YEARS	HISTORICAL	LOCAL	STATISTICAL

As an illustration, two cases:

First the airplane -

The airplane moves fast relative to storms. Hence, in many cases an observation can be used as a prediction. But it <u>is</u> really a prediction, the prediction of no change.

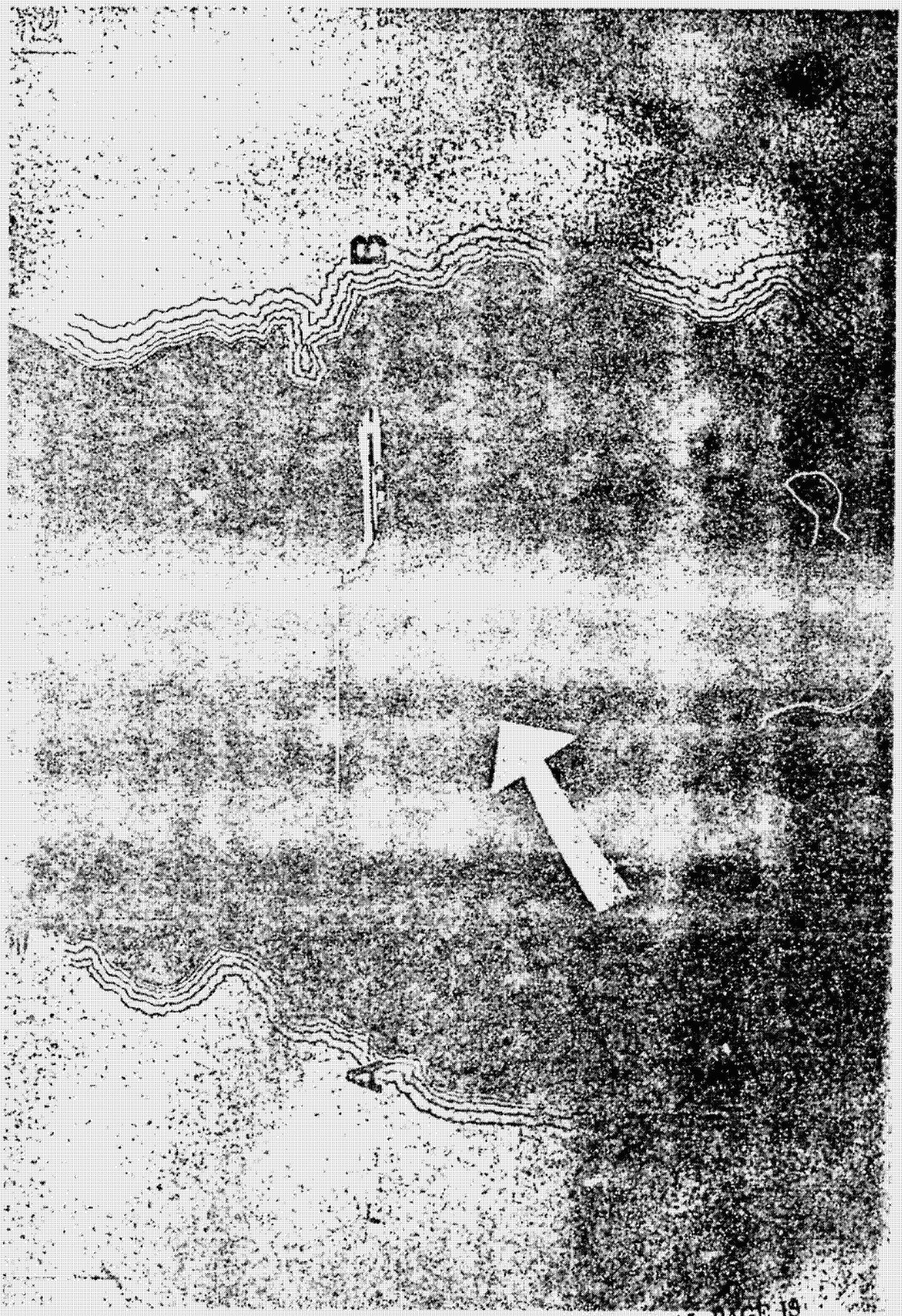

Now, the other extreme—the bain of the ship routers—the tug and tow which can make only a few knots. If he is to avoid disaster, he needs to begin moving out of the path of a storm before the storm has even formed.

- Where does all this lead us?

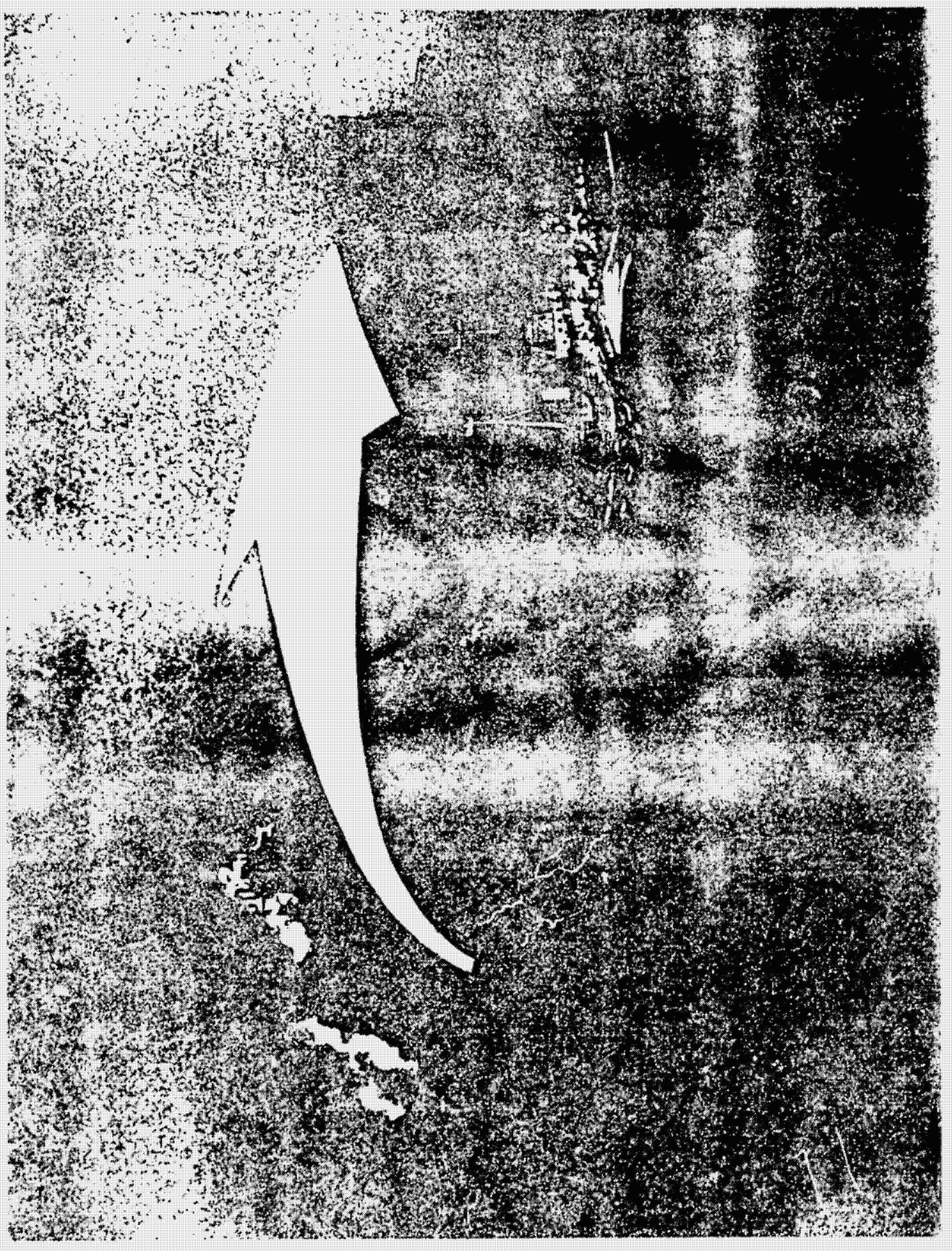

It leads us to a system such as the one installed at FNWC--one which can:

- receive both conventional and satellite observational data for the entire globe.
- integrate all these observations and turn them into predictions rapidly.
- communicate the predictions to the operational user rapidly in a form which relates to his mission.

This requires a ground system with powerful computers and powerful communications.

Fleet Numerical Weather Central
The Navy's Ocean/Atmosphere Data Processing Center

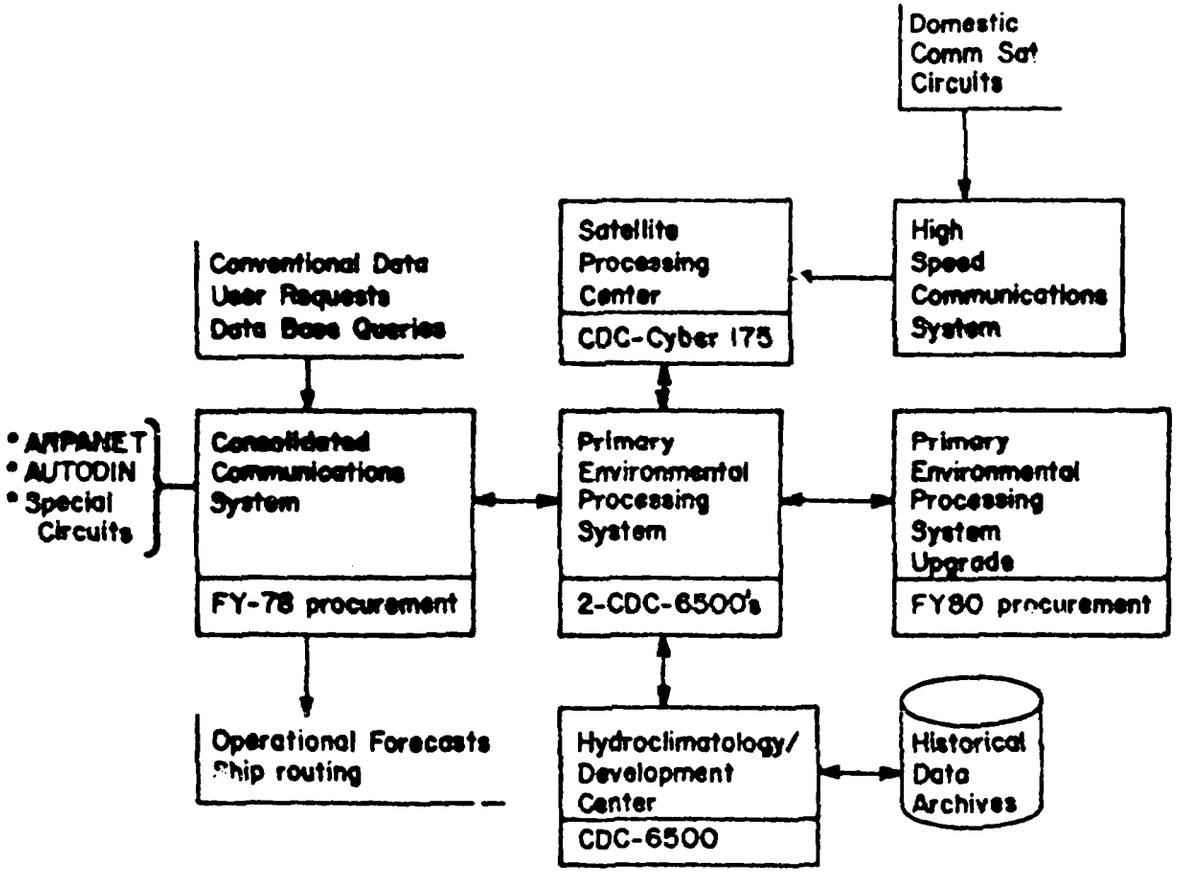

As an example of the complexity of the processing problem, let's look at the need for predicting the sea conditions for tomorrow:

The primary model for this purpose is the Spectral Wave Model. I would like to point out that, at this time, we don't know how to use observations of wave conditions as inputs to such a model. We do need as inputs:

- sea and air temperature observations and predictions to compute stability factors.
- surface wind and pressure observations and the whole atmospheric mass structure.
- a sophisticated model to predict atmospheric mass structure and thus surface winds.

Then we can compute the predicted sea conditions extremely accurately.

C-2

SPECTRAL OCEAN WAVE MODEL

- Predicts energy densities for wave components
- 12 directions
- 15 frequency components
- Generates waves from winds
- Propagates wave components

My final point concerns specifically the distribution of real-time SEASAT-A data. It is now expected that NASA will provide a Satellite Data Distribution System at FNWC which will be operated by the Navy.

Planned FNWC Satellite Data Distribution System

3. The presentation of Mr. David Nippert of BCL.

SEASAT-A

REAL-TIME USER

DATA DISTRIBUTION

SYSTEM

Battelle
Columbus Laboratories

FUNCTIONAL ELEMENTS OF THE SEASAT-A REAL TIME USER DATA DEMONSTRATION SYSTEM

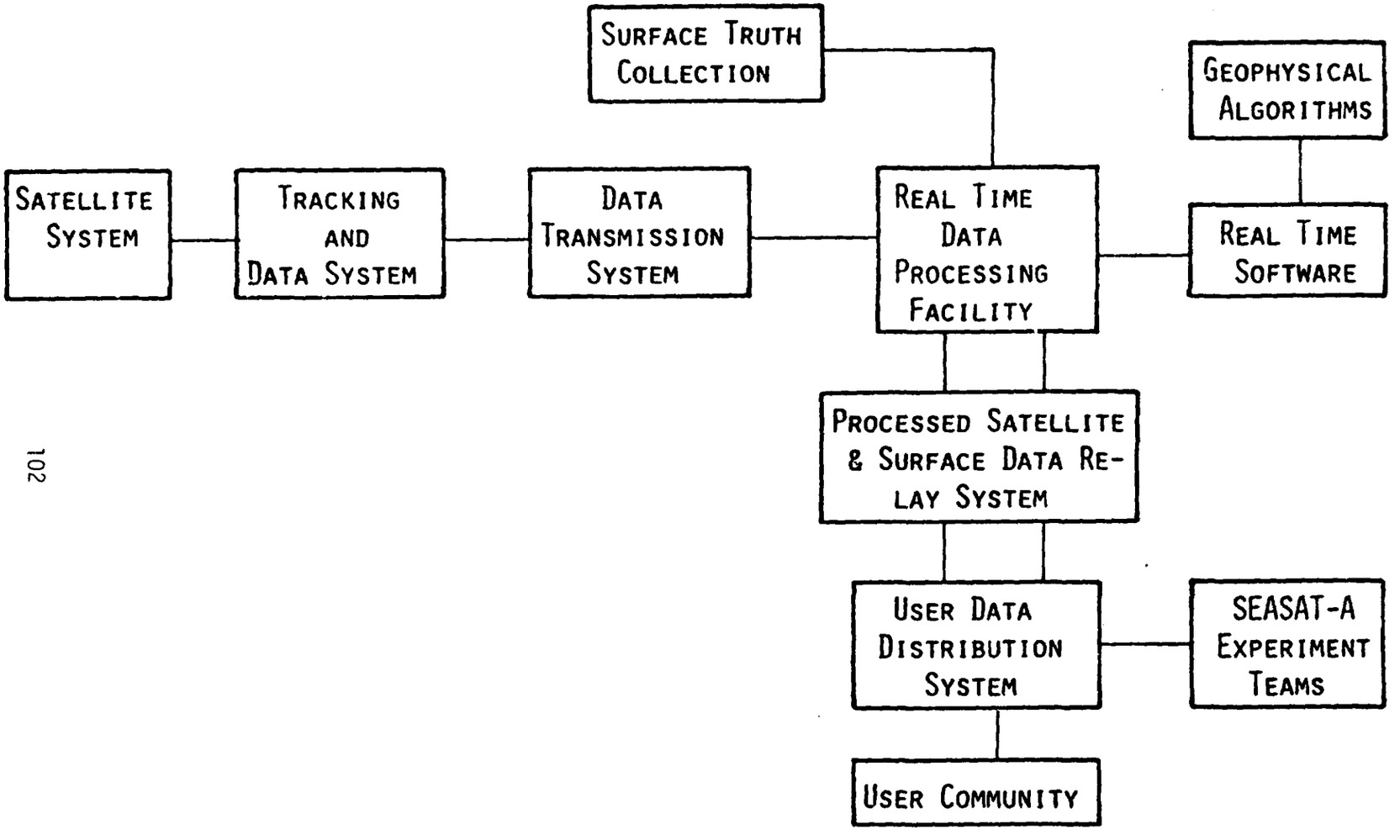

DATA PRODUCTS

SEASAT OBSERVATIONS

- Winds (Scatterometer and Microwave Radiometer)
- Wave Heights (H 1/3) (Altimeter)
- Sea Surface Temperature

FNWC ANALYSES AND FORECASTS

- Marine Winds
- Wave Heights (H 1/3)
- Primary Wave Direction
- Primary Wave Period
- Sea Level Pressure
- Sea Surface Temperatures
- Spectral Wave Data

DATA FORMATS

GRAPHICS

CHARTS WITH CONTOURS OR ISOPLETHS FOR SPECIFIC GEOGRAPHICAL REGIONS

TABLES

LISTS OF DATA VALUES FOR SPECIFIC LOCATIONS (LATITUDES AND LONGITUDES) AND TIME

BINARY DATA

A FORM FOR COMPUTER-TO-COMPUTER TRANSMISSION OF DATA PRODUCTS

MAGNETIC TAPE

ARCHIVED DATA FOR USE IN NON REAL-TIME ANALYSES

ORIGINAL PAGE IS
OF POOR QUALITY
WHAT NEXT (REPLOT/OR STOP)

DATA PRODUCTS/DATA FORMATS

	GRAPHICS	TABLES	BINARY	MAG TAPE
SEASAT OBSERVATIONS				
Winds		X	X	X
Wave Heights		X	X	X
Sea Surface Temperature		X	X	X
FNWC ANALYSES & FORECASTS				
Marine Winds	X		X	
Wave Heights	X		X	
Primary Wave Direction	X		X	
Primary Wave Period	X		X	
Sea Level Pressure	X		X	
Sea Surface Temperatures	X		X	
Spectral Wave Data		X	X	

REQUIRED USER TERMINALS

GRAPHICS

Terminals

Tektronix Storage Tube Terminals

4006, 4010, 4012, 4013, 4014, 4015 and 4051

or Any Plotter which can be driven with Tektronix graphic codes

Hardcopy Devices

Tektronix

or Electrostatic Plotters

TABLES

Any terminal, CRT or Hardcopy, which can operate at 110-300 baud

BINARY

A computer

USER COMMUNICATION EQUIPMENT

TELEPHONE

- STANDARD PHONE
- DATA ACCESS ARRANGEMENT
- DATA PHONE

MODEM

- 110-300 BAUD - ACCOUSTIC COUPLER - MANY BRANDS
- 1200 BAUD (FOR GRAPHICS) VADIC
- 2000 - 4800 (FOR BINARY) BELL

TYPICAL USER EQUIPMENT SCHEMATIC

COMMUNICATIONS ACCESS
TO
REAL-TIME DATA DISTRIBUTION FACILITY

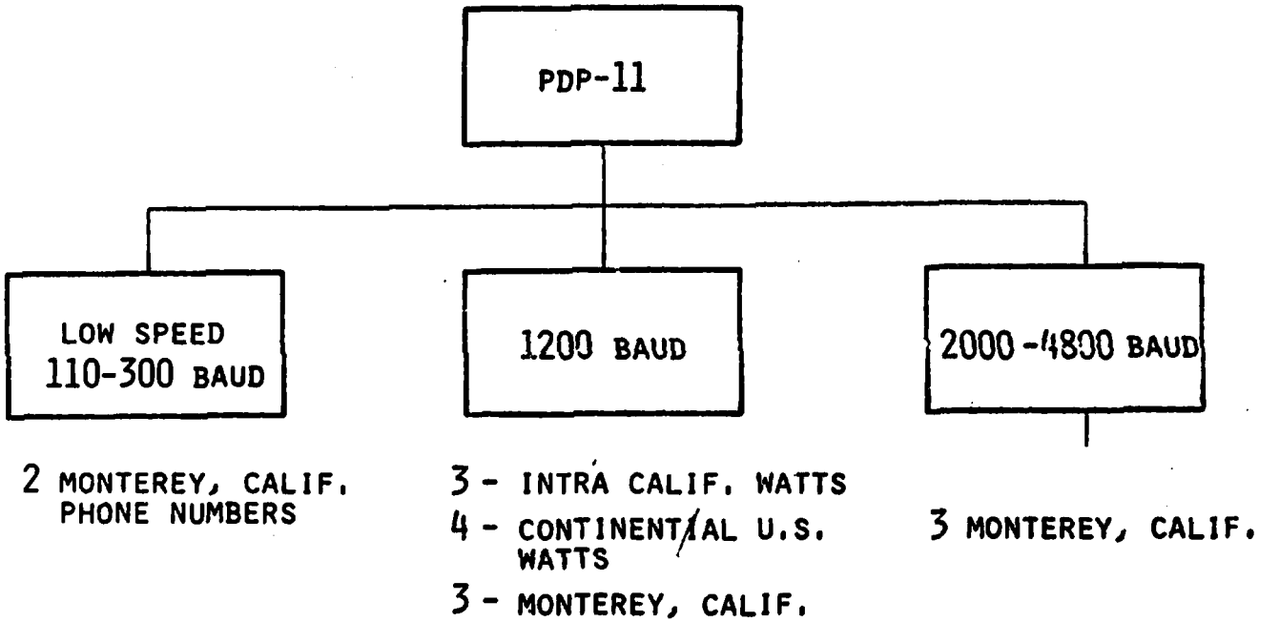

DATA VOLUME
AND
TRANSMISSION TIMES

SEASAT OBSERVATIONS

WINDS (SCATTEROMETER) 100 KM SPACING
30 CELLS/SWATH 1 SWATH EVERY 3.8 SECONDS
24 UP TO 4 VECTORS (MAGNITUDE & DIRECTION)
6 MAGNITUDE ONLY

WINDS (MICROWAVE RADIOMETER)
5 CELLS/SWATH 1 SWATH EVERY 4 SECONDS

SEA SURFACE TEMPERATURE
5 CELLS/SWATH 1 SWATH EVERY 4 SECONDS

WAVE HEIGHT
1 MEASUREMENT EVERY 1 OR 2 SECONDS

EACH MEASUREMENT WILL BE IDENTIFIED
LATITUDE
LONGITUDE
TIME

THERE WILL ALSO BE A "QUALITY" FLAG
INDICATING LIKELIHOOD OF ICE OR LAND

DATA VOLUME
AND
TRANSMISSION TIMES

SEASAT OBSERVATIONS (CONT.)

CHARTS

AN "AVERAGE" TABLE IS 2000 CHARACTERS
- 12 SECONDS @ 1200 BAUD
- 48 SECONDS @ 300 BAUD

BINARY DATA

ONE DAY'S TOTAL OBSERVATIONS IS 97×10^6 BITS - 337 MINUTES @ 4800 BAUD

FNWC CHARTS & FIELDS

CHARTS

10,000 CHARACTERS/CHART X 25 CHARTS/SESSION = 250,000 CHARACTERS/SESSION

250,000 CHARACTERS/SESSION X 2 SESSIONS/DAY = 500,000 CHARACTERS/DAY/USER

10,000 CHARACTERS/CHART ÷ 120 CHARACTERS/SEC (1200 BAUD = 83 SEC/CHART

83 SEC/CHART + 30 SEC (COPY TIME) + 10 SEC = 120 SEC/CHART

2 MIN/CHART X 25/CHARTS/SESSION = 50 MIN/SESSION/USER

BINARY DATA

GLOBAL BAND - 6 PARAMETERS/6 PERIODS	7.26×10^6 BITS
POLAR STEROGRAPHIC - 2 PARAMETERS/6 PERIODS	1.37×10^6 BITS
WAVE SPECTRAL DATA - 14 POINTS	$.06 \times 10^6$ BITS

9×10^6/12 HOURS $\approx$ 30 MINUTES @ 4800 BAUD

FNWC PRODUCTS TIMING

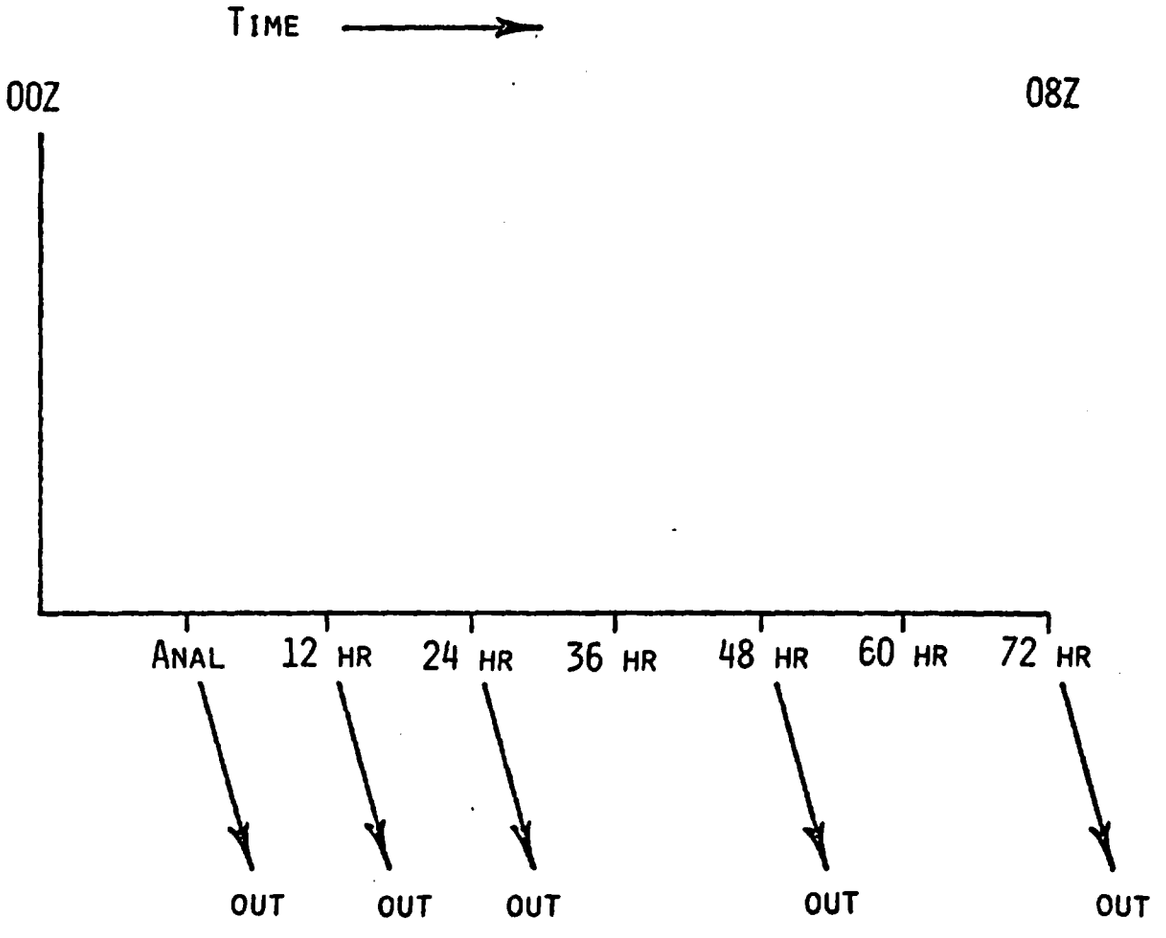

INDUSTRY USERS ACCESS SCHEDULE

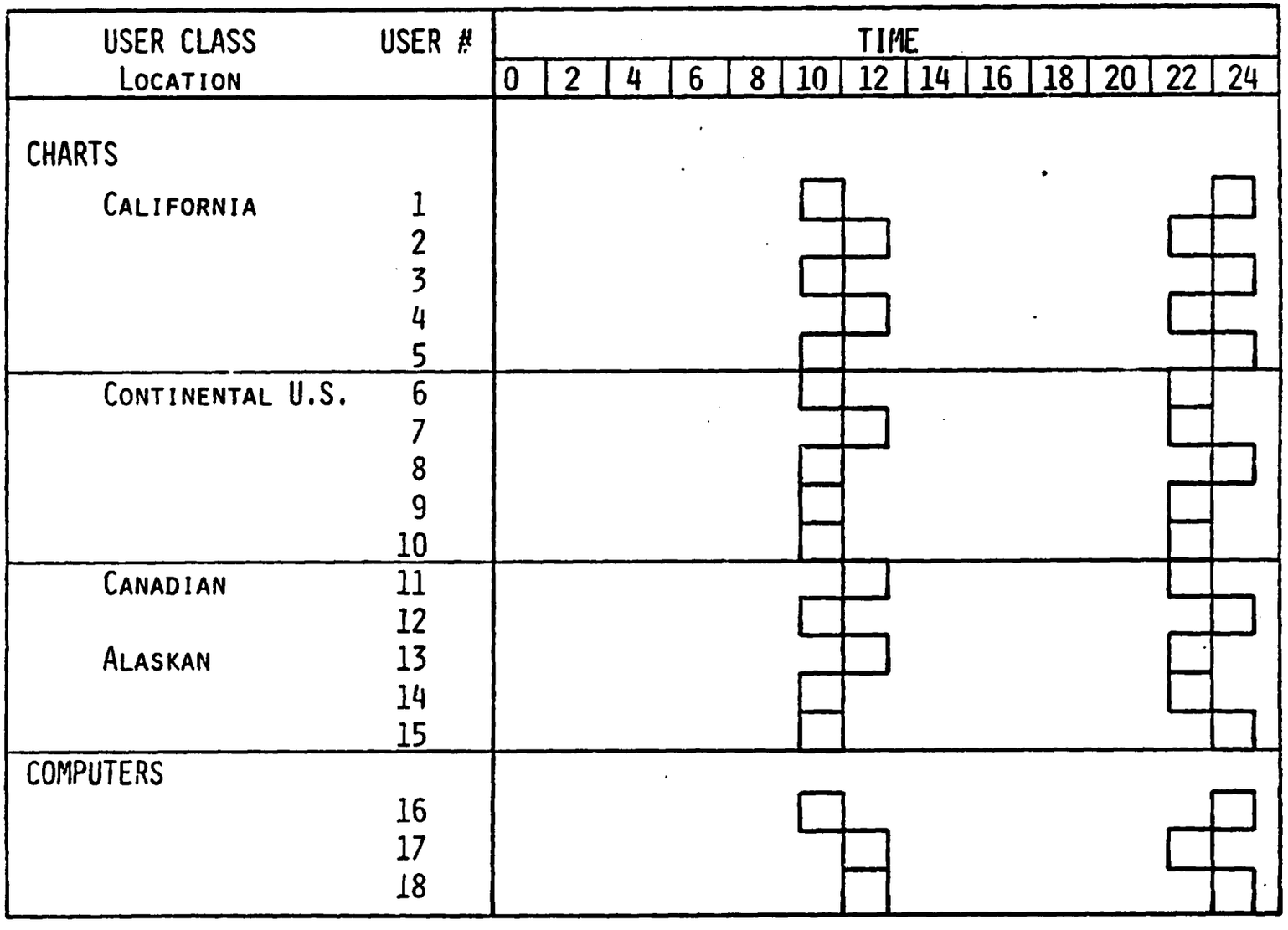

CANADIAN EXPERIMENTS

Canada, through the Canada Centre for Remote Sensing in Ottawa, has had an interest in the SEASAT-A program almost from its inception, since the goals of the SEASAT-A program parallel to a great extent those of the Canadian Government. Until this year no agreement between the governments of the United States and Canada existed to allow Canada's formal participation in the program.

This presentation on Canada's activities was provided by Mr. Donald J. Clough who is both a professor of engineering at the University of Waterloo, Ontario, Canada and a consultant to the Canada Centre for Remote Sensing.

PROPOSED CANADIAN PARTICIPATION

(CANADIAN CENTER FOR REMOTE SENSING)

PROPOSED CANADIAN PARTICIPATION IN SEASAT-A PROGRAM

- CANADA'S OCEAN MANAGEMENT AND REGULATORY RESPONSIBILITIES HAVE RECENTLY INCREASED AS A RESULT OF THE NEW 200-MILE FISHERIES LIMITS AND CONTINENTAL SHELF OIL AND GAS ACTIVITIES. (SEE PLATE 1)

- CONSEQUENTLY CANADA'S OCEAN SURVEILLANCE AND ENVIRONMENTAL MONITORING REQUIREMENTS HAVE INCREASED. AN INTERDEPARTMENTAL TASK FORCE HAS RECENTLY REPORTED TO THE GOVERNMENT OF CANADA ON A POSSIBLE SATELLITE SURVEILLANCE PROGRAM FOR CANADA. (SEE PLATE 2)

- THE CANADIAN GOVERNMENT APPROVED SEASAT-A PARTICIPATION AND A RELATED R AND D PROGRAM. CANADA HAS REQUESTED THAT AN AGREEMENT BE ENTERED INTO BETWEEN CANADA AND THE U.S.A. ON PARTICIPATION IN THE SEASAT-A EXPERIMENT.

- THE CANADIAN CONTRIBUTION TO THE OVERALL SEASAT-A SYSTEM WILL INCLUDE DATA RECEPTION FACILITY AT SHOE COVE, NEWFOUNDLAND, MODIFICATION OF AN EXISTING OPTICAL PROCESSOR AND DEVELOPMENT OF NEW DIGITAL PROCESSOR FOR SAR DATA/IMAGE PRODUCTION, AIRBORNE RADAR APPLICATION STUDIES AND SURFACE TRUTH SUPPORT FOR SEASAT-A, IONOSPHERIC AND SEA CLUTTER STUDIES. FEASIBILITY STUDIES HAVE BEEN CARRIED OUT OVER THE PAST TWO YEARS. (SEE PLATE 3)

- THE CANADIAN CONTRIBUTION TO THE PROPOSED SEASAT-A VERIFICATION AND APPLICATIONS EXPERIMENTS WILL INVOLVE AN INTEGRATED APPROACH IN WHICH THE DATA REQUIREMENTS OF SCIENTIFIC AND INDUSTRY USERS WILL BE ADDRESSED SIMULTANEOUSLY. COOPERATION WILL BE SOUGHT BETWEEN U.S. AND CANADIAN GROUPS INVOLVED IN BOTH SCIENTIFIC AND INDUSTRY EXPERIMENTS. (SEE PLATE 4)

THE CURRENT PLAN IS BASED ON AN APPROVED THREE-YEAR PROGRAM FUNDING LEVEL OF $8.2 MILLION, SPREAD OVER FY77-78, FY78-79, FY79-80. (SEE PLATE 5)

A PROGRAM MANAGEMENT STRUCTURE FOR THE INTERDEPARTMENTAL SURVEILLANCE SATELLITE PROGRAM IS NOW FUNCTIONING. CANADA'S PARTICIPATION IN THE SEASAT-A PROGRAM WILL BE MANAGED WITHIN THIS STRUCTURE. (SEE PLATE 6)

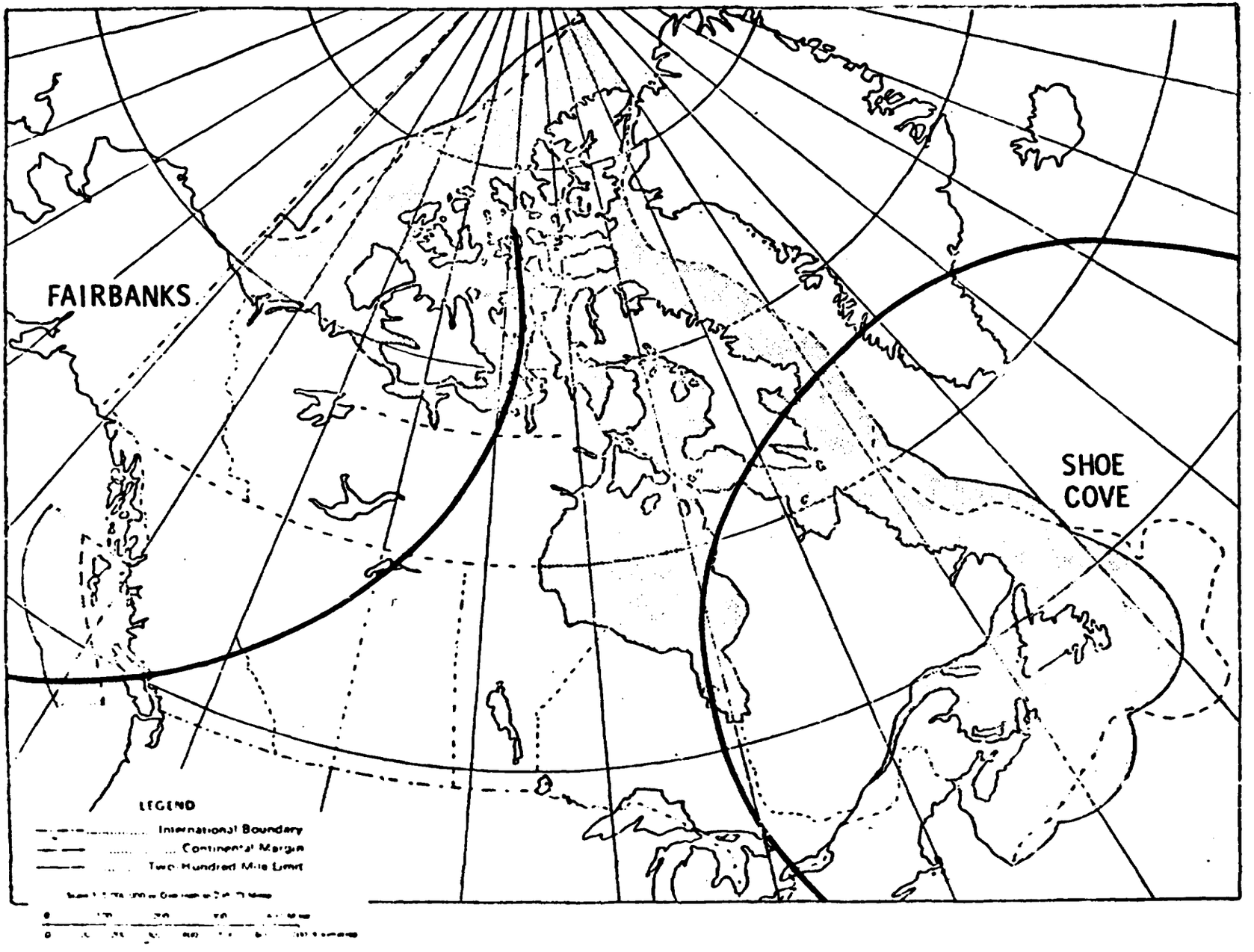
FAIRBANKS
SHOE COVE
LEGEND
International Boundary
Continental Margin
Two Hundred Mile Limit

A POSSIBLE SURVEILLANCE PROGRAM FOR CANADA

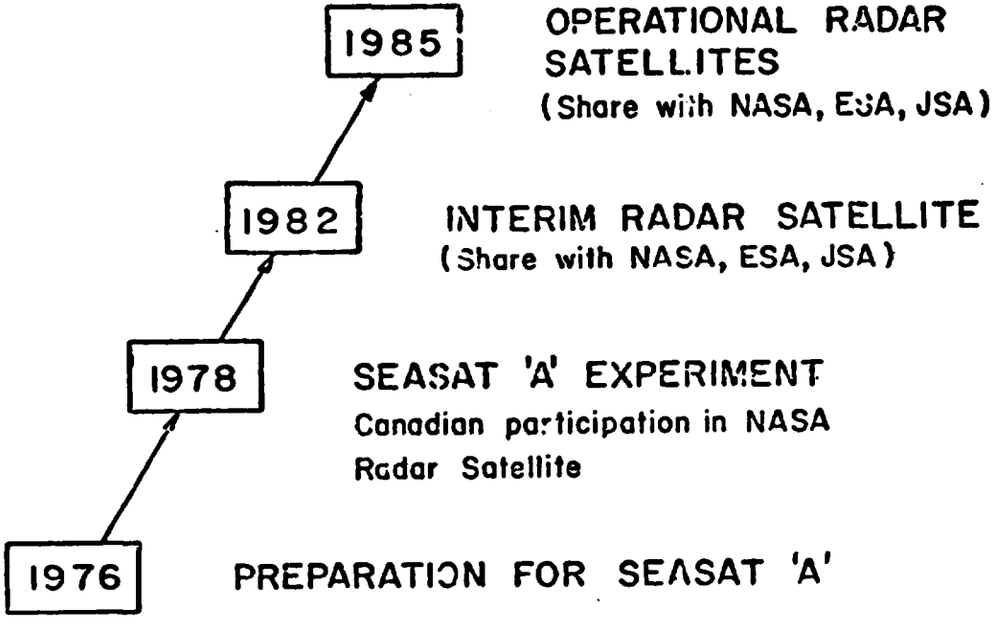

PLATE 2

PROPOSED CANADIAN PARTICIPATION IN SEASAT-A:SYSTEMS

- DIRECT READOUT OF ALL SEASAT-A DATA AT SHOE COVE
  OPERATIONAL AT LAUNCH, MID-1978.

- MODIFICATION OF EXISTING OPTICAL SAR PROCESSOR
  OPERATIONAL LATE 1978.

- DEVELOPMENT OF DIGITAL SAR PROCESSOR
  OPERATIONAL MID-1979.

- AIRBORNE RADAR APPLICATION STUDIES
  CONVAIR 580 WITH ERIM SAR. OPERATIONAL EARLY 1978.

- IONOSPHERIC AND SEA-CLUTTER STUDIES
  ONGOING FROM MID-1977.

PLATE 3

PROPOSED CANADIAN PARTICIPATION IN SEASAT-A:EXPERIMENTS

- COUPLED SCIENTIFIC/INDUSTRIAL USER EXPERIMENTS

- OCEAN ENVIRONMENTAL MONITORING COMBINED WITH SURVEILLANCE OF SHIPS, DRILL RIGS AND OTHER HUMAN ACTIVITIES

- SCOTIAN SHELF	-	OPEN OCEAN
- GRAND BANKS	-	OCEAN WITH ICE
- LABRADOR SHELF	-	OCEAN WITH ICE
- BEAUFORT SEA	-	OCEAN WITH ICE
- WEST COAST	-	OPEN OCEAN
- GREAT LAKES	-	INLAND WATER
- HIGH ARCTIC	-	ICE, HUMAN ACTIVITY

- LANDMASS - QUEBEC AND MARITIMES - GEOLOGY, WATER RESOURCES, FORESTRY AND AGRICULTURE

PLATE 4

THREE-YEAR DIRECT PROGRAM FUNDING ($THOUSAND)*

• PROGRAM MANAGEMENT	199
• SEASAT-A DATA RECEPTION (SHOE COVE STATION)	995
• SEASAT-A IMAGE PROCESSING	225
• SAR OPTICAL DATA PROCESSOR MODS	130
• SAR DITIGAL DATA PROCESSOR DEVELOPMENT	2,550
• AIRBORNE DATA ACQUISITION & PROCESSING	2,685
• RADAR RESEARCH	230
• VERIFICATION/APPLICATIONS EXPERIMENTS	1,010
• EVALUATION STUDIES	175
THOUSAND DOLLARS TOTAL	8,199

*DOES NOT INCLUDE ACTIVITIES OF FUNDING FROM INDUSTRY OR SECONDARY USERS.

PLATE 5

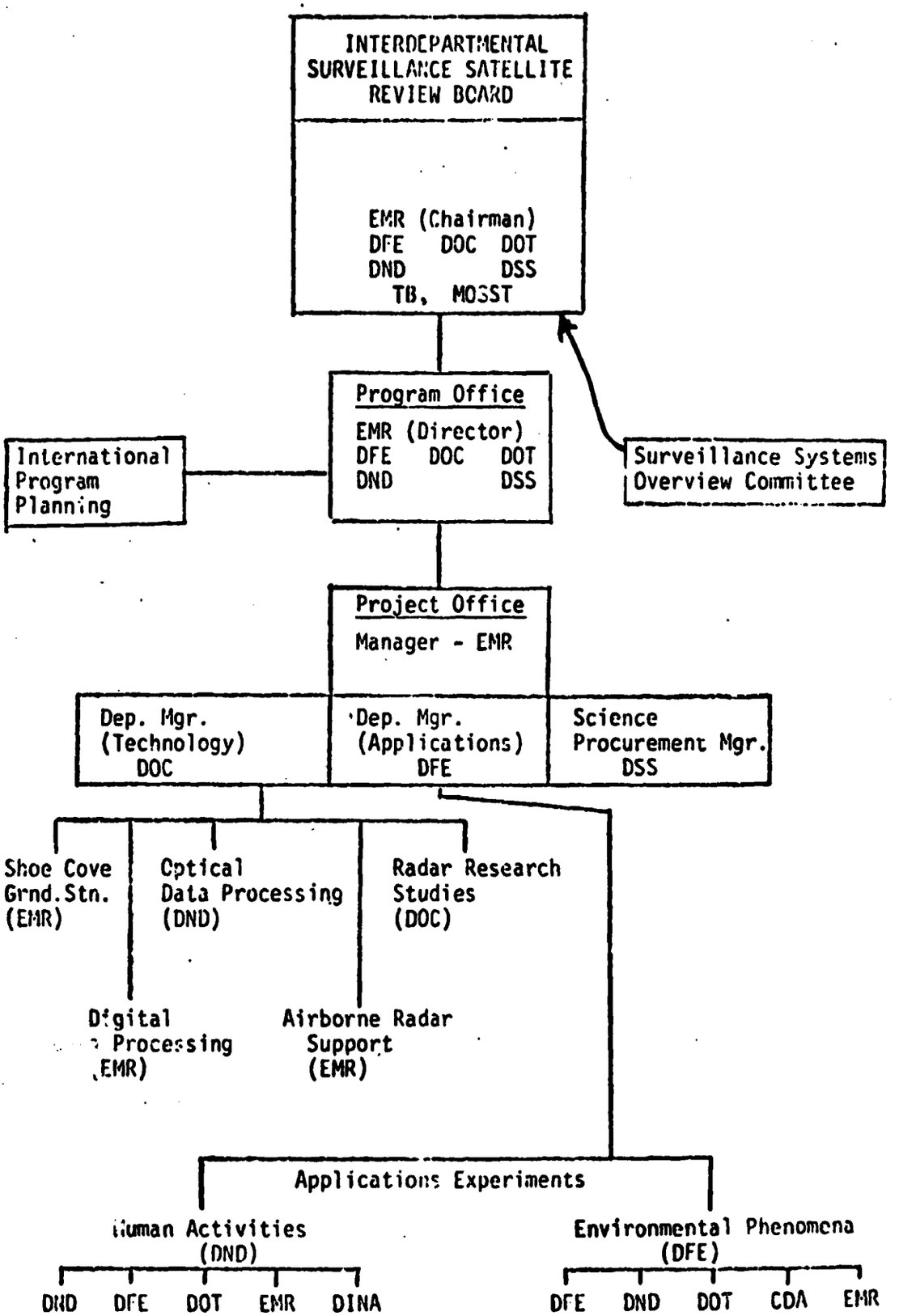

Plate 6 Program Management Structure

EXPERIMENTERS WORKSHOPS

On the second day of the workshop, experimenters, having been briefed on the current status of the SEASAT-A program and the associated data dissemination approaches, were asked to document the requirements of their experiments. This documentation was undertaken under the guidance of coordinators and with easy access to resource personnel, identified and present at the workshop.

The experimenters identified 22 different experiments of which 19 were actually documented. The remaining 3 were not documented, either because the experiment details had not yet been developed or because there was no experimenter representation at the workshop.

The association between experiments and experimenters is tabulated and the documentation of the experiments is provided.

Between the time of the workshop and the publication of this document, Experiments 3, 4 and 6 were documented and are now included. Also Dr. George Mourad of Battelle produced a more comprehensive description of the workshop experiments which is included.

This section also contains summary worksheets for all of the experiments described at the workshop. The information contained in these worksheets was provided by the experimeters during the workshop.

WORKSHOP IDENTIFIED EXPERIMENTS

No.	Experiment	Experimenter
1	Canadian Beaufort Sea, Dome Petroleum, Gulf and/or Imperial Oil	Glenn Davis
2	Labrador Sea or West Africa, Texaco and Gulf	Daniel H. Macy
3	Labrador Sea (Canadian), EPOA	*A. George Mourad
4	Gulf of Mexico, AGA/PRC	*A. George Mourad
5	U.S. East Coast, Conoco	Frank Rose
6	Offshore West Africa, Getty and Texaco	*A. George Mourad
7	North Sea, Union	Mike Utt
8	Equatorial East Pacific Ocean Mining	Bill Siapno, Atle Steen
9	Ocean Thermal Energy Conversion	Paul Wolff
10	Bering Sea Ice Task Group	Fredric H. Deily
11	Ship Navigation Gulf of Alaska	George Christoph
12	Ship Navigation Simulation	George Christoph
13	Ice Monitoring Experiment for Tanker Design	George Christoph
14	Marine Environmental Forecasting	Ray Mayer
15	Optimum Ship Routing	Ray Mayer
16	North American Goose Nesting Habitat	Robert E. Munro
17	International Ice Patrol--Northern Survey	Lt. G. Ketchen, USCG
18	International Ice Patrol--Environmental Data	Lt. G. Ketchen, USCG
19	International Ice Patrol--Repetitive Coverage Drift Analysis	Lt. G. Ketchen, USCG
20	Tropical Tuna Fishery	Merritt Stevenson
21	Salmon--Albacore Fishery	Fred Jurick
22	Alaskan Crab Fishery	Sigfryed Jaeger

*Experiments identified but not documented at workshop.

WORKSHOP EXPERIMENTS (BCL)

	Experiment Title/Type	Location	Organization(s)	Principal Contact	U.S. Coordinator
1.	Beaufort Sea (Oil and Gas and Arctic Operation)	200 Miles Offshore Between Longitudes 125° and 140°W	(1) Gulf Oil Canada Ltd. (2) Imperial Oil (Canada) (3) Dome Petroleum (Canada) (4) AOGA/ARC (US)	B. Wright/J. Hnatiuk G. Spedding G. Davis T. Hudson, Chairman (Chevron)	A. G. Mourad (BCL) and R. Gedney (NASA/LeRC) R. Ramseier (Canadian Coordinator)
2. & 3.	Labrador Sea (Oil & Gas and Sea Ice)	150 Miles Offshore Between Latitudes 33° and 63°N	(1) EASTCAN Exploration (Canada) (2) Gulf Oil Canada Ltd. (3) Imperial Oil (Canada) (4) Texaco (US)	P. Buemi B. Wright/J. Hnatiuk G. Spedding G. F. Mott/D. Macy	A. G. Mourad (BCL) and R. Gedney (NASA/LeRC) R. Ramseier (Canadian Coordinator)
4.	Gulf of Mexico (Oil & Gas and Pipelines)	Northern half of the Gulf of Mexico	(1) AGA/PRC (2) Getty Oil (3) Texaco	R. J. Simmons Jr., Chairman (United Gas Pipeline Co.) H. A. DeMirjian G. E. Mott/D. Macy	A. G. Mourad (BCL)
5.	U.S. East Coast	(1) Georges Bank (2) Baltimore Canyon Trough (3) Georgian Embayment	CONOCO, et al.	F. Rose	A. G. Mourad (BCL)
6.	Offshore West Africa (Oil & Gas & Drilling)	Western & Southern Coast of Africa	(1) Getty Oil, et al. (2) Texaco	H. A. DeMirjian G. E. Mott/D. Macy	A. G. Mourad (BCL)
8.	Equatorial East Pacific (Ocean Mining)	Offshore Southern Calif. and Central America in a corridor 15° Wide Extending to Southeast of Hawaii	Kennecott Exploration Deepsea Ventures	B. Livesay/A. Steen W. Siapno	A. G. Mourad (BCL)
10.	Bering and Chukchi Seas (Oil & Gas & Ice)	Offshore Alaska to U.S.-U.S.S.R. Border	AOGA/Bering Sea Task Force on Ice	Fred W. Ng, Chairman (ARCO)	A. G. Mourad (BCL) and R. Gedney (NASA/LeRC)
7.	North Sea (Oil & Gas)	United Kingdom area of Northern North Sea (52°N-65°N and 4°W-3°E)	(1) CONOCO (2) Union Oil	F. Rose M. Utt	A. G. Mourad (BCL)
9.	Ocean Thermal Power (Thermal Resources)	Many Sites Offshore the U.S. East and West Coasts	Ocean Data Systems	P. Wolff	D. Montgomery (JPL)

WORKSHOP EXPERIMENTS (BCL)

	Experiment Title/Type	Location	Organization(s)	Principal Contact	U.S. Coordinator
16.	North American Goose Nesting Habitat	Four Sites in Alaska's Coastal and Inland Marsh Nesting Areas	USDI/F&WS	A. Marmelsteen/R. E. Munro	D. Montgomery (JPL) and R. Gedney (NASA/LeRC)
13.	Ice Monitoring For Tanker Design	Beaufort Sea/Northwest Passage	Sun Shipbuilding and Dry Dock Co.	G. Christoph	D. Montgomery (JPL) and R. Gedney (NASA/LeRC)
11.& 12.	Optimum Ship Routing	Shipping Lanes Between Tacoma, Washington and Anchorage, Alaska	Sun Shipbuilding and Dry Dock Co.	G. Christoph	D. Montgomery (JPL)
17.	International Ice Patrol - Northern Survey	Coasts of Labrador and Baffin Island	USCG	Lt. G. Ketchen	R. Gedney (NASA/LeRC)
19.	International Ice Patrol - Drift	Grand Banks	USCG	Lt. G. Ketchen	R. Gedney (NASA/LeRC)
18.	International Ice Patrol - Environment	43°-49°N & 44°-50°W	USCG	Lt. G. Ketchen	R. Gedney (NASA/LeRC)
15.	Ocean Routing & Environmental Predictions	West Pacific & Gulf of Alaska	Ocean Routes, Inc.	R. Mayer	D. Montgomery (JPL)
14.	Gulf of Alaska (Oil Exploration)	Gulf of Alaska And Bering Sea	Ocean Routes, Inc.	R. Mayer	D. Montgomery (JPL)
22.	Alaskan Crab Fisheries	Gulf of Alaska and Bering Sea	Pacific Fishing Vessel Owners Assoc.	S. Jaeger	D. Montgomery (JPL)
22.	Alaskan Crab Fisheries	Gulf of Alaska and Bering Sea	Kodiak	F. Bohannon	D. Montgomery (JPL)
20.	Eastern Tropical Pacific Tuna Fisheries	From the Coast of Chile North to Northern California and Offshore 100's to 1000's of Miles	Inter American Tuna Commission (IATTC)	M. Stevenson/R. Kirkham	D. Montgomery (JPL)

WORKSHOP EXPERIMENTS (BCL)

	Experiment Title/Type	Location	Organization(s)	Principal Contact	U.S. Coordinator
21.	Salmon - Albacore	Offshore Southeastern Alaska to Guadalupe Island	Oregon State University/ Marine Adv. Prog. and Humboldt State University/Marine Adv. Ext. Soc.	R. Jacobson F. Jurick	D. Montgomery (JPL)

Key

APOA: Arctic Petroleum Operators Association
EPOA: Eastcoast Petroleum Operators Association
UKOOA: United Kingdom Offshore Operators Association
AGA/PRC: American Gas Association/Pipeline Research Committee
DOE: U.S. Department of Energy
BCL: Battelle Columbus Laboratories
JPL: Jet Propulsion Laboratory
AOGA/ARC: Alaska Oil And Gas Association/Arctic Research Committee
USDI/F&WS: U.S. Department of Interior/Fish and Wild Life Service
USCG: U.S. Coast Guard
NASA/LeRC: NASA/Lewis Research Center

EXPERIMENT 1: Canadian Beaufort Sea, Joint Dome Petroleum, Gulf Oil and Imperial Oil

EXPERIMENTER: Glenn Davis - Dome Petroleum/P.O. Box 200 Calgary, Alberta, Canada T2P 2H8

OBJECTIVE/PURPOSE: Evaluate SEASAT A sensors for operational applications in meteorologic, oceangraphic and sea ice monitoring in the Canadian Beaufort Sea offshore location.

LOCATION(S)	DATE (S)	FREQUENCY/DURATION
Canadian Beaufort Sea, approximately delineated Long: 125° - 140° W Long: Shoreline - 72° N	May, 1978 to end of program	As often as SEASAT A passes plus FNWC daily synopsis, forecasts and GDR.
COMMUNICATIONS	**PERSONNEL**	**SPECIAL EQUIPMENT**
Provide FNWC real time GDR's synopsis and forecasts to Calgary and Beaufort Advance Base, Tuktoyuktuk, N.W.T. Historical data on C.C.T.	Approx. 6 man months per year.	6 digital integrator anenometers Tektronex terminal
EXPERIMENTERS CONTRIBUTION	**EXPERIMENTERS OUTPUT**	**ECONOMIC BENEFITS**
a) hourly meteorological & oceanographic data, offshore location from June-Oct. each year. b) ground truth for SAR passes on ice during winter (approx. once a month, Dec.-March. c) Remote sensing overflights.	a) Real time transmission to FNWC, of meteorologic and oceanographic data. b) Yearly interim summary evaluation reports until termination c) Final evaluation report d) Remote sensing data collected in a sample area of study.	
DATA CHARACTERISTICS	**DATA FORMAT**	**DATA DELIVERY**
a) Real time data - Scat wind (magnitude&dir.) - SMMR " " - SMMR - SST - Altimeter H-1/3 AGC &confidence level - FNWC products - winds, waves, direction height period.	-Tables for G.D.R. synopsis and forecasts in real time; -CCT for historical data; -Interpreted ice concentration on charts (Fleet Weather Suitland) for SMMR data -would like wind & wave data from scatterometer even	Telephone for real time

SPECIAL ORBITAL REQUIREMENTS

(cont'd on attached sheet)

Canadian Beaufort Sea

DATA CHARACTERISTICS

-Sea Surface pressure
-SST
-Synopsis and forecasts
Non real time data
 - winds)
 - SST) SAR imagery
 - H-1/3)

-Ic· Concentration)
-Ice Types) SAR imagery

-Currents & Tides(if possible)

FNWC products, would like to have
 1. Observation file - sfc
 ships
 upper air
 other satellite

 2. Upper air analysis

 3. Forecasts - storm warnings
 winds
 wave heights
 (maximum & H-1/3)
 4. G.D.R.s tables
 5. Quality control
 (statement with each product)

DATA FORMAT

when flag for ice and land is set.
-SAR imagery
-SMMR & IR imagery

Canadian Beaufort Sea

Glenn Davis

Experiment's Contribution (cont'd. from previous page)

Dome Petroleum will have three drillships moored in locations in the Beaufort Sea. The drillships will be located in water depths between 90 feet and 200 feet approximately and distances from shore between 50 and 100 nautical miles.

Each drillship will have an experienced environmental observer aboard who will collect hourly meteorologic and oceangraphic data. Daily water column data will also be collected.

Hourly data collections include:

> Air temperature, barometric pressure, wind velocities, wind direction, humidity, cloud cover, wave heights, wave periods and sea surface temperature. Whenever sea ice is in the vicinity of the drilling vessel, ice flows are monitored on radar, visually and with on board computer-coupled, automatic, omega ice tracking transmitters. Wave heights are recorded every four hours, on charts and magnetic tape, with wave rider buoys. Currents are continually monitored and recorded at near surace, 5 meters and 10 meters at each drillship. Water column data, collected once a day, includes temperature, salinity and turbidity. Daily ice reconaissance flights are undertaken by experienced ice observers.
>
> Imperial Oil Ltd. will collect similar data at their artificial islands, which are nearer to shore than Dome's drillships. Meteorological data are collected at Beaufort Advance Base, Tuktogaktuk also.
>
> This data can be made available to FNWC in near real time or for historical analysis, while such data are being collected (during normal operations).
>
> All ground truth data (ice thickness, ridge heights, ridge frequencies), that are being collected during the winter ice research programs, will be available to the SEASAT project.
>
> Aerial photography, laser profiles, SLAR and Thermal I-R will be collected during the winter months over Sherefort ice and the Shear zone in the Beaufort Sea. Attempts will be made to coincide their flights with SEASAT SAR overpasses.

RAMS buoys will be placed on sea ice in the Shear zone of the Beaufort Sea.

Experimenters Output

a) Interim summary reports:

- assess capability of Scatterometer to determine wind velocity and direction in open water area of Beaufort Sea (between sea ice and land).
- provide an assessment of Scatterometer capability to determine wave heights, wind velocity and direction in water that is at freezing temperature.
- compare FNAC forecasts, with SEASAT impact, with Canadian A.E.S. Beaufort Advance Base forecast.
- assess whether SMMR data (sea surface temperature) will be useful for freezeup prediction model.
- assess SAR capability for collecting sea ice data ice type, ice concentrations, leads, ridges and pack ice compactness (degree of pressure)
- assess capability of radar altimeter for determining wave heights in the Beaufort Sea.

b) Final report at project end - conclusions and recommendations.

EXPERIMENT 2: Labrador Sea or West Africa - Texaco, Inc. & Gulf of Mexico
(THIS SHEET IS FOR LABRADOR ONLY)

EXPERIMENTER: Daniel Macy/Texaco, Inc./P. O. Box 60242/New Orleans, LA 70160

OBJECTIVE/PURPOSE: OCEANOGRAPHIC VERIFICATION OF SEASAT -
FOR UTILITY OF DATA FOR OFFSHORE DRILLING & PRODUCING OPERATORS

LOCATION(S)	DATE (S)	FREQUENCY/DURATION
In order of priority: 1) Labrador Sea - Offshore Newfoundland 2) Offshore Africa (specific Pt.Loc. ?)	Drill Season (July-Oct.) 1979 1978 intermittent as activity requires	As often as SEASAT Transits location
COMMUNICATIONS	**PERSONNEL**	**SPECIAL EQUIPMENT**
Real time data at drill vessel via fascimile. Historical data at New Orleans/Houston	6 man-months for one year	To be determined
EXPERIMENTERS CONTRIBUTION	**EXPERIMENTERS OUTPUT**	**ECONOMIC BENEFITS**
Ground truth data from our orig. vessel either area as available.	Report summarizing the verification or assessment of instruments data and ground truth for reliability and utility to our operations and design	Estimation of projected benefits based on both real time and historum data to form an environmental data base for design purposes and operational efficiency.
DATA CHARACTERISTICS	**DATA FORMAT**	**DATA DELIVERY**
FNWC real time data (see back) and historical data aircraft necessary to perform data verification sea ice and iceberg	Real time data on currents, tables or graphics (see back) Historical data on magnetic tape SAR & SMMR imagery V/IR imagery	Real time data to ground base operation compatible with weather facsimile transmission from Newfoundland. Historum data to New Orleans/Houston

SPECIAL ORBITAL REQUIREMENTS

Labrador Sea or West Africa

DATA CHARACTERISTICS

1) Observation File: SFC
SHIPS
Upper Air — 1^{o} 8 bits day
Other Satellites

2) Tailored Charts and Forecasts:

Storm warning
Area, any scale, any projected
Selected plotted data

3) GDR's plotted w/geograhical background

4) Quality control statement w/each product

(prepared by A. G. Mourad/Battelle)

EXPERIMENTER: EPOA (Eastcan Exploration: P. Bugmi; Gulf Oil: B. Wright/Hnatiuk; Imperial: G. Spedding; Canadian Coordinator: R. Ramseier/Sursat Proj.) and Texaco/U.S.: C. Mott/D. Macy

OBJECTIVE/PURPOSE:

(1) to improve wind, wave, freezeup and breakup forecast
(2) to locate icebergs
(3) to assess the utility of SEASAT data for offshore facilities design and operations.

LOCATION(S)	DATE (S)	FREQUENCY/DURATION
150 miles offshore west and 33° - 63°N	Throughout the life of the SEASAT experiment	As often as SEASAT-A passes are available over the test area plus FNWC daily synopsis and forecasts.
COMMUNICATIONS	**PERSONNEL**	**SPECIAL EQUIPMENT**
Transmission Lines; Phone, FAX Receiving Equipment: Graphic terminal Alpha numeric CRT Teletype	Approximately 6 man-months/year	?
EXPERIMENTERS CONTRIBUTION	**EXPERIMENTERS OUTPUT**	**ECONOMIC BENEFITS**
Data from drill ships, platforms and ice surveys on: - waves (height,period,dir) - wind speed/dir - current speed/dir - iceberg size, position & route -sea ice type,leads,roughness, pressure ridges, etc.	- Surface truth data to NASA and/or FNWC - Interim and Final reports evaluating the accuracy and utility of SEASAT data in design and operations for offshore oil and gas purposes.	Assess the economic benefits of SEASAT data utility.
DATA CHARACTERISTICS	**DATA FORMAT**	**DATA DELIVERY**
- GDR: (Scat wind, SMMR wind, SMMR SST, alt. $H_{1/3}$ - FNWC Products: Marine winds, waves ($H_{1/3}$, dir. period, spectra), SSP & SST in nowcast and forecast at 12,24,48 & 72 hrs ship obser.files, plots of GDR's,quality (over)	- tables for GDR synopsis and forecasts - tables, charts & graphs for FNWC real time and forecast products - CCT for historical data - SAR, SMMR & V/IR imagery	Telephone for real time data, and mail historical data to Calgary, Alberta, Canada ?

SPECIAL ORBITAL REQUIREMENTS

Labrador Sea

Data Characteristics (Con't.)

control statements with each product

- Non-real time data:

  Winds, waves ($H_{1/3}$), SST

  SAR, SMMR & V/IR imagery
  Ice concentration & types
  Currents and tides if possible

(Prepared by A. G. Mourad/Battelle)

EXPERIMENTER: American Gas Association/Pipe Line Research Committee (J. Simmons, Jr. Chairman); Getty Oil and Texaco are also interested in this area.

OBJECTIVE/PURPOSE:

(1) to improve the design criteria for pipeline and correlate the effect of surface environmental data with subsurface and ocean bottom conditions
(2) to improve real-time prediction capability and the accuracy of predicting severe storms.

LOCATION(S)	DATE (S)	FREQUENCY/DURATION
26°N - 30°N 80°W - 97°5W	Throughout the duration of the experiment Priority times during the hurricane season for SAR data	All available pertinent data and as often as passes are taken over the test area plus FNWC daily synopsis and forecasts
COMMUNICATIONS	**PERSONNEL**	**SPECIAL EQUIPMENT**
Transmission Lines: Phone, FAX Receiving Equipment: Graphic terminal Alpha numeric CRT Teletype	2-4 man-month/year depending on the accuracy and usefulness of the data	None
EXPERIMENTERS CONTRIBUTION	**EXPERIMENTERS OUTPUT**	**ECONOMIC BENEFITS**
Surface data (wave spectra, wind speed/direction, water temperature, air temperature and water vapor) from platforms and subsurface instrument packages	- Surface truth data to NASA and/or FNWC - Verification of the accuracy and utility of SEASAT data - Write final report	Assess potential economic benefits of SEASAT data in offshore pipeline and facilities design and operations
DATA CHARACTERISTICS	**DATA FORMAT**	**DATA DELIVERY**
(1) GDR: (Scat. wind, SMMR wind, SMMR SST, Altimeter $H_{1/3}$ (2) FNWC Products: marine winds, waves ($H_{1/3}$, direction, period, spectra), SSP and SST nowcast and forecast at 12,24,48,&72 hrs. (over)	- Tables for GDR synopsis and forecasts in real time - CCT for historical data - SMMR V/IR and SAR imagery - Tables, charts and graphs for real time data and forecast	Telephone for real time data in Houston, Texas. Mail historical data to ____

SPECIAL ORBITAL REQUIREMENTS

Gulf of Mexico

Data Characteristics (Con't.)

Ship obs. files, storm warning plot of GDR's with geographic coordinates and quality control statements of data

(3) Non-real time data:

SAR, SMMR & V/IR imagery
Currents, tides

EXPERIMENT 5: **OFFSHORE OIL AND GAS**

EXPERIMENTER: Frank Rose Conoco/P.O. Box 2197/Houston, TX 77001

OBJECTIVE/PURPOSE:

LOCATION(S)	DATE (S)	FREQUENCY/DURATION
North Atlantic with Ground Truth Stations in Baltimore Canyon and North Sea Area	From initiation or data disimination to end of project.	See Attached sheet
COMMUNICATIONS	**PERSONNEL**	**SPECIAL EQUIPMENT**
Bell Modem	---	To be studied
EXPERIMENTERS CONTRIBUTION	**EXPERIMENTERS OUTPUT**	**ECONOMIC BENEFITS**
$H_{1/3}$ Wind Speed & Direction Sea Surf Temp Surf Current		1. Assist in calibration of Hindcast models 2. More accurate forecasts 3. Indication of applicability to Development of long term data bases for structural design&operational consideration 4.Develop Directional Spectra for design
DATA CHARACTERISTICS	**DATA FORMAT**	**DATA DELIVERY**
	Graphics Tabulars	Houston/Ponca City

SPECIAL ORBITAL REQUIREMENTS

Offshore Oil and Gas

FREQUENCY - DURATION

Real Time:

I. GDR Data - Need Data whenever Satellite passes over North Atlantic between 20°N and 80°N

II. Forecast/Predicts/OBS

Ship, Buoy, Military OBS - 4 times per day for above area

Surface Analysis Chart - 4 times per day.

Upper Air Charts - 2 times/day for above area

Sea Temp. Charts - 1 time/day (not forecast)

$H_{1/3}$ Charts - 2 times/day (not forecast)

$H_{1/3}$ Point Predictions - This info. required at 12 hour intervals for site specific points and should include the 12, 24, 36, 48 & 72 hour point forecast for each 12 hour interval.

HISTORICAL

Tide/Current Data from range info for area mentioned above for each pass.

EXPERIMENT 6: (prepared by A. G. Mourad/Battelle)

EXPERIMENTER: Getty Oil Co., et al (H. DeHirjian) and Texaco (G. Nott/D. Macy)

OBJECTIVE/PURPOSE:

To assess the utility of SEASAT historical and real time data for offshore oil and gas and drill ship design and operations.

LOCATION(S)	DATE (S)	FREQUENCY/DURATION
Exact area may not be known until 2-3 months prior to operations. Approximately: 0-12°N and 18°S-35°S up to 2000-m contour west	During the drill ship operations for real time data and throughout the SEASAT experiment program for historical data.	All available pertinent data and as often as passes are available over the test areas plus FNWC daily synopsis and forecasts.
COMMUNICATIONS	**PERSONNEL**	**SPECIAL EQUIPMENT**
Transmission Lines: Phone, FAX Receiving Equipment: Graphic terminal Alpha numeric CRT Teletype	1 man-month prior to verification 2 man-month/year after, depending on SEASAT data utility.	None
EXPERIMENTERS CONTRIBUTION	**EXPERIMENTERS OUTPUT**	**ECONOMIC BENEFITS**
Data from drill ship and wave rider buoy such as water temp. and salinity, waves (height, period, dir.), wind speed/direction, current speed/direction, air temperature	- Surface truth data to NASA and/or FNWC - verification of accuracy and utility of SEASAT data - final report	Assess potential economic benefits of SEASAT data for offshore oil and gas operations and for drill ship design and operations
DATA CHARACTERISTICS	**DATA FORMAT**	**DATA DELIVERY**
(1) GDR: (Scat.wind, SMMR wind SMMR SST, altimeter $H_{1/3}$ (2) FNWC Products: Marine winds, waves ($H_{1/3}$, dir., period, spectra) SSP and SST in newcast, and forecast at 12,24,48,72 hrs. Ship obs. files, storm warning plot (over)	- Tables for GDR synopsis and forecasts - tables, charts & graphs for FNWC real time and forecast data - CCT for historical data - SMM & V/IR imagery	Telephone for real time data, mail historical data to Houston, Tex.

SPECIAL ORBITAL REQUIREMENTS

Offshore West Africa

Data Characteristics (Con't.)

of CDR's with geographic coordinates, and quality control statements, if possible

(3) Non-real time data: SMMR and V/IR imagery waves, currents, tides, winds and temperature

EXPERIMENT 7: UNION OIL NORTH SEA

EXPERIMENTER: Mr. Mike Utt - Union Oil Research/P.O. Box 76/Brea, CA 92621

OBJECTIVE/PURPOSE: SEASAT Data Verification and Assessment of the Utility of the Data for Analysis and Design

LOCATION(S)	DATE (S)	FREQUENCY/DURATION
Northern North Sea -(within 100 km of Heather production platform) $52^{o}N$ - $65^{o}N$ and $40^{o}W$ - $3^{o}E$	From start of SEASAT-A (Nov. '78) for at least one year.	As often as SEASAT passes are available (estimated less than 1 pass/day)
COMMUNICATIONS	**PERSONNEL**	**SPECIAL EQUIPMENT**
Phone line or magnetic tape, non-real time.	1 Research Engineer and computer support personnel at Union Research Center (estimated 2 man-months)	none
EXPERIMENTERS CONTRIBUTION	**EXPERIMENTERS OUTPUT**	**ECONOMIC BENEFITS**
Surface data (wind, waves and temp.) from fixed platform	Report summarizing statistical comparisons of SEASAT and surface data	direct - none indirect: -NASA gets verification of SEASAT data -Union gets experience with satellite data
DATA CHARACTERISTICS	**DATA FORMAT**	**DATA DELIVERY**
GDR's only real time not required. week or 10 days delivery time okay	Wave height - tabular data Wind and temperature - Desirable to have estimate at a point (platform location) for each pass encompassing the point.	To: Union Research Center Brea, CA via phone line or by mag.tape.

SPECIAL ORBITAL REQUIREMENTS NO PREFERENCE

EXPERIMENT 8: EQUATORIAL EAST PACIFIC/OCEAN MINING

EXPERIMENTER: Bill Siapno - Deepsea Ventures/Gloucester Point, VA 23062
Atle Steen - Kennecott Exploration, Inc./3377 Carmel Mountain Road/ SAN Diego,CA 92121

OBJECTIVE/PURPOSE: Receive & Assess SEASAT Data Utility for Ocean Mining Design and Operation

LOCATION(S)	DATE (S)	FREQUENCY/DURATION
Area included within 5°N - 20°N; 110°W - 150° W plus Storm area of West Coast of N. America 5°N - 40°N and West to 150°W.	Oct. 1978 to end of program Especially between June 1 thru Oct. 1	As often as SEASAT passes area plus all FNWC forecasts.
COMMUNICATIONS	**PERSONNEL**	**SPECIAL EQUIPMENT**
Provide all data by Weatherfax. Provide historic data once/month	6 x man months/year	To be determined
EXPERIMENTERS CONTRIBUTION	**EXPERIMENTERS OUTPUT**	**ECONOMIC BENEFITS (Anticipated)**
Surface Temp. Air, Sea. Wind: Direction & Speed Wave/Swell: Height,Period, Direction These data could be made available to NASA orFNWC by radio or whatever means available to receive them.	Report summarizing results: 1)Verification of SEASAT data accuracy and their utilities in mining operations and design 2)Assessment of potential benefits of a projected SEASAT operational system.	Increase environmental data base, minimize increase efficiency of operation.
DATA CHARACTERISTICS	**DATA FORMAT**	**DATA DELIVERY**
1)Real time data (copy) (see back) 2)FNWC forecast products (see back) 3)Storm Advisory 4)Spectral points for each experiment.Historical data - 3[illegible] data block,SAR, SMR&V/IR,Currents,tides,etc	Historical data on Computer tape. Real Time - Tables, Charts, Graphs Forecasts - Tables, Charts, Graphs V/IR facsimilies	1 - Weatherfax 2 - Kennecott, S.D.,CA Deep Sea - Venturus, VA INCO - Wash. State Lockheed, CA

SPECIAL ORBITAL REQUIREMENTS

Equatorial East Pacific/Ocean Mining

DATA CHARACTERISTICS

Quality Control Statements with each product
GDR's plotted w/grey background
Tailored charts & forecasts

Real time data from SEASAT (GDR)
Scat. wind (magnitude and direction)
SMMR wind and SST
Altimeter $H_{1/3}$

AGC on confidence level

FNWC products nowcast and forecast at 12, 24, 48, 72 hrs.
(winds, $H_{1/3}$, direction, period, wave spectra)
spectral date points

Historical data on -
(winds, SST, $H_{1/3}$, SAR and SMMR and V/IR imagery

EXPERIMENT 9: OCEAN THERMAL ENERGY CONVERSION

EXPERIMENTER: Mr, Paul Wolff - Ocean Data Systems/2400 Garden Rd./Monterey,CA 93940

OBJECTIVE/PURPOSE: SURVEY DATA FOR PLANT SITES, THERMAL RESOURCE EVALUATION, ENGINEERING DATA ON WINDS, WAVES AND CURRENTS

LOCATION(S)	DATE (S)	FREQUENCY/DURATION
Gulf of Mexico 10 1° Square Florida Straits 6 " Florida East Coast 8 " Hawaii 6 " Guam 4 " 10 other 1° Lat. Long areas in Tropical oceans	Continuing full period for which data are available.	All available pertinent observations
COMMUNICATIONS	**PERSONNEL**	**SPECIAL EQUIPMENT**
Direct line to FNWC computer 4 transmissions/day.	P. Wolff + 3 Dr. Lloyd Lewis DOE	
EXPERIMENTERS CONTRIBUTION	**EXPERIMENTERS OUTPUT**	**ECONOMIC BENEFITS**
Computers & Comm line plotters - previous engineering data specifications OTEC observations	Comparison of this data with OTEC obs and previous estimates of thermal resource, wind, wave mean values and extremes. Currents if discernible	Changes in engineering design specifications. Warnings of high seas and winds during operations.
DATA CHARACTERISTICS	**DATA FORMAT**	**DATA DELIVERY**
SST obs H1/3 obs Wind obs Spectral Sea State analyses for each point twice a day. MLD data or analyses	FNWC packed binary or any other computer to computer protocol.	Direct line from ODSI computer to FNWC computer.

SPECIAL ORBITAL REQUIREMENTS Prefer Baseline Orbit

OCEAN THERMAL ENERGY CONVERSION

These plants expect to use the thermal difference between the warm upper layer of the ocean and the cold water available at 1000 meter depths.

Test operations of components have begun off Hawaii and Puerto Rico. A small test plant is planned for the N. Gulf of Mexico with a larger movable plant soon thereafter.

Ocean Data Systems has been working under contract to DOE to evaluate environmental conditions especially thermal resource availability.

Specifically the plant operation is possible only in areas with warm surface water throughout the year. Depth of the mixed layer is needed also.

In addition, the plants are affected by strong winds, wave action and currents which influence design of hull, piping mooring, etc.

Sites are identified in 1^{o} Lat. Long squares. All are in ocean areas where environmental observations are sparse in both space & time.

ODSI has prepared monthly values and limits for temperature structures monthly. Engineering design specs define wind, waves and currents.

This experiment has the following purpose initially:

a) verify environmental design values

b) determine diurnal variations

c) compare these new observations with specified envelopes.

Changes in engineering design characterictics may be possible from this study. Any environmental values outside current design characteristics will have expensive engineering impacts.

When plants are in operation -

a) provide warnings of extreme winds, seas, currents

b) detect any change in sea surface temperature caused by plant operation.

EXPERIMENT 10: BERING SEA ICE

EXPERIMENTER: Fredric H. Daily, Exxon Production Res/PO Box 2189/Houston,TX 77001

OBJECTIVE/PURPOSE: Use Data from SEASAT-A to study ice coverage and movement to see if it is feasible to use data for Offshore Operations.

LOCATION(S)	DATE (S)	FREQUENCY/DURATION
54° N - 70° N 157° W - 175° W To the US, USSR borders	Nov. 1978 - May 1979 Nov. 1979 - May 1980	As many SAR passes as possible SMMR data once/week. In non-ice areas Wind, Wave and SST requirements to be determined.
COMMUNICATIONS	**PERSONNEL**	**SPECIAL EQUIPMENT**
Data not required in real time	Outside contractor funded AOGA will perform analysis	
EXPERIMENTERS CONTRIBUTION	**EXPERIMENTERS OUTPUT**	**ECONOMIC BENEFITS**
Aircraft under flight. Stereo aerial photography. LANDSAT and NOAA analysis payed for by AOGA	Verify SEASAT data. Attempt to assess utility Submit report	
DATA CHARACTERISTICS	**DATA FORMAT**	**DATA DELIVERY**
SAR imagery 2 copies film positives 10% data as CCT's	SMMR - % of ice concentration. Open water areas, wind, wave height, SST	1 month after acquisition.

SPECIAL ORBITAL REQUIREMENTS Desire Cambridge Orbit

EXPERIMENT 11: SHIP NAVIGATION IN GULF OF ALASKA

EXPERIMENTER: George Christoph - Sun Shipbuilding and Dry Dock Co./Chester, PA 19013

OBJECTIVE/PURPOSE:

LOCATION(S)	DATE (S)	FREQUENCY/DURATION
Along Great Circle Routes 1) From Puget Sound to Mouth of Cook Inlet and 2) From Los Angeles to the Mouth of Prince William Sound.	As available	Continuously throughout the orbital life of SEASAT A.
COMMUNICATIONS	**PERSONNEL**	**SPECIAL EQUIPMENT**
Data Broker, FNWC to Sun Shipbuilding and Dry Dock Company Chester, PA 19013 215-876-9121		
EXPERIMENTERS CONTRIBUTION	**EXPERIMENTERS OUTPUT**	**ECONOMIC BENEFITS**
Analysis of the influence of SEASAT A data on the operation of two ships sailing at regular intervals in the above region of interest.	A report on their findings. Definition of operational system requirements.	Expected to result from scheduling improvement, fuel conservation and damage avoidance.
DATA CHARACTERISTICS	**DATA FORMAT**	**DATA DELIVERY**
R T)Surface Wind Speed and E I)Direction - Wave Spectra A M)Significant Wave Height L E)Wave Length)10Meter wind velocity & direction Non Real time Sea Surface Temperature Air Temp.--Currents.	1) Digital tables in CRT Compatible form a) Graphics compatible with Tektronics CRT	FNWC Analysis and Forecasts (6,12,18,24,72 hours) 4 times per week on demand GDR data every 6 - 12 hours continuously.

SPECIAL ORBITAL REQUIREMENTS

EXPERIMENT 12: SHIP NAVIGATION SIMULATION

EXPERIMENTER: George Christoph - Sun Shipbuilding and Dry Dock Co./Chester, PA 19013

OBJECTIVE/PURPOSE:

LOCATION(S)	DATE (S)	FREQUENCY/DURATION
As yet undefined Ocean Trade Routes	As available after first year of SEASAT A Launch.	On demand throughout the orbital life of SEASAT A.
COMMUNICATIONS	**PERSONNEL**	**SPECIAL EQUIPMENT**
Data, Broker, FNWC to Sun Shipbuilding and Dry Dock Company, Chester, PA 19103 215-876-9121		
EXPERIMENTERS CONTRIBUTION	**EXPERIMENTERS OUTPUT**	**ECONOMIC BENEFITS**
In association with Ship Navigation in Gulf of Alaska experiment, simulate ship operations on other trade routes	A report on their findings Definition of operational system requirements	Expected to result from reduced passage time, fuel conservationand damage avoidance.
DATA CHARACTERISTICS	**DATA FORMAT**	**DATA DELIVERY**
Surface wind, speed and direction. Wave spectra. Significant wave height. Currents. Wave length. 10 Meter Wind speed and direction. Sea Surface temperatures/air temperatures.	1) Digital tables in CRT compatible form 2) Graphics compatibles with Tektronics CRT	FNWC Analysis and forecasts (6,12,18,24 and 72 hours) on demand. GDR on demand.

SPECIAL ORBITAL REQUIREMENTS

EXPERIMENT 13: ICE MONITORING EXPERIMENT FOR TANKER DESIGN

EXPERIMENTER: George Christoph - Sun Shipbuilding and Dry Dock Co./Chester, PA 19013

OBJECTIVE/PURPOSE:

LOCATION(S)	DATE (S)	FREQUENCY/DURATION
Beaufort and Chukchi Seas beyond 10-fathom line from coast	Experiment Period Dec. 78 - March 79 Dec. 79 - March 80	6 SAR passes per month during experimental period. SMMR coverage every two weeks
COMMUNICATIONS	**PERSONNEL**	**SPECIAL EQUIPMENT**
JPL to Sun Ship Building and Dry Dock Co.,Chester, PA 19013 (214-TR6-9121)	NASA personnel will provide assistance for SAR image interpretation and CCT evaluation.	None
EXPERIMENTERS CONTRIBUTION	**EXPERIMENTERS OUTPUT**	**ECONOMIC BENEFITS**
Will interpret data made available in terms of economic significance to tanker design, in simulation model.	A report on their findings Definition of operational system requirements	These are expected as a consequence of more effective ship design by having adequate ice information.
DATA CHARACTERISTICS	**DATA FORMAT**	**DATA DELIVERY**
SAR data will beam-lyse to determine 1)frequency and distribution of ice ridges 2) ice type 3)inferred ice thickness. SMMR data required is %ice, % 1st yr. and % multiyear	As required by experimentor SAR-1. Film Positive (2 copies) 2. CCT'S of selected area 3. Location Accuracy ±5 Km. SMMR-1 Chart	One to two months after acquisition

SPECIAL ORBITAL REQUIREMENTS Cambridge Orbit Preferred

EXPERIMENT 14: MARINE ENVIRONMENTAL FORECASTING

EXPERIMENTER: Mr. Ray Mayer - Oceanroutes/3260 Hillview Ave./Palo Alto,CA 94034

OBJECTIVE/PURPOSE: Sea Truth Determination - Forecast Model Improvement

LOCATION(S)	DATE (S)	FREQUENCY/DURATION
Gulf of Alaska or North Sea or East Coast US	1 year after Algorithm. validation	Continuously
COMMUNICATIONS	**PERSONNEL**	**SPECIAL EQUIPMENT**
4800 band line to FNWC ORJ unique Access to DDF 4800 preferred 1200 acceptable Link Palo Alto to Anchorage 1200 band on higher	ORI Staff	Graphics terminal in Alaska
EXPERIMENTERS CONTRIBUTION	**EXPERIMENTERS OUTPUT**	**ECONOMIC BENEFITS**
	Evaluation of GDR data with ground truth Evaluation of value of SEASAT data as input to real time forecast system.	Higher platform, semi-submissible, and helicopter utilization.
DATA CHARACTERISTICS	**DATA FORMAT**	**DATA DELIVERY**
GDR and FNWC products. Will utilize all available products in forecast system. Selected FNWC special points SAR for evaluation as operational ice forecast tool	Binary CRT graphic	Real time on 3 hourly(GDR) basis or more if available.

SPECIAL ORBITAL REQUIREMENTS

EXPERIMENT 15: OPTIMUM SHIP ROUTING

EXPERIMENTER: Mr. Ray Mayer - Oceanroutes, 3260 Hillview Ave./Palto Alto, CA 94034

OBJECTIVE/PURPOSE: Determine Incremental Savings Accruing to Ship Operators through Integration of SEASAT Data into FNWC Products

LOCATION(S)	DATE (S)	FREQUENCY/DURATION
Palo Alto	1 year after Algorithm validation	Continuously
COMMUNICATIONS	**PERSONNEL**	**SPECIAL EQUIPMENT**
4800 band line to FNWC ORI unique. Access to DDF @ 4800 preferred	ORI Staff	Graphics Terminal in Palo Alto
EXPERIMENTERS CONTRIBUTION	**EXPERIMENTERS OUTPUT**	**ECONOMIC BENEFITS**
	Evaluation of changes in fleet efficiency for 1 or more U. S. Flag operators after integration of SEASAT data into FNWC product.	Reduced time in transit Reduced Hull and Cargo damage Reduced probability of catastrophic loss
DATA CHARACTERISTICS	**DATA FORMAT**	**DATA DELIVERY**
FNWC products pre and post SEASAT	Binary CRT Graphic	Real time At least twice daily

SPECIAL ORBITAL REQUIREMENTS

EXPERIMENT 16: NORTH AMERICAN GOOSE NESTING HABITAT

EXPERIMENTER: Mr. Robert E. Munro USF&WS/Patuxent Wildlife Res.Center/Laurel, MD 20811

OBJECTIVE/PURPOSE: Evaluate the Utility of SAR and Data Products from FNWC in Assessment of Habitat Conditions on Arctic Goose Nesting Grounds.

LOCATION(S)	DATE (S)	FREQUENCY/DURATION
Clarence Rhode National Wildlife Refuge Yukon - Kuskokwim, Delta Alaska* *see attached figure	Mid to end May 1978 (doubtful) Mid to end May 1979	Continuous during dates
COMMUNICATIONS	**PERSONNEL**	**SPECIAL EQUIPMENT**
FNWC, JPL Migratory Bird & Habitat Research Lab., Laurel, MD 20811	NASA Lewis assistance in SAR interpretation	Graphics terminal & 1200 baud coupler NASA aircraft over-flight
EXPERIMENTERS CONTRIBUTION	**EXPERIMENTERS OUTPUT**	**ECONOMIC BENEFITS**
USFWS personnel at location	Comprehensive report to NASA; ground truth such as description of ice conditions on selected lakes in test areas.	Estimatable from improved waterfowl species management
DATA CHARACTERISTICS	**DATA FORMAT**	**DATA DELIVERY**
SAR 1) images ——→ SMMR 2) data ——→ VIRR images ——→ 1 JPL 2 Real-Time from FNWC 3 Near Real-Time from __?	Images Graphics, tables Images	ASAP

SPECIAL ORBITAL REQUIREMENTS Cambridge Orbit

North American Goose Nesting Habitat

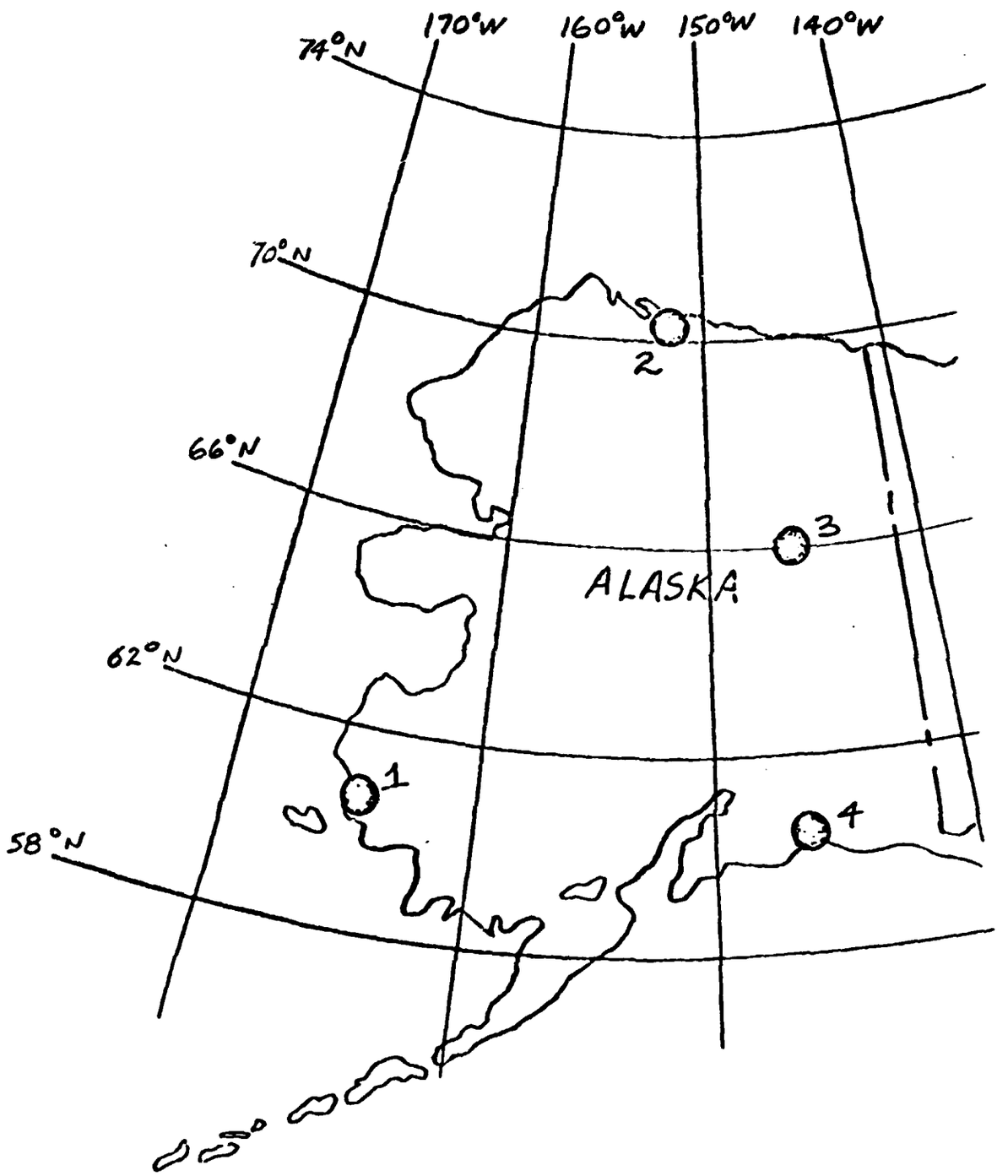

EXPERIMENT 17: Application of SEASAT-A for International Ice Patrol (Northern Survey)

EXPERIMENTER: Lt. Gregory Ketchen, USCG, Staff Oceanographer/International Ice Patrol Building/110/Governor's Island/New York, NY 10004

OBJECTIVE/PURPOSE: A Northern Survey will be performed to demonstrate the feasibility and benefits of conducting a pre-season survey of icebergs and sea ice along the Labrador and Baffin Island Coasts using SEASAT-A SAR in place of aircraft reconnaissance.

LOCATION(S)	DATE (S)	FREQUENCY/DURATION
A region from the coast to 100 miles off shore along Labrador and Southeast Baffim Island and across Davis Straits.	Mid January thru late February 1979	7 SAR passes over 12 days Min: One complete coverage of survey area. Desired: Two complete coverages of the area.
COMMUNICATIONS	**PERSONNEL**	**SPECIAL EQUIPMENT**
Data delivery by physical transport.		
EXPERIMENTERS CONTRIBUTION	**EXPERIMENTERS OUTPUT**	**ECONOMIC BENEFITS**
4 C-130 Aircraft Sorties. SLAR/RIP equipped	1. Ground Truth - Observed Icebergs 2. Data Report and Analyses or Results	If survey using SEASAT-A SAR, elimination of one to two HC-130 pre-season deployments of approximately 12 days each.
DATA CHARACTERISTICS	**DATA FORMAT**	**DATA DELIVERY**
Full resolution SAR processing optimally focused for surface targets.	1. Images 2 CCT's	Within 14 days

SPECIAL ORBITAL REQUIREMENTS Cambridge

EXPERIMENT 18: INTERNATIONAL ICE PATROL ENVIRONMENTAL DATA

EXPERIMENTER: Lt. Gregory Ketchen, USCG, Staff Oceanographer/International Ice Patrol/Bldg. 110/Governors's Island/New York, NY 10004

OBJECTIVE/PURPOSE: To assess the value of using sea surface windvelocity and sea surface slope (i.e. current) data from SEASAT-A in an iceberg drift model and sea surface temperature for iceberg melt prediction.

LOCATION(S)	DATE (S)	FREQUENCY/DURATION
43° N - 49° N 44° W - 50° W	Apr - June 1979	Daily from Mar - Jul
COMMUNICATIONS	**PERSONNEL**	**SPECIAL EQUIPMENT**
Telephone modem to computer terminal		Textronic CRT Terminal for receipt of FNWC Prediction and Analysis CST and Surface Wind.
EXPERIMENTERS CONTRIBUTION	**EXPERIMENTERS OUTPUT**	**ECONOMIC BENEFITS**
1. Ship surface truth data: time ave.winds, sea surface temperature and geostrophic current measurements 2. Data analysis and comparison	1. Iceberg drift & melt predictions 2. Data report and analyses of results	Improved iceberg drift predictions could lead to reduction in dist.of detour of some vessels around ice limits and thus reduce vessel transit time.
DATA CHARACTERISTICS	**DATA FORMAT**	**DATA DELIVERY**
1. Wind velocity (Knots & °T) 2. Current velocity (cm/s & °T) 3. Temperature (°C) FNWC Anal & Predict Surface Winds for 40° - 52° N and 39° - 57° W	BCD	Within 8 hours after Anal. end and Predict Start time

SPECIAL ORBITAL REQUIREMENTS

EXPERIMENT 19: Application of SEASAT-A for International Ice Patrol (Repetitive Coverage Drift Analysis)

EXPERIMENTER: Lt. Gregory Ketchen, USCG, Staff Oceanographer/International Ice Patrol Building/110 Governor's Island/New York, NY 10004

OBJECTIVE/PURPOSE: Primary - To determine how reliably icebergs could be tracked using the SAR
Secondary - Use repetitive iceberg drifts observed with SAR to validate and adapt the operational Keberg Drift Model.

LOCATION(S)	DATE (S)	FREQUENCY/DURATION
43° - 50° N 45° - 52° W	March - June 1979	4 SAR passes required over a 3 day period Min: one survey Desired: two surveys
COMMUNICATIONS	**PERSONNEL**	**SPECIAL EQUIPMENT**
Data delivery by physical transport.		
EXPERIMENTERS CONTRIBUTION	**EXPERIMENTERS OUTPUT**	**ECONOMIC BENEFITS**
1) Aircraft side-looking radar and ship surface truth 2) Surface truth data analysis	1) Iceberg drift model validation 2) Analyses & report	Improved iceberg drift predictions could lead to reduction in distance detoured around ice limits by some vessels reducing vessel transit time.Possible reduction of deployed forces
DATA CHARACTERISTICS	**DATA FORMAT**	**DATA DELIVERY**
Full resolution SAR processing optimally focused for surface targets	1) Images 2) CCT'S	For one pass, would like fastest practical delivery to determine possible operational application.

SPECIAL ORBITAL REQUIREMENTS

EXPERIMENT 20: TROPICAL TUNA FISHERY

EXPERIMENTER: Dr. Merritt Stevenson - Inter-Am. Tropical Tuna Commission/ c/o Scripps Institute of Ocean./ LaJolla, CA 92037
OBJECTIVE/PURPOSE: Use of SEASAT-A Products by the Eastern Tropical Pacific Tuna Fishery

LOCATION(S)	DATE (S)	FREQUENCY/DURATION
80°W - 145°W 34°N - 10°S	Annual Fishing Season Jan. 1 - Dec. 31	Daily (every two days as necessary)
COMMUNICATIONS	**PERSONNEL**	**SPECIAL EQUIPMENT**
Need link from FNWC to IATTC and hence to WWD for radio transmission to fleet vessels	a) Tuna boat captains b) Tuna boat Assoc. (for info purposes at least) c) 1. IATTC Staff 2. R. Kirkham 3. M. Stevenson 4. Support Personnel	Terminal, tape recorder and FACS machine at IATTC (La Jolla) for receiving & copying charts.
EXPERIMENTERS CONTRIBUTION	**EXPERIMENTERS OUTPUT**	**ECONOMIC BENEFITS**
a) Plan and supervise distribution of charts b) Liaison with boat Captains c) Prep. of questionnaire d) Summarization of results of questionnaire in form of Final Findings Report e) Vessel participation	Preparation of Final Technical Report which summarizes findings of experiment	a) Reduced trip & fuel usage b) Increased fishing efficiency statistics c) Improved safety for vessels
DATA CHARACTERISTICS (Charts)	**DATA FORMAT**	**DATA DELIVERY**
Sea Surface temperature (°C; inlcude °C/°F scale) (1°C contour interval) Surface Winds - Steamlines (in kts) contour interval could be 2 kt + intervals wave heights-stream lines (contour interval in feet)	Map Scale 1" (MAP) =4° Lat Chart Size 18" (Long) x 14" (For Lat.) Mercator type projection	Daily, via data line & terminal then FACS machine for retransmittal to fleet

SPECIAL ORBITAL REQUIREMENTS

Tropical Tuna Fishery

DATA CHARACTERISTICS

Thermal front - shows Axis of Fronts as line segments; Frontal gradient is given as # $^{\circ}C/_{10}$ nmi; also warm/cold sides; possibly length of front:
Thermal Front is generated from SST Field and should show:

(a) Axis of Front
(b) Labelled Warm (w) and Cold (c) sides
(c) Scale of Front, that is, thermal gradient and length of front i.e., 3/150 means $3^{\circ}C/_{10}$ nmi and 150 means estimated front length is 150 nmi

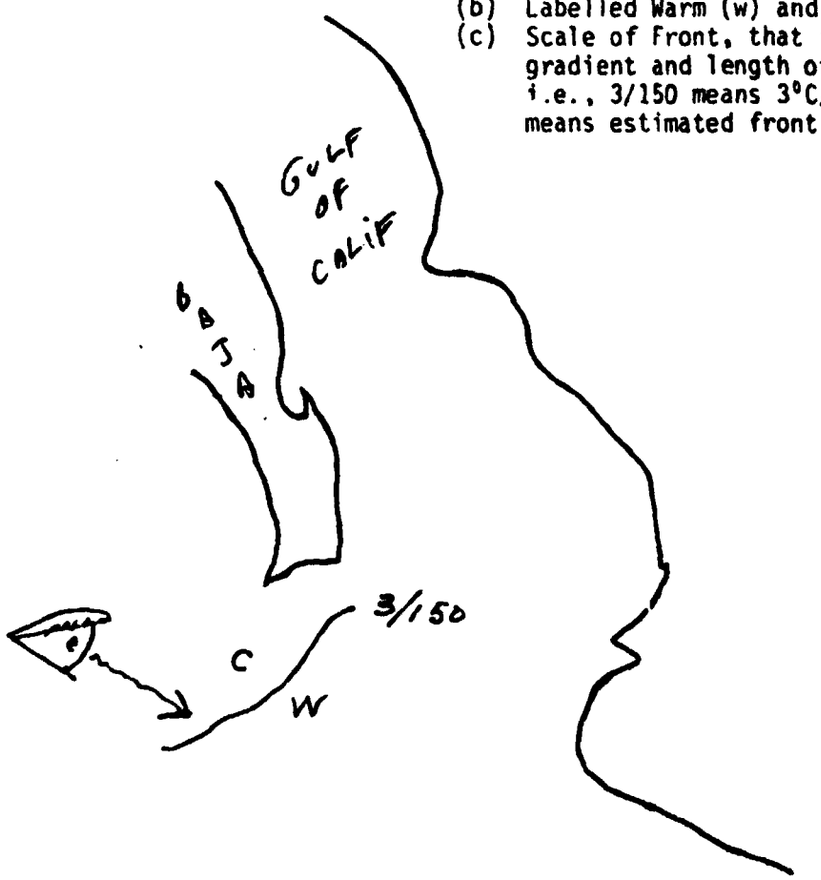

"FNWC Charts only" first for several weeks, then desire "SEASAT only" charts for a specific period of time, then followed by SEASAT & FNWC charts

---

Alternative: FNWC charts only first, followed in time by FNWC & SEASAT Charts

EXPERIMENT 21: **Salmon - Albacore Experiment**

EXPERIMENTER: FredJurick Humboldt State University/Marine Adv.-Ext.SVC./ Arcata, CA 95521

OBJECTIVE/PURPOSE: Fishing Environmental Data Charts

LOCATION(S)	DATE (S)	FREQUENCY/DURATION
34^{o} N - 50^{o} N @1/2"= 1^{o} lat. Coast - 135^{o} Wide	Crab Season Dec.-March Salmon March - Sept. Albacore June - Nov.	Daily forecasts which are composite of 2 days data.
COMMUNICATIONS	**PERSONNEL**	**SPECIAL EQUIPMENT**
FAX transmission	A. Boat Captains (6-12) B. Bob Jacobson C. Fred Jurick	Communication receiving equipment for vessels
EXPERIMENTERS CONTRIBUTION	**EXPERIMENTERS OUTPUT**	**ECONOMIC BENEFITS**
Vessel time Manpower Evaluation	1) Selected observation 2) Log	1) Savings time 2) Savings fuel 3) Better weather data
DATA CHARACTERISTICS	**DATA FORMAT**	**DATA DELIVERY**
1) SST.5C^{o} with Conversion Table to F^{o} 2) Wind Speed mph 3) H-1/3 ft. 4. Frontal location w/warm & cold locations and gradient. Same as tuna frontal chart.	Chart Loran A overlay	1) Surface - wind direction & wind speed 2) H-1/3 3) SST 4) Frontal location chart 4 charts: 2 morning 2 evening-SST & Front

SPECIAL ORBITAL REQUIREMENTS

EXPERIMENT 22: ALASKA CRAB FISHERY

OBJECTIVE/PURPOSE: BEGIN THE TECHNOLOGY TRANSFER PROCESS FROM NASA TO COMMERCIAL MARINE FISHERIES & TO ACCELERATE THE RATE AT WHICH SEASAT BENEFITS ARE OBTAINED BY THE COMMERICAL CRAB INDUSTRY

LOCATION(S)	DATE (S)	FREQUENCY/DURATION
Gulf of Alaska 140°W - 160°W, 50°N - 62°N. Bering Sea 160°W - 175°W 50°N - 65°N	Preferably a period covering 2 seasons of King & Tanner Crab beginning Fall 1978 thru Spring 1980.	Data Product Transmission Once per day to each participating vessel.
COMMUNICATIONS	**PERSONNEL**	**SPECIAL EQUIPMENT**
Land data line or satellite channel from FNWC to a TBD point in Alaska for subsequent radio facsimile transmission to each participating vessel.	Vessel coordinators are Sig. Jaeger for vessels operating out of Dutch Harbor and Frank Bohannon for vessels out of Kodiak. Candidate vessels & operators are shown on attached pages.	Leased data terminal (w/graphics) located at TBD in Alaska. Some leased Fax receivers to be located on some participating vessels.
EXPERIMENTERS CONTRIBUTION	**EXPERIMENTERS OUTPUT**	**ECONOMIC BENEFITS**
Crab vessels & crew. Some data analysis and surface OBS. reports back to FNWC.	Final Report with results analysis	Potential Benefits: Improved Fuel Efficiency Reduced Dead Loss Reduced Equipment Loss Improved Vessel & Crew Safety
DATA CHARACTERISTICS	**DATA FORMAT**	**DATA DELIVERY**
SEASAT-A Unique Products: Winds--Waves--SST FNWC Analysis & Forecast Products: Winds--Waves--SST-- Air Temp.--Ice Info.	SEASAT-A Unique Products Tabular, Alpha-Numeric Format. FNWC Analysis & Forecast Products: All graphics w/ Loran-C Mylar overlay Windfield-Vector presentation Waves - H 1/3 values	

SPECIAL ORBITAL REQUIREMENTS SST - Temp. Values Plus 50°F, 55°F, & 60°F Isotherms; Air temp - Temp. Values; Ice - Boundaries

Alaska Crab Fishery Experiment — CANDIDATE PARTICIPANTS

Vessel Name	Owner/ Operator	Vessel Type/Size	Catch Capacity	Principal Catch	Communication Equipment	On Board Environmental Sensors
Viking	Carl Perovich	120' steel Value - $1.8M	225,000# (King)	King Tanner Bottom Fish		
American Viking	Terry Buholm	95' steel Value - $900K	150,000#	King Tanner		
Ocean Leader	Mogney Nes	120' steel Value - $2.0M	225,000#	King Tanner Bottom Fish		
Pacific Viking	Kaare Ness	108' steel Value - $1.3M	175,000#	King Tanner		
Intrepid	Sigmdno Andreassen (Rudy Peterson)	120' steel Value - $1.8M	225,000#	King Tanner		

Table 1

Alaska Crab Fishery Experiment

Vessel Name	Owner/ Operator	Vessel Type/Size	Catch Capacity	Principal Catch	Communication Equipment	On Board Environmental Sensors
Alyeska	Jeff Hendicks	120' steel Value - $1.8M	225,000#	King Tanner		
Provider	John Hall			King Tanner		

Table 1

COOPERATIVE AGREEMENT

A preliminary draft of a cooperative agreement was provided to each experimenter, for his assessment and comments.

The objective is to develop an agreement whose language is satisfactory to both an experimenter and NASA so that the cooperative agreement can form the basis of a mutual exchange of services between NASA and the experimenter.

A copy of the preliminary draft of the cooperative agreement follows.

PRELIMINARY DRAFT

COOPERATIVE AGREEMENT
NASA AND CONTINENTAL OIL COMPANY

Introduction

This Agreement pertains to activities involving a proof of concept, oceanographic satellite called SEASAT-A; geophysical parameters derived from the processing of a signals acquired by SEASAT-A sensors and the application of these geophysical parameters to operations of various industrial users.

It is the mutual desire of the National Aeronautics and Space Administration, subsequently referred to as NASA, and each one of these industrial users to mutually conduct experiments which will

i) demonstrate and evaluate the operational and economic utility of SEASAT-A geophysical data.

ii) initiate transfer of SEASAT-A technology to the user industry, if it proves to be beneficial.

The characteristic geophysical parameters are specific to sea wave heights; sea surface winds; sea surface temperature; and ice which covers sea surfaces, not all of which are necessarily pertinent to every NASA-user experiment.

It is the intent of each Agreement to establish the basis for a cooperative experiment between NASA and a user from which will result a successful completion of the experiment and which will provide NASA with a complete, independent documentation of the results of the experiment.

General Intent of Agreement

By this Agreement, NASA and Continental Oil Company hereinafter referred to as CONOCO, enter into a cooperative agreement which will endure no more than three years beyond the date of the last signature. The Agreement may, however, be terminated earlier by mutual concurrence of both parties.

The Cooperative Agreement involves only a mutual exchange of services between the parties by which the parties discharge their responsibilities to the agreement. The Agreement does not provide for any exchange of monetary payments either by the parties or between the parties and it should not be construed to imply such an exchange.

A document entitled "Project Plan, SEASAT-A Industrial Demonstration Program", which is attached to this Agreement, describes the details of implementation of this Cooperative Agreement. These details can be expected to undergo some modification and amendment during the course of the experiment to successfully achieve the mutual objectives of the Agreement. Such changes will be jointly agreed on by NASA and CONOCO.

It is understood and agreed that the responsibilies of NASA to this Agreement will be discharged by;

i) Providing SEASAT-A derived geophysical parameters, at an agreed point of use, in the formats and units necessary to the execution of the experiment, through an access to be agreed upon, for the duration of the experiment.

ii) Providing certain types of forecast products at an agreed point of use

iii) Providing, as necessary and required, consultation support to configure the experiment; to interpret the geophysical parameter data provided and to effectively accomplish the reporting, to NASA, of the results of the experiment.

It is understood and agreed that the responsibilities of CONOCO to this Agreement will be discharged by;

i) Assuming total responsibility for the conduct and execution of the experiment of this cooperative agreement.

ii) Assuming total responsibility for documenting the evaluated results and the procedures of both the experiment and the evaluation, as they pertain to SEASAT-A data operational utility and to SEASAT-A data economic utility, to the extent possible, of the experiment in an approved final report to NASA before the termination of this Agreement or within ninety (90) days of the concurrent termination of this Agreement, as appropriate.

Liability For Loss or Damage

NASA agrees to pay for any claims of property damage or bodily injury to the extent required by the Federal Tort Claims Act. The NASA's obligation includes, in addition to the Federal Tort Claims Act, other liabilities pursuant to law, including but not limited to the National Aeronautics and Space Act of 1958, as amended. CONOCO agrees to indemnify the NASA and save it harmless from all claims, demands, actions, costs, and charges which the NASA may have to pay, by reason of any injury to any person or property or loss of life or property, suffered or sustained during the period of this agreement when the injury, loss of life, or property damage is caused by any act or omission of any agent or employee of CONOCO.

Property Rights In Inventions

The term "invention" includes any invention, discovery, improvement, or innovation. Any invention conceived or first actually reduced to practice in the performance of work under

this agreement shall be reported promptly to the Patent Counsel of NASA/Headquarters, such report containing full and complete technical information concerning the invention. Any invention so reported shall be presumed to have been made under the conditions described in paragraphs (1) and (2) of Section 305(a) of the National Aeronautics and Space Act of 1958, as amended. The rights of the United States to such invention shall be determined in accordance with Section 205 of the Space Act, and CONOCO and the NASA shall cooperate in execution of documents, furnishing of further information or data otherwise appropriate to that end.

Review Of Information Releases

During the performance of this agreement, if technical data relating to this agreement is proposed to be used in oral or written presentations at professional meetings, seminars and symposia or in articles to be published in professional, scientific, technical journals and similar media, CONOCO will request a review by the NASA/Headquarters of such proposed publication. Such requests should be forwarded to the NASA/Headquarters Public Affairs Office (Code EN) at least (4) weeks in advance of the desired NASA/Headquarters response date, to provide sufficient time for review and comments to CONOCO.

Nothing herein is intended to control news releases or advertisements which CONOCO deem appropriate. Credit for joint support by CONOCO and NASA shall be given in all written and oral presentations.

Officials Not To Benefit

No member of or delegate to Congress or resident commissioner, shall be admitted to any share or part of this agreement, or to any benefit that may arise therefrom; but, this

provision shall not be construed to extend to this agreement if made with a corporation for its general benefit.

Reduction In Satellite Capabilities

If SEASAT-A, to be launched in May 1978, fails to orbit the responsibilities of both parties to this Agreement will be null and void.

If SEASAT-A, during the duration of the Agreement, should undergo either a failure or degradation of its expected capabilities, the responsibilities of both parties to the Agreement will be modified or amended, as required by the satellite operating conditions that then prevail.

This Agreement is entered into by the Administration of the NATIONAL AERONAUTICS AND SPACE ADMINISTRATION in accordance with the authority set forth in Sections 202 (c) (5) and 203 (c) (6) of the National Aeronautics and Space Administration Act of 1958, as amended. It is executed in duplicate originals on the dates indicated below.

FOR

_____ _____
Date

FOR National Aeronautics and Space Administration

_____ _____
Date

SUMMARY

In a sense, this two-day workshop represented the formal kickoff meeting for the SEASAT-A Industry Demonstration Program. The workshop provided the first opportunity for all of the industry experimenters and the NASA program personnel to meet at one time for a discussion of the proposed experiments and the capabilities of the SEASAT-A system. In this workshop, the experimenters were assured of the continuing progress of SEASAT-A toward a successful launch in May 1978 as subsystem and system testing has advanced satisfactorily. Experimenters, also, were able to query the developers of the instrumentation on many points of concern to them and to receive satisfactory answers. In addition, the experimenters were introduced to the processes through which data and information involving the processed signals from the instrumentation would be made available to them and to clarify their needs for display terminals and for associated hardcopy terminals that would be compatible with the sources of data and information supply.

Subsequent to their briefing on the status of the SEASAT-A program and its proposed dissemination of information, the majority of the experimenters were able to document their experimental objectives and requirements with support and technical help from resource personnel present at the workshop. In reviewing the experiments proposed, all experimenters became acquainted with the diversity of experiments to be undertaken and, in some instances, with the commonality of the elements of the experiments.

It was clear that some confusion existed for the experimenters about NASA's goals and objectives from the results of the experiments, and this matter was discussed in detail during the summation.

In the future, at some undefined date, what is generally described as an operational SEASAT system may exist and become the principal provider of synoptic data from which oceanographic and meteorological information may be derived. Today such a system does not exist and indeed has no official sanction. What is about to appear is SEASAT-A, a satellite whose instrumentation will provide experimental data which needs experimental evaluation to define its effectiveness and acceptability to users. A positive evaluation will support the concept of valid information supply by satellite. A negative evaluation will not. Thus an important goal of this experiment program is the independent evaluation of the data and information made available through SEASAT-A and its dissemination system. Clearly the criteria for decision concerning an effectiveness evaluation must come from the community of users most likely to be concerned about the existence of such data.

SEASAT-A data will be available explicitly as GDRs and images, which will permit direct comparison as "point" data with sea truth measurements. Thus, in general, the GDR sea-truth evaluations can determine the relative utility of remote sensing as a substitute for sea truth and identify remote sensing as an economic substitute for sea truth.

When GDRs are incorporated as another data source into the operations of FNWC, their explicit contribution is no longer readily apparent. The analysis programs of FNWC will, as with all input data, evaluate the consistency of SEASAT-A data with all other sources, but after such an evaluation no record is kept of the data included in subsequent processing. Consistent GDRs, that is those consistent with FNWC techniques, will be introduced into forecasts provided by FNWC. Because FNWC is an operational forecasting organization, its continual search to provide the best operational forecasts

it can implies that the sources of data and methods of proces- g may change with time. Thus it will not be possible to identify explicitly the contribution to forecasting quality arising from SEASAT-A data's existence, except possibly as an improvement in forecast quality over an extended period of time. Experiments which are concerned with forecasting efficacy will only be able to measure or identify the effectiveness of the forecasts obtained for their operational applica- s and to indicate or measure the economic advantage arising from the total forecasting process.

Evaluation of the contribution of SEASAT-A data to the forecasting quality requires either an explicit determination by FNWC or a tentative determination employing historic forecasts where the experiments will allow.

The overall goals and objectives of the SEASAT-A Industry Demonstration Program are to evaluate the effectiveness and operational and economic utility of SEASAT-A data within the major categories of operations performed in the marine environment. The experiments are an independent means of obtaining the goals and objectives, and require from the experimenters careful reporting to validate and substantiate the results.

In addition, recognizing that SEASAT-A and its data dissemination system are experimental and not operational, NASA seeks from all experimenters a considered opinion, judgemental or otherwise, of how these systems could be improved. Thus, these experiments will provide guidance to NASA for future system design, as well as assisting the experimenters in gaining an understanding of the potential that these future systems may offer.

During the workshop several of the experimenters expressed concern that more time should have been provided for discussion of the proposed experiments. The time allocations in this workshop were a compromise between the

objectives of educating the experimenters in the capabilities of SEASAT-A and educating those concerned with the SEASAT-A program with the desires of the experimenters. In subsequent workshops, it is planned that a greater percentage of time will be allocated to discussion of the experiments. Between workshops it will be necessary to complete the plans for the experiments and the data dissemination so that the final details of the implementation can be resolved at the next workshop. As a follow-up to the workshop, individual meetings will be held between the experimenters and SEASAT-A program personnel to complete the proposed experiment plans.

LISTING OF WORKSHOP ATTENDEES

Attendees were recorded and a listing is supplied. The two day meeting resulted in some attendance at one day or the other and as a consequence the listing may not be complete.

Revised

ATTENDEES AT THE SEASAT INDUSTRIAL USERS WORKSHOP

Princeton, New Jersey

29/30 November 1977

Name	Company Name and Address	Telephone
B. P. Miller	ECON, Inc./900 State Road/Princeton, NJ 08540	(609) 924-8778
Dave Nippert	Battelle/505 King Avenue/Columbus, OH 43201	(614) 424-5120
R. L. Stone	NASA Headquarters/Code EK/Washington,DC 20546	(202) 755-8611
J. N. Perdue	Fleet Numerical Weather Control/Monterey,CA 93940	(408) 646-2670
Harry Nicholson	Fleet Numerical Weather Control/Monterey,CA 93940	(408) 646-2384
R. L. Matthews	Sun Shipbuilding and Dry Dock Co./Chester,PA 19013	(215) 876-9121 X673
G. Christoph	Sun Shipbuilding and Dry Dock Co./Chester,PA 19013	(215) 876-9121
D. Dunbar	NORDCO, Ltd./St. John's, Newfoundland	(709) 754-2401
Paul Wolff	Ocean Data Systems/2400 Garden Rd./Monterey,CA 93940	(408) 373-2011
Ted Pounder	JPL/Pasadena, CA	(213) 354-5490
Byron D. Tapley	University of Texas/Austin, TX 78712	(512) 471-1356
Larrain Luckl	ECON, Inc./900 State Road/Princeton, NJ 08540	(609) 924-8778
Charles Raquet	NASA-Lewis/21000 Brookpark/Cleveland, OH 44135	(216) 433-4000 X291 (FTS) 294-6291
Robert E. Munro	USF&WS/Patuxent Wildlife Res.Center/Laurel,MD 20811	(301) 776-4880 X331 (FTS) 937-7331
A. George Mourad	Battelle/505 King Avenue/Columbus, OH 43201	(614) 424-5097
Fredric H. Deily	Exxon Production Res./P.O. Box 2189/Houston, TX 77001	(713) 965-4574
Merritt Stevenson	Inter-Am. Tropical Tuna Commission/c/o Scripps Institute of Ocean./LaJolla, CA 92037	(714) 453-2820
Fred Jurick	Humboldt State University/Marine Adv.-Ext.SVC./ Arcata, CA 95521	(707) 443-8369
W. Linwood Jones	NASA-Langley RC, M/S-490/Hampton, VA 23665	(804) 827-3651 (FTS) 928-3651
Dick Gedney	NASA-Lewis Research Center/Cleveland,OH 44135	(216) 433-4000 X209 (FTS) 294-6209

Name	Company Name and Address	Telephone
Sung L. Suh	Kennecott Exploration, Inc./3377 Carmel Mountain Road/San Diego, CA 92121	(714) 453-3751
Atle Steen	Kennecott Exploration, Inc./3377 Carmel Mountain Road/San Diego, CA 92121	(714) 453-3751
Allan Reece	Shell Development Co./P.O.Box 481,Houston,TX 77001	(713) 663-2437
S. W. Selfridge	Oceanroutes/3260 Hillview Ave./Palo Alto,CA 94304	(415) 493-3600
Bill Siapno	Deepsea Ventures/Gloucester Point, VA 23062	(804) 642-2121
Daniel H. Macy	Texaco, Inc./P.O. Box 60242/New Orleans,LA 70160	(504) 524-5311
Dr. Reggie J. Caudill	Princeton University/Eng.Quad.E-420/Princeton, NJ 08540	(609) 452-4596
Mike Utt	Union Oil Research/P.O. Box 76/Brea, CA 92621	(714) 528-7201
Frank Rose	Conoco/P. O. Box 2197/Houston, TX 77001	(713) 965-2614
Doug Jones	Continental Oil Co./R&D Dept./Ponca City,OK 94601	(405) 762-3456 X4437
Ray Mayer	Oceanroutes/3260 Hillview Ave./Palo Alto,CA 94034	(415) 493-3600
Glenn Davis	Dome Petroleum/P.O. Box 200/Calgary, Alberta, Canada T2P 2H8	(403) 232-5550
Walter M. Thiebaut	European Space Agency/955 L'Enfant Plaza, S.W. Suite 1404/Washington, DC 20024	(202) 488-4158
W. T. Eaton	LMSC 0/66-01, Sunnyvale, CA 94088	
Ed Langham	SURSAT Project Office/c/o Canada Centre for Remote Sensing/520 Preston St./Room 1195/Ottawa, Ontario, Canada K1A0Y7	
William C. Squillarid	Exxon International Co./Tanker Research and Development/Florham Park, NJ 07932	(201) 474-1896
Dick Hale	Technology Development Corp./155 Moffett Park Drive/Sunnyvale, CA 94086	(408) 734-5500
Donald J. Clough	Professor of Engineering/University of Waterloo/ Waterloo, Ontario, Canada Systems Engineering Associates Ltd./R.R. 2/ Braden, Ontario, Canada N0B 1G0--Consultant to Canada Centre for Remote Sensing/Ottawa, Canada	(519) 885-1211
Don Montgomery	NASA Headquarters/Code ESE/Washington, DC 20546	(202) 755-1201

Name	Company Name and Address	Telephone
H. Gregory Ketchen, Lt., USCG	Staff Oceanographer/International Ice Patrol/ Building 110/Governor's Island/New York,NY 10004	(212) 264-4798
Richard M. Hayes	U. S. Coast Guard/Oceanographic Unit/Building 159E/ Navy Yard Annex/Washington, DC 20590	(202) 426-4636
Fred G. Rea	Battelle/505 King Avenue/Columbus, OH 43201	(614) 424-5101
Ken Hicks	ECON, Inc./900 State Road/Princeton, NJ 08540	(609) 924-8778
Pierre Hartman	NASA Headquarters/Code GK/Washington, DC 20546	(202) 755-3161
S. W. McCandless, Jr.	NASA Headquarters/Code ESE/Washington, DC 20546	(202) 755-1201
James G. Marthaler	Lieutenant, USCG Headquarters/Sensor Tech. Branch (G-DOE-2/TP54)/Washington, DC 20590	(202) 426-1013
Omar M. Shemdin	JPL, M.S. 183-50 - 4800 Oak Grove Dr. Pasadena, CA 91103	(213) 354-2447
Al Robinson	Battelle/505 King Ave./Cleveland,OH 43201	(614) 424-5097

APPENDIX A SASS

These reprints were provided by Dr. Jones as a replacement for his presentation material.

Aircraft Measurements of the Microwave Scattering Signature of the Ocean

W. LINWOOD JONES, SENIOR MEMBER, IEEE, LYLE C. SCHROEDER, AND JOHN L. MITCHELL

Abstract—Microwave scattering signatures of the ocean have been measured over a range of surface wind speeds from 3 m/s to 23.6 m/s using the AAFE RADSCAT scatterometer in an aircraft. Normalized scattering coefficients are presented for vertical and horizontal polarizations as a function of incidence angle (nadir to 55°) and radar azimuth angle (0° to 360°) relative to surface wind direction. For a given radar polarization, incidence angle, and azimuth angle relative to the wind direction, these scattering data exhibit a power law dependence on surface wind speed. The relation of the scattering coefficient to azimuth angle obtained during aircraft circles (antenna conical scans) is anisotropic and suggests that microwave scatterometers can be used to infer both wind speed and direction. These results have been used for the design of the Seasat-A Satellite Scatterometer (SASS) to be flown in 1978 on this first NASA oceanographic satellite.

Manuscript received December 15, 1975; revised July 30, 1976.

W. L. Jones and L. C. Schroeder are with NASA Langley Research Center, Hampton, VA 23665.
J. L. Mitchell is with the Vought Corporation, Hampton, VA 23666.

INTRODUCTION

SINCE THE invention of radar, the scattering properties of the ocean surface have been of interest to researchers. For years the noiselike backscattered signal from the ocean

 Annals No. 701AP0C3

called sea clutter was a source of interference which had to be overcome by radar system designers. Early attempts to characterize sea clutter were concerned with measurements at near grazing incidence angles and were frequently obtained without a good knowledge of the state of the sea [1], [2]. During the 1960's, the Naval Research Laboratory (NRL) conducted an extensive aircraft measurements program [3]–[5] to provide quantitative information on the parametric behavior of the electromagnetic scattering coefficient (often called normalized radar cross section) σ^0 of the ocean. Measurements were obtained as a function of polarization, incidence angle, and azimuth angle using pulse radars operating at 0.4, 1.2, 4.5, and 8.9 GHz. Other aircraft measurements [6], [7] were later performed by the National Aeronautics and Space Administration, Johnson Space Center (NASA-JSC) using a fan-beam Doppler radar operating at 13.3 GHz. The NRL and NASA-JSC data sets were subsequently used to propose a microwave scatterometer technique [8] for remotely sensing surface wind speed over the ocean.

During the early 1970's, an aircraft microwave scatterometer was developed under the NASA Langley Research Center's Advanced Applications Flight Experiments (AAFE) program. This instrument was subsequently used to make ocean scattering measurements to evaluate the viability of radar remote sensing of surface wind vector. The purpose of this paper is to present the results of this ocean measurements program. Every attempt has been made to include all significant σ^0 data along with the corresponding ocean wave and wind vector measurements. It is our hope that these data will clarify the relationship between K_u-band radar backscatter coefficient and the ocean surface wind vector.

Experiment Description

A combined microwave radiometer-scatterometer (RADSCAT) operating at 13.9 GHz was developed to measure the microwave brightness temperature and scattering coefficient of the ocean from aircraft altitudes. A detailed description of AAFE RADSCAT and its operation is given in [9]; therefore, only a brief description of the scatterometer portion is given herein. A simplified scatterometer subsystem block diagram is shown in Fig. 1. During normal operation, the passive and active measurements are time shared through the use of a single pencil beam antenna.

For the scatterometer measurement, "long" pulses are transmitted to the surface such that the area illuminated is defined by the antenna pattern, that is, beam limited conditions. RADSCAT uses a dual polarized, high beam efficiency, parabolic antenna with a half power beam width of about 1.5°. While the transmitter is off, a 2-μs sample of the received pulse is processed. In the scatterometer processor, a single spectral line is selected by passing the sampled received pulse through a narrow bandwidth filter.

For smooth seas and light winds, the backscattered signal has a dynamic range of approximately 60 dB [illegible] surements at the nadir to 55° incidence angle. [illegible] useful

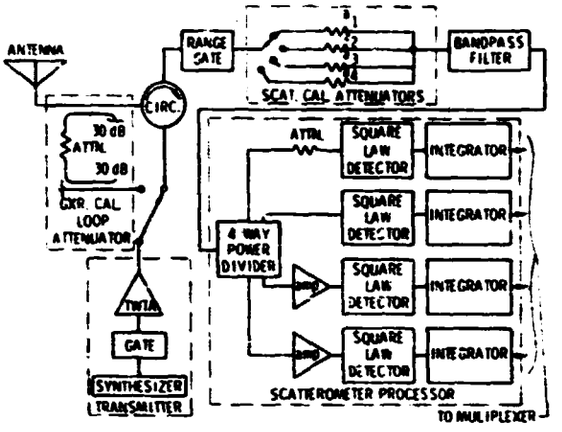

Fig. 1. Simplified diagram of RADSCAT (scatterometer subsystem).

power measurement range of a square law detector is typically 20 dB, four receiver channels are used in parallel with staggered sensitivities to insure continuous operation over the complete receiver dynamic range. In each channel, the signal is square law detected and then integrated for a selectable period ranging from 300 to 924 ms. The integrator outputs are analog-to-digital converted and recorded in a PCM format on an analog magnetic tape recorder.

In making scatterometer measurements, the quantity of interest is the scattering coefficient σ^0 of the ocean. This quantity is independent of the type of radar performing the measurement and is defined from the radar equation to be

$$\sigma^0 = \frac{P_r (4\pi)^3 R^4}{P_t G^2 \lambda^2 A_T} \tag{1}$$

where

- P_r received power,
- P_t transmitted power,
- G antenna gain,
- R slant range,
- λ free-space wavelength,
- A_T effective antenna footprint on ocean surface.

For the RADSCAT case of beam limited conditions

$$A_T = \frac{\pi (\beta_{eq} R)^2}{4 \cos \theta} \tag{2}$$

where β_{eq} is the effective pencil-beam antenna width (approximately equal to the half power antenna beam width), and θ is the incidence angle. The scattering coefficient thus becomes

$$\sigma^0 = \frac{P_r (16\pi)^2 R^2 \cos \theta}{P_t G^2 \lambda^2 \beta_{eq}^2}. \tag{3}$$

Referring to the block diagram of Fig. 1, the P_r/P_t ratio was measured in two steps. First, a sample of the transmitter power, attenuated by a known value GXR, was diverted into the receiver. This produced a "calibration" output voltage V_{cal} in each receiver channel pro-

Fig. 2. RADSCAT installed on NASA 929 aircraft.

portional to P_r.[1] Next, the transmitter was connected to the antenna and an output voltage V_{sea} proportional to P_r was obtained in a particular channel. Solving for the received to transmitted power ratio (in terms of the voltage from a particular channel) yields

$$\frac{P_r}{P_t} = \frac{V_{sea}}{V_{cal}} \frac{\tau_{cal}}{\tau_{sea}} \alpha GXR \tag{4}$$

where

- V output voltage of RADSCAT integrator,
- τ integration time for RADSCAT integrator
- α calibration attenuator value (selected from a_1 to a_4),
- GXR receiver calibration loop attenuation,

and subscripts are

- cal during calibration,
- sea during ocean operation.

Finally, in terms of the RADSCAT transfer function [9], the expression for σ^0 is

$$\sigma^0 = (16\pi)^2 \frac{A^2}{\lambda^2} \frac{V_{sea}}{V_{cal}} \frac{\tau_{cal}}{\tau_{sea}} \frac{\alpha GXR}{G^2 \cos \theta(\beta_{eq})^2} \tag{5}$$

where A is the altitude of aircraft (antenna).

The measurements presented in this paper were obtained with RADSCAT operating on a Lockheed C-130B cargo aircraft. Fig. 2 is a photograph of RADSCAT in its operational configuration on the NASA-JSC C-130 aircraft, NASA-929. The instrument was mounted on rails attached to the cargo ramp (lower door in the aft of the aircraft). The radar was retracted inside the aircraft and the doors were closed for take-off and landing. For in-flight ocean measurements, the upper cargo door was raised, the ramp was lowered, and the RADSCAT was extended to its operational position outside the fuselage. In this configuration, the antenna had an unobstructed view of the ocean surface without the use of a radome. The antenna elevation was mechanically scanned to the aft in six steps from 0° (nadir) to approximately 55° incidence angle.

[1] Automatic instrument calibrations are performed after every 2 min of operation to minimize the effect of long-term changes in the instrument gain.

Aircraft Experiment Description and Results

During the aircraft experiments, the radar backscattering coefficients of the ocean were measured and correlated with the near simultaneously observed surface wind vector and sea state. For the most part, flights were performed in the open ocean, at distances greater than 100 km from shore, where uniform wind and wave conditions existed. Measurements were obtained under a variety of conditions from light winds and calm seas to gale conditions.

Surface Truth Measurements

For each flight, the local ocean surface wind speed and wave conditions were measured by either *in situ* instrumentation or by onboard aircraft sensors. Typical *in situ* measurements consisted of 10 min averages of wind speed and direction, air temperature, and near-surface sea temperature obtained hourly during the scatterometer experiment. For the aircraft case, "surface truth" was usually obtained at the beginning and the end of the flight which resulted in observations separated by 3 to 4 h. During these measurements, flight lines about 30 km long were flown at low altitudes (100–150 m) in the upwind and downwind directions. Wind speed and direction measurements were obtained from the aircraft inertial navigation system (Litton LTN-51), and wave measurements were obtained from a laser profilometer (Spectra-Physics Geodolite 3A).

From electromagnetic (Bragg) scattering theory, the RADSCAT radar return for incidence angles tens of degrees off nadir is proportional to the spectrum of water waves a few centimeters long. Although the open ocean measurement of these short waves is currently beyond the state of the art, researchers usually use wind speed measurements within the surface boundary layer for surface truth. These wind speed measurements can be used to infer the wind stress at the sea surface, which is the generating force of the resulting short waves. To be consistent with previous investigators, the "surface" wind measurements are presented at 19.5 m altitude. The wind direction measured at 100–150 m was assumed to be the same as at 19.5 m. The wind speed, however, was extrapolated using a boundary-layer wind profile described by Cardone [10]. In this model, the wind speed was first extrapolated to the ocean's surface using the profile determined by the air-sea temperature difference and then extrapolated back to 19.5 m using a logarithmic profile for zero air-sea temperature differential (neutral stability conditions).

This procedure produces a wind speed that would have been measured at 19.5 m in a neutrally stratified atmosphere with an adiabatic lapse rate. Moreover, this wind speed is proportional to the surface wind stress rather than the actual wind at 19.5 m. During the flight the required air and sea surface temperatures were measured using a Barnes PRT-5 infrared radiometer (sea surface temperature)

TABLE I
SURFACE TRUTH DATA AND SOURCES

Mission/flight date	Mean test location		19.5 m wind vector		Wind vector source	RMS wave height, m	Wave height source
	Latitude	Longitude	Speed, m/s	Direction			
230/FCF April 11, 1973	38.1°	-73.1°	13.5 to 15.0	270° to 290°	Wind hindcast (supplemented with inertial navigator)	0.69 to 1.07	Wave hindcast
238/20 June 5, 1973	25°	-92.6°	6.5	130°	Inertial navigator	0.29 to 0.31	Laser
238/27 June 11, 1973	26.5°	-89.3°	3.0	100°	Inertial navigator	0.08 to 0.15	Laser
288/2 Nov. 11, 1974	57.5°	1.9°	23.6	228°	Inertial navigator	1.4	DFS*
288/6 Nov. 14, 1974	56.3°	3.5°	13.47	180°	Inertial navigator	1.04 0.83	Laser DFS

*Technique described in. Weissman, D. E., and Johnson, J. W.: Dual Frequency Radar Measurements of the Height Statistics of Ocean Waves. Paper in this issue.

and a Rosemont model 103 temperature sensor (total air temperature).

The aircraft derived ocean wave height was computed from the laser profilometer time series; however, a subjective analysis was required to eliminate errors caused by short-term aircraft altitude variations during the laser measurements. The procedure was to perform a Fourier analysis and produce a wave height spectrum. Next, the spectrum was examined to estimate the high-frequency cutoff of altitude changes (typically 0.3 Hz) and the low-frequency cutoff of wave information. The laser recordings were high-pass filtered and digitized, and then transformed to a stationary coordinate system and Fourier analyzed. Finally, the corrected spectrum was integrated to yield the rms wave height.

A summary of the flight dates and locations and the "surface truth" measurements are given in Table I.

RADAR SCATTERING MEASUREMENTS

During a typical flight, σ^0 was measured as a function of radar incidence angle and polarization while the aircraft flew specific patterns. Two major types of flight lines were used and are discussed below.

A. Fixed Wind Direction Lines

These flight lines consisted of flying the aircraft "straight and level" along a constant heading with the antenna pointing in the desired direction relative to the surface wind. Flight lines where the antenna was pointing into the wind were designated upwind, with the wind were designated downwind, and 90° azimuth with respect to the wind were designated crosswind. It should be noted that the winds at the RADSCAT measurement altitudes were usually not aligned with surface winds. The aircraft, therefore, experienced yaw and cross track drift. Although this produced a ground track which was diagonal to the surface winds, the antenna azimuth during the line was in the proper direction. Generally, the flight lines were flown at 3000 m, the maximum altitude tolerable without aircraft pressurization, to provide the largest antenna footprint and greatest spatial sample of ocean surface.

A study of aircraft radar sea return by Pierson and Moore [11] was used to define the RADSCAT flight line length requirements. They showed that for numerical weather prediction, the desired quantity is the mean synoptic scale wind. For a surface anemometer, this corresponds to wind measurements that have been averaged for tens of minutes to remove the microscale turbulence in the planetary boundary-layer wind field. They estimated the equivalent averaging time for an airborne radar using the Taylor's hypothesis.

From this analysis, the aircraft measurement time T_{ac} was given by

$$T_{ac} = \frac{T_{an} v_0}{v \pm v_0}$$

where

- T_{an} equivalent anemometer measurement time,
- v_0 mean wind speed,
- v aircraft velocity,
- $+$ upwind,
- $-$ downwind.

For a typical case with wind speed of 10 m/s and aircraft velocity of 100 m/s, the required aircraft measurement time is about one-tenth that of the anemometer

Based on typical correlation lengths in the atmosphere, for the RADSCAT measurement, statistically independent samples are defined to be those separated by 600 m. Assuming an aircraft ground speed of 100 m/s and the above sample length, the aircraft measurement time was converted to the number of independent samples that must be averaged. The results are plotted in Fig. 3 versus mean wind speed for upwind and downwind flight lines.

Typical flight lines were 50 km length and 8 min duration. While on line, the scatterometer polarization alternated

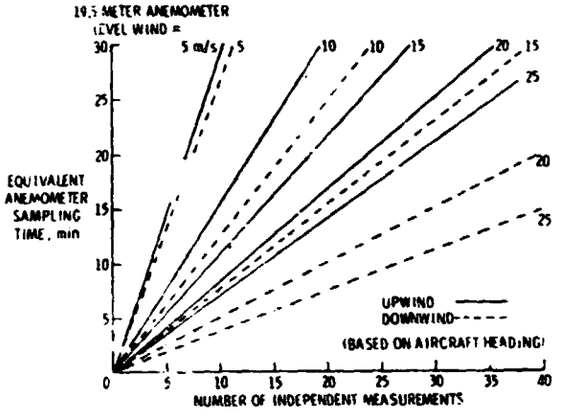

Fig. 3. Number of independent measurements required to sample mean synoptic wind speed.

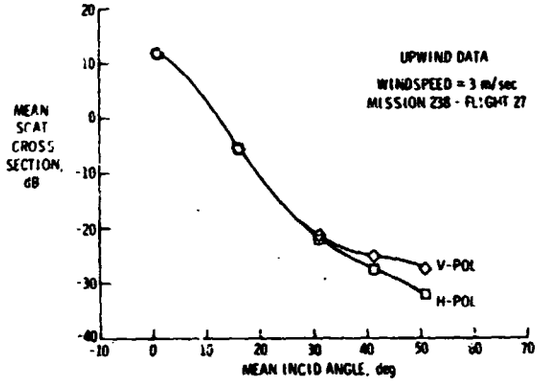

Fig. 4. Upwind σ^0 versus incidence angle for low wind speed.

between vertical and horizontal every 3 s and the antenna elevation angle was stepped every 30 s. The lines were generally repeated until a minimum of an equivalent 10-min anemometer average was obtained. For each incidence angle and polarization, σ^0 (in ratio form) from upwind, downwind, and crosswind lines were averaged, respectively. These mean scattering coefficients were then converted to decibels and plotted versus incidence angle to produce the scattering signature for that wind speed and flight direction. A typical plot for upwind observation and a low surface wind speed is shown in Fig. 4. The symbols are the experimental data, and the curves are computer-generated fourth-order polynomials through the data. The values of σ^0 for both polarizations are nearly equal from nadir to about 25° incidence angle, but at higher angles, $\sigma_{VV}{}^0$ (transmit/receive vertical) becomes increasingly greater than $\sigma_{HH}{}^0$ (transmit/receive horizontal). The shape of the curves from near the nadir to about 15° agree with those predicted by geometric optics scattering theory. Beyond 30°, the separation of the polarized scattering coefficients and the general shape of the curves agree qualitatively with first-order Bragg scattering calculations.

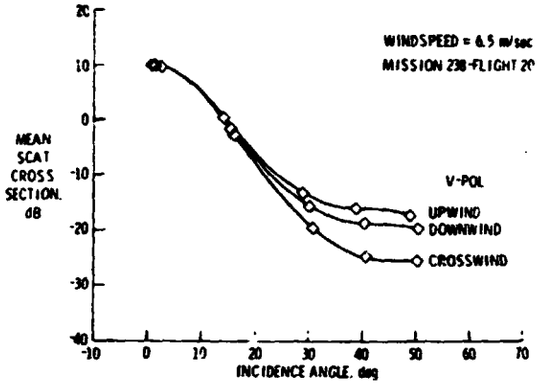

Fig. 5. Upwind, downwind, and crosswind σ^0 versus incidence angle.

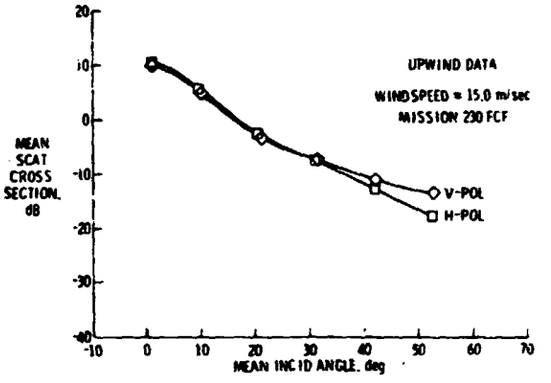

Fig. 6. Upwind σ^0 versus incidence angle for higher wind speed.

The effect of changing antenna azimuth relative to the surface wind direction is demonstrated in Fig. 5. Here, upwind, downwind, and crosswind scattering characteristics are presented for the same flight and nearly constant wind conditions. As would be expected, these measurements are approximately equal at the nadir; but in the Bragg scattering region, the three scattering characteristics are different. The magnitude is maximum for upwind and minimum for crosswind. As will be shown in a later section, this sensitivity of σ^0 to radar azimuth (flight direction) enables one to infer wind direction from scatterometer measurements.

The upwind scattering signature for a higher wind speed is shown in Fig. 6. The shape of these curves is similar to those of Figs. 4 and 5; although the range of σ^0 versus angle is considerably less for this higher wind speed case. For example, compared to Fig. 4, the scattering coefficient at nadir has decreased 3 dB; while at 50° both the horizontal and vertical values have increased about 14 dB. These examples illustrate the apparent sensitivity of the ocean scattering signature to wind speed which is the basis for the wind speed remote-sensing technique.

RADSCAT ocean scattering signature measurements have been obtained over a wind speed range of 3 to 24 m/s. Data from fixed wind direction lines from five flights are tabulated in Table II. The normalized standard deviation

TABLE II
STATISTICS OF SCATTERING COEFFICIENT, σ^0

(a) [illegible] m/s

Antenna position	H-POL θ mean	H-POL θ std dev	H-POL σ^0 mean, dB	H-POL $\frac{\Delta\sigma^0}{\sigma^0}$ *	H-POL σ^0 error, ±dB	H-POL No. independent samples	V-POL θ mean	V-POL θ std dev	V-POL σ^0 mean, dB	V-POL $\frac{\Delta\sigma^0}{\sigma^0}$ *	V-POL σ^0 error, ±dB	V-POL No. independent samples
Upwind 1	1.26	0.38	11.87	17.52	0.72	42	1.25	0.39	11.51	17.37	0.72	42
Upwind 2	16.45	0.49	-5.90	25.98	0.27	39	16.46	0.48	-6.21	26.62	0.27	39
Upwind 3	31.37	0.48	-22.24	32.65	0.38	36	31.36	0.49	-21.59	28.59	0.37	36
Upwind 4	41.43	0.33	-27.20	26.28	1.23	40	41.42	0.33	-24.67	23.19	1.12	38
Upwind 5	51.32	0.35	-31.96	42.52	2.12	37	51.32	0.34	-26.80	35.29	1.66	37
Downwind 1	0.82	0.22	12.49	18.24	0.76	7	0.77	0.19	12.16	18.80	0.76	8
Downwind 2	16.07	0.29	-3.66	25.19	0.30	8	16.08	0.31	-4.09	27.23	0.30	8
Downwind 3	31.24	0.31	-21.17	23.96	0.37	8	31.26	0.28	-20.07	23.46	0.36	8
Downwind 4	41.10	0.23	-27.38	30.70	1.23	6	41.08	0.20	-23.83	23.37	0.80	8
Downwind 5	50.74	0.40	-33.05	33.86	1.93	6	50.69	0.43	-26.83	30.16	1.45	6
Crosswind 1	0.69	0.34	13.44	12.04	0.72	15	0.94	0.40	12.86	13.13	0.72	31
Crosswind 2	16.19	0.28	-4.46	30.57	0.27	8	16.32	0.35	-5.79	49.99	0.27	24
Crosswind 3	31.16	0.28	-24.36	15.51	0.95	8	30.95	0.31	-22.80	45.66	0.[illegible]	24
Crosswind 4	41.41	0.18	-30.22	15.24	1.32	4	40.94	0.35	-26.30	61.40	1.23	19
Crosswind 5	51.60	0.24	-32.31	25.49	4.07	4	51.11	0.35	-26.96	65.85	2.49	19

(b) 6.5 m/s

Antenna position	H-POL θ mean	H-POL θ std dev	H-POL σ^0 mean, dB	H-POL $\frac{\Delta\sigma^0}{\sigma^0}$ *	H-POL σ^0 error, ±dB	H-POL No. independent samples	V-POL θ mean	V-POL θ std dev	V-POL σ^0 mean, dB	V-POL $\frac{\Delta\sigma^0}{\sigma^0}$ *	V-POL σ^0 error, ±dB	V-POL No. independent samples
Upwind 1	1.10	0.76	11.19	27.53	[illegible]	64	0.89	0.53	11.17	20.43	[illegible]	49
Upwind 2	15.61	0.87	-0.38	40.17	0.29	66	15.75	0.74	-0.92	41.50	0.29	63
Upwind 3	30.29	0.88	-14.78	29.68	0.37	51	30.31	0.88	-14.19	26.49	0.37	51
Upwind 4	40.39	0.99	-19.65	28.68	0.43	56	40.39	0.99	-17.90	29.85	0.42	54
Upwind 5	50.23	0.96	-22.76	22.66	1.88	53	50.21	0.96	-18.06	29.20	1.55	54
Downwind 1	1.06	0.64	9.67	12.44	0.[illegible]0	15	1.05	0.60	9.39	16.02	0.69	15
Downwind 2	15.43	0.54	-1.07	24.70	0.35	7	15.43	0.47	-1.57	16.72	0.35	8
Downwind 3	30.69	0.51	-17.42	21.27	0.[illegible]6	10	30.52	0.51	-16.00	20.27	0.36	9
Downwind 4	40.81	0.56	-23.22	17.21	0.46	12	40.80	0.57	-18.89	15.03	0.38	12
Downwind 5	50.63	0.50	-26.26	18.92	1.66	10	50.87	0.48	-20.00	20.43	1.06	10
Crosswind 1	1.34	0.23	11.[illegible]	26.08	0.67	8	1.37	0.22	10.77	26.48	0.64	8
Crosswind 2	16.03	0.25	-1.23	32.23	0.31	[illegible]	16.08	0.24	-1.56	32.33	0.30	7
Crosswind 3	30.77	0.18	-18.55	16.72	0.36	6	30.76	0.14	-18.52	15.15	0.36	5
Crosswind 4	40.75	0.26	-24.18	11.40	1.21	9	40.73	0.26	-23.57	13.59	0.44	9
Crosswind 5	50.31	0.41	-28.44	18.61	1.32	9	50.29	0.44	-24.31	14.06	1.31	9

(c) 13.47 m/s

Antenna position	H-POL θ mean	H-POL θ std dev	H-POL σ^0 mean, dB	H-POL $\frac{\Delta\sigma^0}{\sigma^0}$ *	H-POL σ^0 error, ±dB	H-POL No. independent samples	V-POL θ mean	V-POL θ std dev	V-POL σ^0 mean, dB	V-POL $\frac{\Delta\sigma^0}{\sigma^0}$ *	V-POL σ^0 error, ±dB	V-POL No. independent samples
Upwind 1	0.12	0.64	9.12	10.60	0.59	11	0.12	0.64	9.04	10.04	0.59	11
Upwind 2	10.58	0.56	5.60	9.31	0.30	14	10.56	0.58	5.54	10.68	0.30	15
Upwind 3	23.35	0.48	-2.82	12.70	0.35	14	23.40	0.50	-2.65	13.52	0.34	14
Upwind 4	32.72	0.64	-9.[illegible]	12.37	0.37	17	32.70	0.64	-8.60	10.26	0.39	14
Upwind 5	42.17	0.78	-13.[illegible]	14.10	1.50	18	42.13	0.72	-11.03	11.84	1.49	19
Upwind 6	51.69	0.58	-16.50	14.02	2.24	20	51.70	0.53	-12.29	11.37	1.98	19
Downwind 1	0.11	0.54	9.51	8.56	0.59	11	0.11	0.58	9.41	9.07	0.59	9
Downwind 2	10.76	0.47	6.50	8.93	0.37	12	10.77	0.47	6.36	9.98	0.37	12
Downwind 3	23.34	0.44	-3.43	11.89	0.42	14	23.34	0.43	-2.73	10.89	0.37	15
Downwind 4	32.98	0.43	-11.46	14.99	0.40	19	32.93	0.46	-9.79	14.50	0.40	15
Downwind 5	42.25	0.45	-17.06	19.76	0.45	20	42.30	0.52	-13.26	16.77	0.37	15
Downwind 6	51.73	0.49	-21.59	14.59	1.22	19	51.80	0.51	-16.00	12.39	0.41	16
Crosswind 1	1.04	0.27	9.26	10.83	0.55	10	1.06	0.27	9.34	11.28	0.55	10
Crosswind 2	11.51	0.27	4.76	9.00	0.29	15	11.50	0.26	4.97	9.33	0.29	15
Crosswind 3	24.26	0.35	-7.24	11.57	0.39	13	24.26	0.33	-6.91	11.67	0.39	14
Crosswind 4	34.07	0.65	-15.08	12.82	0.42	15	33.97	0.56	-13.57	10.82	0.40	17
Crosswind 5	43.14	0.43	-20.75	17.44	1.93	17	43.14	0.46	-17.42	13.61	1.56	18
Crosswind 6	52.69	0.63	-24.79	23.90	2.62	20	52.70	0.60	-19.45	27.13	2.58	19

*Normalized standard deviation, percent.

TABLE II *Continued*

(d) 15 m/s

Antenna position	H-POL θ_{mean}	$\theta_{std\ dev}$	σ^o_{mean}, dB	$\frac{\Delta\sigma^o}{\sigma^o}$ *	σ^o_{error}, ±dB	No. independent samples	V-POL θ_{mean}	$\theta_{std\ dev}$	σ^o_{mean}, dB	$\frac{\Delta\sigma^o}{\sigma^o}$ *	σ^o_{error}, ±dB	No. independent samples
Upwind 1	1.33	0.56	10.41	13.30	0.75	13	1.28	0.51	9.96	15.68	0.74	18
2	9.39	0.55	5.78	19.97	0.38	18	9.61	0.62	5.07	10.91	0.33	15
3	20.51	0.69	-2.82	28.84	0.26	14	20.84	0.62	-3.41	30.85	0.28	15
4	31.07	0.51	-7.94	24.76	0.29	13	31.09	0.87	-7.39	22.09	0.32	14
5	42.18	0.79	-13.18	32.01	1.04	15	42.01	0.79	-10.91	24.15	1.05	16
6	52.78	0.70	-17.65	29.91	1.88	20	52.67	0.49	-13.71	15.58	1.84	18
Crosswind 1	1.42	0.55	9.69	18.25	0.77	6	1.76	0.34	9.55	18.13	0.74	6
2	8.91	0.40	5.55	35.59	0.39	10	9.12	0.39	5.28	14.31	0.39	6
3	20.29	0.81	-5.17	24.04	0.29	6	19.81	0.66	-4.76	26.47	0.29	6
4	30.78	0.35	-11.27	23.41	0.36	6	30.83	0.43	-10.95	14.83	0.36	8
5	41.80	0.16	-16.04	20.44	0.38	6	42.08	0.44	-14.07	18.00	0.71	7
6	52.56	0.10	-20.35	21.06	1.02	8	52.76	0.34	-16.98	13.54	1.05	7

(e) 23.6 m/s

Antenna position	H-POL θ_{mean}	$\theta_{std\ dev}$	σ^o_{mean}, dB	$\frac{\Delta\sigma^o}{\sigma^o}$ *	σ^o_{error}, ±dB	No. independent samples	V-POL θ_{mean}	$\theta_{std\ dev}$	σ^o_{mean}, dB	$\frac{\Delta\sigma^o}{\sigma^o}$ *	σ^o_{error}, ±dB	No. independent samples
Upwind 1	0.41	0.75	6.93	10.60	0.54	9	0.35	0.78	6.67	8.58	0.53	9
2	10.50	0.65	4.24	13.53	0.29	10	10.55	0.64	4.76	13.85	0.30	10
3	23.30	0.31	-1.75	11.71	0.31	9	23.31	0.32	-1.72	13.43	0.30	10
4	32.81	0.29	-6.07	15.16	0.51	8	32.85	0.30	-5.44	12.49	0.59	9
5	42.09	0.46	-8.10	12.80	2.99	8	42.42	0.44	-6.97	10.83	2.10	7
6	51.85	0.59	-10.53	12.35	1.73	10	51.88	0.58	-8.29	7.96	1.32	10
Downwind 1	1.03	0.86	6.58	15.16	0.54	17	1.05	0.80	6.54	14.67	0.54	16
2	11.71	0.63	4.78	17.79	0.32	17	11.66	0.65	4.82	20.63	0.32	18
3	24.34	0.71	-2.38	22.88	0.50	15	24.35	0.71	-1.90	22.69	0.28	14
4	34.08	0.61	-7.84	12.49	0.46	19	34.18	0.55	-6.52	17.70	0.50	18
5	42.94	0.86	-11.41	14.62	0.36	21	42.94	0.86	-9.37	12.48	0.38	21
6	52.56	0.89	-15.25	14.49	0.37	23	52.55	0.86	-12.31	11.91	0.36	23
Crosswind 1	0.30	0.14	6.38	12.56	0.53	16	0.27	0.14	6.38	10.16	0.53	17
2	11.17	0.79	3.50	12.01	0.37	14	11.19	0.77	3.64	12.13	0.37	13
3	23.92	0.68	-5.14	14.34	0.39	12	23.88	0.69	-4.52	12.31	0.36	14
4	33.29	0.66	-10.73	13.51	0.41	17	33.35	0.68	-9.67	12.78	0.43	16
5	42.62	0.58	-14.66	18.04	0.36	17	42.63	0.57	-12.45	14.23	0.36	17
6	52.36	0.77	-18.07	14.79	0.43	16	52.29	0.74	-14.64	13.21	0.37	17

*Normalized standard deviation, percent.

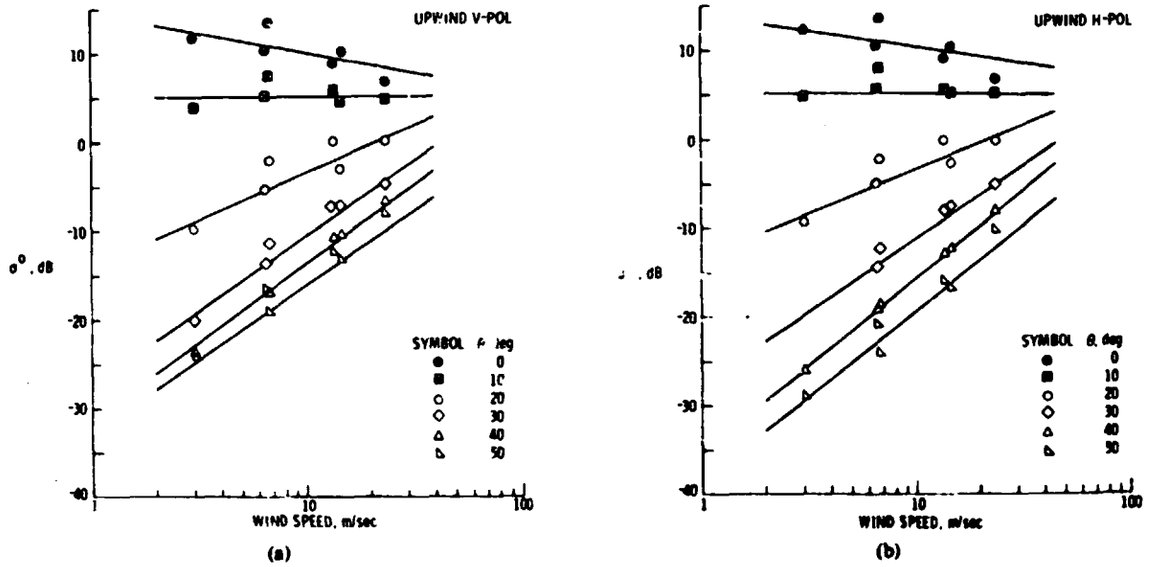

Fig. 7. σ^o versus wind speed for constant incidence angles and wind direction. (a) Upwind, V-POL. (b) Upwind, H-POL. (c) Downwind, V-POL. (d) Downwind, H-POL. (e) Crosswind, V-POL. (f) Crosswind, H-POL.

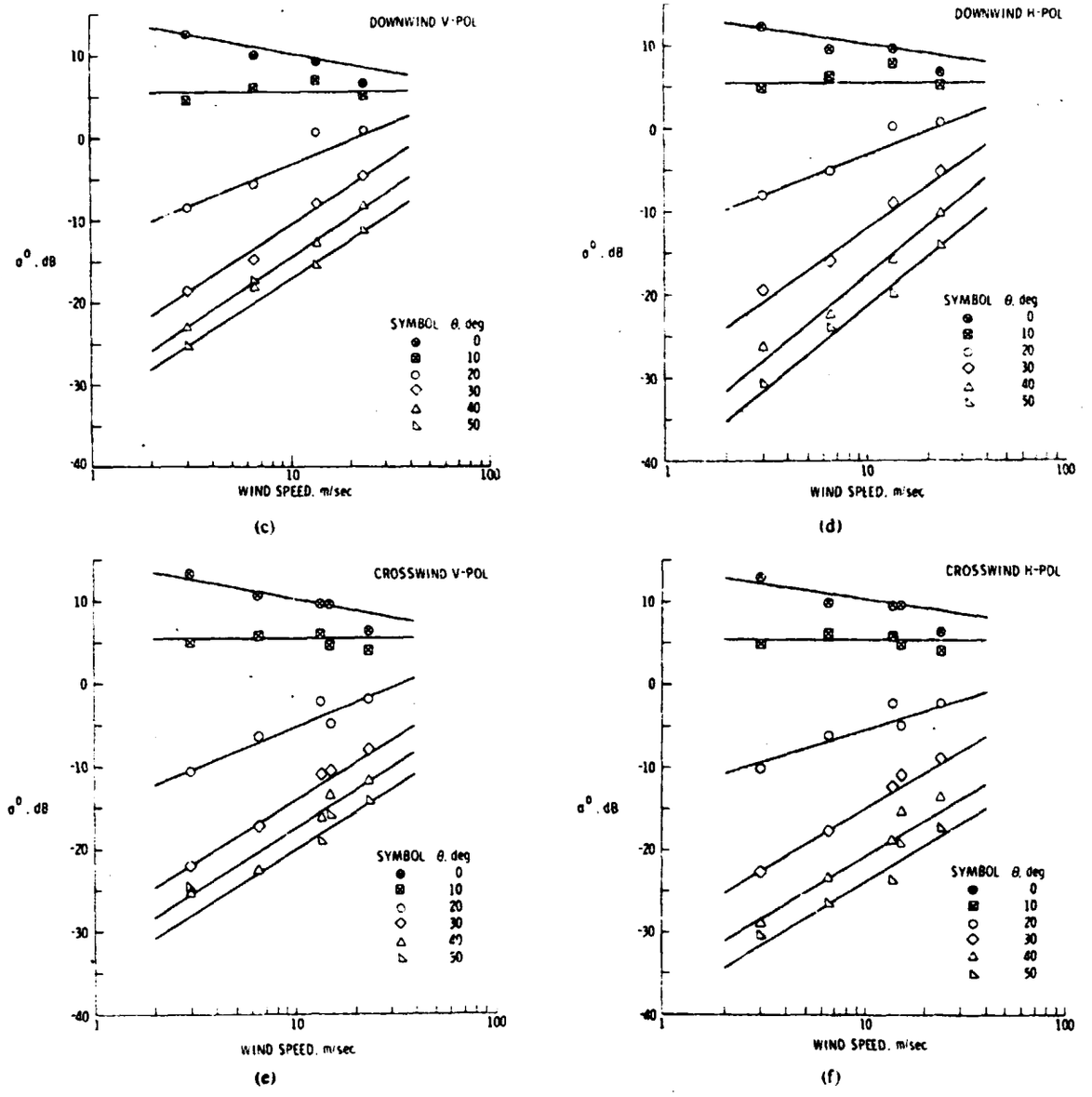

Fig. 7. *Continued.*

of the σ^0 measurements is the result of two random processes. The first is the "Rayleigh fading" of the radar return which for the number of radar measurements averaged and for the scatterometer integration times is typically 5 to 15 percent. The remaining scatter is produced by the natural fluctuation of the ocean surface σ^0 with wind turbulence. Also included in Table II are the number of independent radar samples used to produce the mean and the rms relative error in the mean σ^0 due to RADSCAT and aircraft attitude/altitude measurement inaccuracies [12]. In addition, all cross sections include a bias which was determined in absolute calibrations of the RADSCAT using precision spheres and discussed in [13]. The level of this bias is -2.40 dB, with an rms uncertainty of ± 0.72 dB. Furthermore, for mission 288 flights 5 and 6, the data have been decreased by an additional 0.33 dB bias, required because the absolute calibration factor of [13] was for a different instrument configuration. The bias level is the amount required to match σ^0 at 10° incidence for these flights to that for previous flights.

To show the wind speed dependence, the data of Table II are also presented in a modified form in Fig. 7. Here, upwind, downwind, and crosswind σ^0 values are displayed versus the neutral stability 19.5 m wind speed for constant

TABLE III
WIND SPEED POWER COEFFICIENTS

Frequency	Direction	Polarization	Exponent	Incidence angle, θ					
				0°	10°	20°	30°	40°	50°
13.9 GHz	Upwind	VV	v	-0.46	0	1.05	1.68	1.77	1.66
	Downwind			-0.46	0	.98	1.56	1.62	1.55
	Crosswind			-0.46	0	.98	1.49	1.52	1.51
13.9 GHz	Upwind	HH	v	-0.36	0	1.00	1.65	1.98	1.93
	Downwind			-0.36	0	.94	1.68	1.97	1.96
	Crosswind			-0.36	0	.75	1.45	1.46	1.48

incidence angles. Note that these data are plotted in log-log form (scattering coefficient in decibels versus wind speed on a logarithmic scale). The data in Fig. 7 are interpolated values from the respective scattering signatures.

These data conform to a power law wind speed response such that

$$\sigma^0 = AU^v$$

where

- σ^0 scattering coefficient in ratio form,
- A a constant,
- U wind speed,
- v wind speed power coefficient.

The wind speed power coefficients derived from analyses of these data in Fig. 7 are presented in Table III. It is noted that the present coefficients were obtained using more data, and, hence, are better than those of [14]. However, these differences are not significant as far as the satellite instrument design is concerned.

B. Wind Circle Lines

These flight lines were conducted to measure the anisotropic scattering characteristic of the ocean. During these measurements, the RADSCAT antenna was pointed to the nadir (perpendicular to the aircraft pitch and longitudinal axes) and then the aircraft was flown in a series of high banked 360° turns. This resulted in the antenna being conically scanned over the ocean's surface at an incidence angle equal to the aircraft bank (roll) angle (nominally 30°–40°). Scattering data from these lines were averaged in azimuth over 10° sectors, and typically five or more circles were flown to obtain a statistically representative sample. Aerodynamic disturbances during the 360° turns caused the aircraft bank angle and, hence, the radar incidence angle to vary by several degrees. The scattering data were corrected for these incidence angle changes by computing the instantaneous incidence angle and then adjusting the value of σ^0 (using the interpolated correction factor from the upwind, downwind, and crosswind scattering characteristics) to correspond to that value for the desired incidence angle. In general, these σ^0 corrections were sinusoidal in azimuth and were less than 1 dB in magnitude.

Anisotropic scattering characteristics for three flights are shown in Fig. 8. The abscissa is the radar azimuth relative to the crosswind direction. Again, the larger σ^0 values are associated with the higher wind speed. The

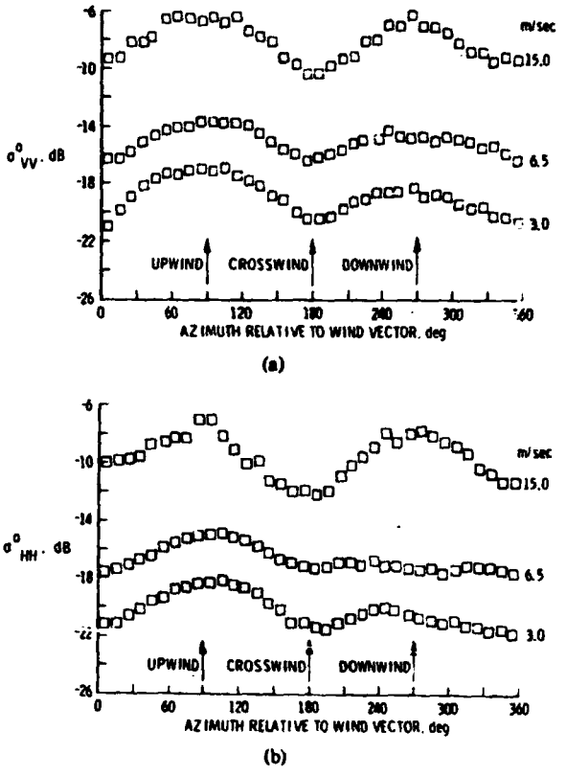

Fig. 8. Anisotropic scattering characteristics for 30° incidence measurements during flights at three different wind speeds. (a) Vertical polarization. (b) Horizontal polarization.

anisotropic scattering characteristic is a quasi-sine of twice the azimuth angle curve with the peaks in the upwind and downwind directions and the minima in the crosswind. Additionally, the upwind peak is slightly greater than the downwind peak. These data illustrate the potential of obtaining both wind speed and wind direction from multilook (azimuth) radar measurements of the ocean's surface.

Concluding Remarks

Microwave backscatter signatures of the ocean have been measured from a C-130 aircraft using the RADSCAT scatterometer. The σ^0 measurements were obtained for both vertical and horizontal polarizations as a function of incidence angle and azimuth angle relative to surface winds over a range of surface wind speeds from 3 to 23.6 m/s.

The ocean scattering coefficient for a given polarization and incidence angle exhibits a power-law dependence on wind speed. For these data, the effects of fetch and nonlinear wave interactions have not been investigated. These effects must be considered in a complete model and are the subject of continuing research. The aircraft data reported here suggest that to the first order, microwave scatterometers can be used to infer surface wind vector over the ocean. In fact, these results have been used for the design [14] of a satellite instrument to be flown in 1978 on the first NASA oceanographic satellite—SeaSat-A.

References

[1] P. Beckmann and A. Spizzichino, *The Scattering of Electromagnetic Waves From Rough Surfaces*. New York: Macmillan, 1963.

[2] M. Skolnik, "A review of radar sea echo," Memo. Rep. 2025, July 1969, U.S. Naval Research Lab., Washington, D.C. (Available from DDC as AD693452.)

[3] N. W. Guinard and J. C. Daley, "An experimental study of sea clutter model," *Proc. IEEE*, vol. 58, no. 4, pp. 543–550, April 1970.

[4] G. R. Valenzuela, M. B. Laing, and J. C. Daley, "Ocean spectra for the high frequency waves as determined from airborne radar measurements," *Journal of Marine Research*, vol. 29, no. 2, pp. 69–84, May 1971.

[5] J. Daley, "An empirical sea clutter model," NRL Memo. Rep. 2668, U.S. Navy, Oct. 1973.

[6] K. Krishen, "Correlation of radar backscattering cross sections with ocean wave height and wind velocity," *J. Geophys. Res.*, vol. 76, pp. 6528–6539, Sept. 20, 1971.

[7] G. A. Bradley, "Remote sensing of ocean winds using a radar scatterometer," Ph.D. dissertation, University of Kansas Center for Research, Inc., Sept. 1971.

[8] R. K. Moore and W. J. Pierson, Jr., "Worldwide oceanic wind and wave predictions using a satellite radar radiometer," *Journal of Hydronautics*, vol. 5, no. 2, pp. 52–60, April 1971.

[9] L. C. Schroeder, W. L. Jones, Jr., and J. L. Mitchell, "RADSCAT calibration data report," NASA TM X-73900, 1976.

[10] V. J. Cardone, "Specification of the wind distribution in the marine boundary layer for wave forecasting," Report TR 69-1, New York University School of Engineering and Science, University Heights, New York 10453, March 1970. (Available as DDS No. AD702 490.)

[11] W. J. Pierson and R. K. Moore, "The extrapolation of laboratory and aircraft radar sea return data to spacecraft altitudes," in *Proc. Fourth Annual Earth Resources Review*, NASA-JSC, Houston, Texas.

[12] W. L. Jones, M. Komen, and L. C. Schroeder, "RADSCAT error analysis," NASA TM X-72743, 1976.

[13] W. L. Grantham, L. C. Schroeder, and J. L. Mitchell, "Absolute calibration of the RADSCAT scatterometer using precision spheres," NASA TN D-8259, 1976.

[14] W. L. Grantham *et al.*, "An operational satellite scatterometer for wind vector measurements over the ocean," NASA TM X-72672, March 1975.

The SeaSat-A Satellite Scatterometer

WILLIAM L. GRANTHAM, MEMBER, IEEE, EMEDIO M. BRACALENTE,
W. LINWOOD JONES, SENIOR MEMBER, IEEE, AND JAMES W. JOHNSON

Abstract—This paper describes the methods used to develop performance requirements and design characteristics for the microwave scatterometer (SASS)[1] ocean-surface wind sensor on the NASA SeaSat-A satellite. Wind vector measurement requirements from the SeaSat user community such as wind speed and direction accuracy, resolution cell size, grid spacing, and swath width formed the basis for defining instrument characteristics. The resulting scatterometer is designed for 14.6 GHz using four fan beam antennas to measure wind speed and direction over a 1000-km swath width with a resolution cell size 50 × 50 km. Results presented show scatterometer accuracy satisfies user requirements for wind speed from 4 m/s to greater than 24 m/s for the nominal SeaSat-A orbit of 790 km altitude, 108° inclination, and 0.001 eccentricity.

I. INTRODUCTION

GLOBAL MEASUREMENT of ocean winds has been established by the SeaSat-A user panel as one requirement of the oceanographic satellite program [1]. Surface winds are required as inputs to ocean wave forecast models and can also be helpful in weather forecasting. The lack of sufficient wind and pressure data over the oceans has thus far precluded better long-range weather forecasting for continental areas.

Microwave scatterometers have been shown to be sensitive to surface winds in previous aircraft programs and the Skylab S-193 experiment [2]-[6]. The scatterometer wind sensor[1] will be used on the SeaSat-A satellite along with the following remote sensors (Fig. 1): a radar altimeter, an imaging radar, and microwave and infrared/optical radiometers. Together, this complement of instruments will provide the SeaSat-A user community with scientific and operational-type data in the areas of oceanography, meteorology, and geodesy. Several configurations of the scatterometer were considered so that tradeoffs could be made in designing the overall payload. The scatterometer options[2] included fan beam antenna systems, scanning pencil beams, and mixtures of the two. Decisions have now been made to use a fixed fan beam antenna design combined with electronic Doppler filtering to achieve the swath width and resolution cell size required by the user panel.

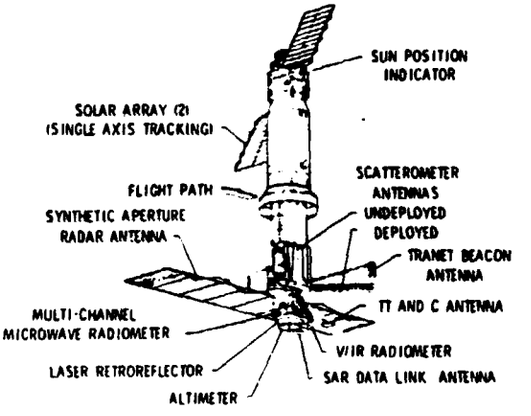

Fig. 1. SeaSat-A satellite configuration.

Special attention was also given to instrument require-

Manuscript received October 8, 1976; revised December 16, 1976

The authors are with the NASA Langley Research Center, Hampton, VA.

[1] SeaSat-A Satellite Scatterometer, SASS.

[2] The reader is referred to [7, ch. 25] for a description of microwave scatterometry technique.

ments so that data would be available to improve future scatterometer designs and provide a broad data base to improve understanding of microwave backscatter from the sea. A comprehensive description of ocean backscattering mechanisms has been compiled by Ruck *et al.* [8] and will not be discussed here.

II. INSTRUMENT DESCRIPTION

A. General

A block diagram of the SeaSat scatterometer is shown in Fig. 2. This system uses a frequency synthesizer to generate the RF signals needed by the transmitter, mixers, and scatterometer processor, thus assuring coherency throughout the sensor. The low-level microwave output of the synthesizer is amplitude gated to insure high isolation (typically ≥ 60 dB) between the ON and OFF states. The pulsed RF is then amplified in the final output stage by a traveling-wave tube amplifier. The 100-W peak power output pulse is directed to the antennas through a series of waveguide components, circulators, and a 1 × 8 waveguide switching matrix. Each antenna has two ports, one for each polarization, which are switched in a preset fashion by the timing and control electronics.

Received RF energy from the proper antenna is directed through the eight-way switch, the *T/R* circulator, and receiver protection circulator to the low-noise preamplifier, bandpass filter, and first conversion mixer (Fig. 2). A local oscillator signal is added to the return signal in the mixer to produce a coherent IF signal which is then fed to the scatterometer processor. The scatterometer processor contains an IF amplifier, a second IF conversion mixer, and 15 processing channels. Each processing channel consists of a range gate, bandpass Doppler filter, square-law detector, and gated signal integrator. Fifteen Doppler filters and range gates are used to electronically subdivide the fan beam into separate resolution cells and to exclude interfering signals from the side lobes. The timing and control for the processor are provided by a digital controller (not shown).

The function of the digitial controller is to accept spacecraft commands and power, to generate the precise timing and control logic needed by the scatterometer to form RF pulses, and operate the processor. In addition, it accepts the scatterometer science data and instrument housekeeping parameters and formats them so they are compatible with the spacecraft data system.

The scatterometer design incorporates four dual polarized antennas which produce a starlike pattern of illumination on the earth (Fig. 3). The peak of the antenna beam is centered at 47° incidence angle to favor the outer swath section where the received signals are weaker due to increased range and lower ocean scattering coefficient σ°. Three Doppler cells provide measurements at earth incidence angles of 0, 4, and 8° to form the 140-km measurement swath centered about the satellite subtrack. Twelve additional Doppler cells will provide σ° values from about 25-65° earth incidence on each side of the subtrack. The effect of earth rotation does cause incidence

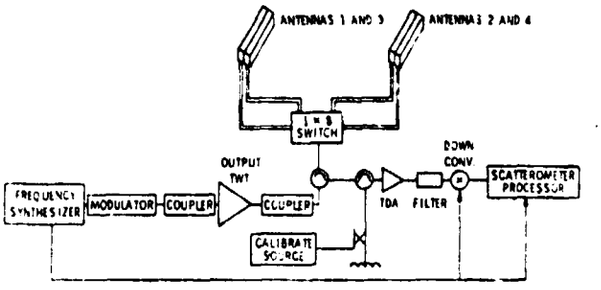

Fig. 2. Scatterometer block diagram.

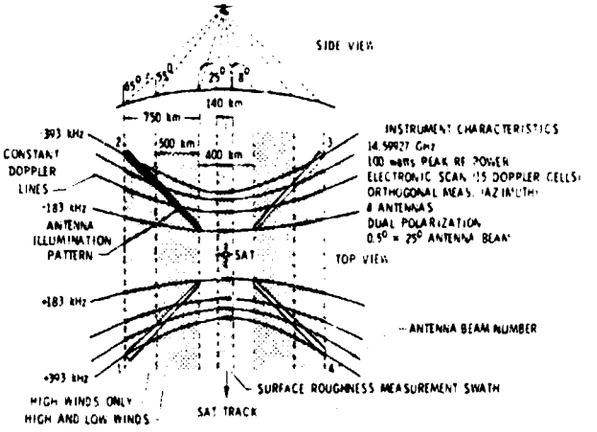

Fig. 3. SeaSat scatterometer characteristics.

angles to change typically 4° during each orbit, but the primary swath width is affected only in a minor way.

The 14.6-GHz signal is switched sequentially through four antenna-polarization combinations taking 1.89 s each for a total 7.56 s to complete one switching sequence. A switching local oscillator is used to allow both positive and negative returning frequencies from the forward and aft footprints to be received by the same bank of 15 Doppler filters. The nine operating modes for the instrument are listed in the table below.

Mode	Measurement Time (Seconds)	Polarization[3] Sequence	Antenna Sequence
1	1.89	VV	1, 2, 3, 4
2	1.89	HH	1, 2, 3, 4
3	1.89	VV, HH	3, 4
4	1.89	VV, HH	1, 2
5	1.89	VV, VV	3, 4
6	1.89	VV, VV	1, 2
7	1.89	HH, HH	3, 4
8	1.89	HH, HH	1, 2
9	Calibrate mode - not polarization or antenna related		

The antenna numbering convention is defined in Fig. 3. Modes 1 and 2 are single polarization measurements over the

[3] VV = Transmit vertical polarizations and receive vertical polarizations. NH = Transmit horizontal polarizations and receive horizontal polarizations.

full swath, modes 3 and 4 are dual polarization measurements over one-half swath, and modes 5-8 are single polarization measurements over one-half swath which allows doubled integration time (through ground computer processing) for improved accuracy without significantly increasing the resolution cell size. The fundamental cycle is through the antenna positions such that in modes 3 and 4, both vertical and horizontal polarization measurements are made before switching antenna positions. A summary of instrument characteristics is given in Fig. 3.

B. Ocean Scattering Coefficient Measurement

The received RF pulses backscattered from the ocean surface will be processed for each Doppler channel using a method described by Grantham *et al.* [9] and Fisher [10] to yield the mean ocean scattering coefficient (σ°) and the error in σ° due to communication noise. In this technique, the instantaneous voltage output of the square-law detector is proportional to the amplitude of the return signal, the receiver noise, and the antenna noise. A gated integrator is used to average the detector output over a number of return pulses (61 pulses) yielding a measurement P_{S+N}, where the subscript $S + N$ refers to both signal and system noise contributing to the measured power. Following this signal-plus-noise measurement, a noise-only measurement P_N is made by integrating the detector output in the absence of radar return pulses. The average power in the received pulses P_R is

$$P_R = P_{S+N} - P_N. \tag{1}$$

The scattering coefficient is computed using the standard radar range equation which for the present satellite/fan beam Doppler scatterometer becomes

$$\sigma^\circ = \frac{(4\pi)^3 R_c^3 P_R}{\lambda^2 \phi G_0^2 \left(\frac{G}{G_0}\right)^2 l P_T L_S} \tag{2}$$

where

R_c	slant range to center of Doppler cell;
P_R	received power;
λ	free-space wavelength;
ϕ	narrow 3-dB antenna beamwidth;
G_0	peak antenna gain;
(G/G_0)	relative antenna gain to center of Doppler cell;
L	length of Doppler cell along broad antenna beamwidth;
P_T	peak transmitted power;
L_S	atmospheric and system losses.

The standard deviation of the σ° measurement divided by the mean value is called the normalized standard deviation K_p, and from [9] and [10] is

$$K_p = \left[\frac{1}{B_c \tau_{SN}}(1 + 2N/S + (N/S)^2)\left(1 + \frac{\tau_{SN}}{\tau_N}\right)\right]^{1/2} \tag{3}$$

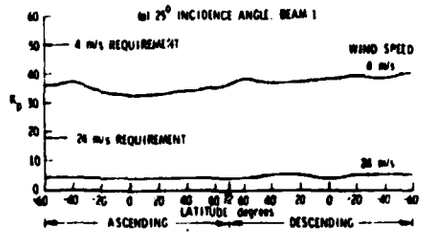

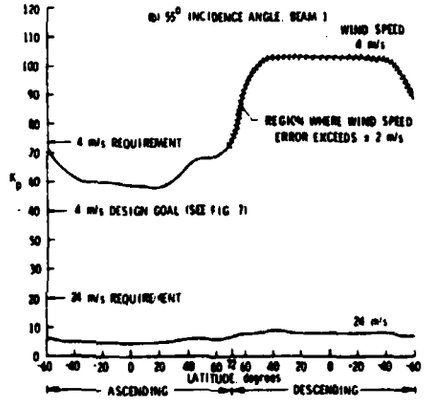

Fig. 4. Normalized standard deviation (K_p) for nominal SeaSat orbit (maximum latitude ±72°).

where

B_c	Doppler bandwidth;
τ_{SN}	integration time for radar return signal plus noise;
τ_N	integration time for noise;
N/S	$KT_s B_c / P_R$ noise-to-signal ratio at input to the square-law detector;
K	Boltzmann's constant;
T_S	system noise temperature.

For each measurement period (1.89 s), 61 RF pulses (~5 ms long) are processed which results in $\tau_{SN} \approx 300$ ms. The noise integration period is 500 ms. Because of these long integration times and large Doppler bandwidths (~20 kHz), the scatterometer provides useful measurements for $N/S \leq +10$ dB.

An analysis of expected K_p for the nominal Seasat-A orbit and a range of wind speeds (σ° values) has been performed. The results are presented in Fig. 4 for two assumed wind speeds (corresponding scattering coefficients) and incidence angles as a function of satellite subtrack latitude. In addition to communication noise errors, there are also static and dynamic uncertainties in the scatterometer from a number of sources. Fixed biases in the instrument will be removed by aircraft underflight calibration measurements with an accuracy goal of ±0.5 dB (12 percent). Dynamic system errors will be held to less than ±0.3 dB (7 percent) by sensor design. Spacecraft attitude determination capability is limited to ±0.2° in pitch and roll and ±0.5° in yaw (three sigma), which converts to a dynamic worst case one sigma error of 8 percent.

Errors due to antenna boresight uncertainty (caused by thermal expansion) will contribute 6 percent maximum over the one-year mission. The total error (root sum square) due to these other sources will be 18 percent which makes them the primary error source for high wind speeds. For low wind speeds the dominant error is due to communication noise. The SASS design satisfies user established wind speed accuracies (discussed in Section III). A minor exception should be noted for the outer portion (55° incidence) of the primary measurement zone (Fig. 4). The cross-hatch curve shows where wind speed error exceeds ±2 m/s for winds ≤4 m/s. This will have the effect of reducing the primary swath width by 10 percent or less during a portion of the orbit. However, measurement accuracy for wind speeds above 5 m/s is sufficient, even considering instrument pointing errors, to avoid swath width reduction.

III. DEVELOPMENT OF INSTRUMENT REQUIREMENTS

A. Wind Measurements (25–65° Incidence Angle Range)

The scatterometer performance requirements have been developed from user requirements of wind vector measurement range and accuracy, swath width, resolution cell size, and measurement grid spacing (Fig. 5). Since the scatterometer is sensitive to both wind direction and wind speed, special techniques are developed to determine both parameters as will be discussed below.

The manner of transforming wind speed accuracy requirements to scattering cross-section (σ°) accuracy is shown in Fig. 6. Using σ° data from the AAFE RADSCAT aircraft instrument [6], vertical polarization and crosswind radar viewing are used in this example. The allowable user wind speed error bar of ±2 m/s or ±10 percent (whichever is greater) is projected on the σ° curves for different incidence angles. By translating this error bar to the σ° axis, as shown, the corresponding σ° error (one sigma) is determined for each incidence angle and wind speed (Fig. 7).

At small incidence angles (less than 25°) the dependence of σ° on wind speed diminishes and the σ° measurement requirements exceed the state-of-the-art measurement accuracy (~0.5 dB). In addition, for the lower incidence angles, σ° is influenced by sea state. For these reasons, earth incidence angles below about 25° are excluded for wind vector measurements. The outer edge of the primary wind vector swath is set at about 55° earth incidence which is approximately the outer angle of present aircraft and S-193 scatterometer data. The swath width thus defined is 500 km wide on each side of the satellite subtrack, giving a total swath of 1000 km for wind vector measurements.

An additional high wind speed measurement zone between about 55 and 65° is specified since returned signals should be large enough to measure for high winds and σ° will remain wind sensitive. The total swath width for high wind measurements is 750 km on each side of the satellite subtrack, giving a total swath width of 1500 km.

As previously stated, radar measurements from aircraft [2], [4], [6] have shown the scattering coefficient to be a function of both wind speed and wind direction. An anisotropic behavior with wind direction is exhibited by σ° having maxima in the upwind and downwind directions and minima in crosswind. Additionally, the upwind σ° peak is slightly greater than the downwind peak. In concept, two radar measurements at different azimuths are sufficient to determine the ocean surface wind vector; however, the near sinusoidal scattering characteristic often yields multiple wind vector solutions from these radar measurements. These mul-

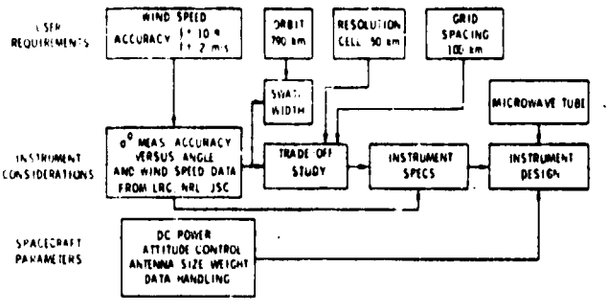

Fig. 5. Development of scatterometer specifications.

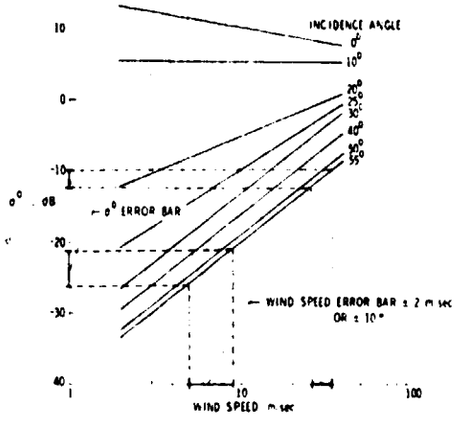

Fig. 6. Wind speed dependence of σ°. Crosswind–AAFE RADSCAT data.

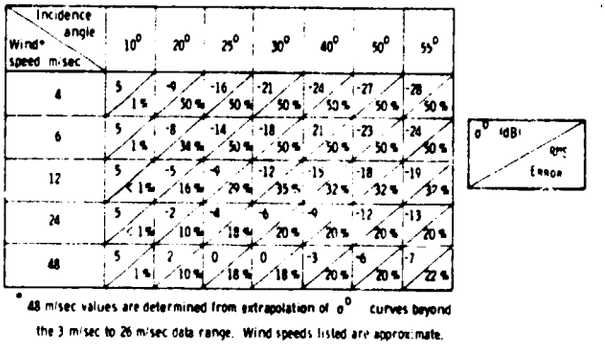

Fig. 7. Required σ° accuracy for scatterometer wind speed accuracy of ±2 m/s or ± 10 percent.

tiple solutions are approximately equal in speed but different in direction. Frequently, the quadrant of wind direction can be determined from conventional meteorological data and/or satellite obtained cloud mosaics, thereby providing a means for selecting the correct solution. A first attempt to use aircraft measurements to model the anisotropic scattering coefficient has been made by Pierson *et al.* [11]. Further development is being pursued by several researchers using presently unpublished AAFE RADSCAT data which cover a wide range of wind speeds and sea states.

To infer wind vector from satellite radar measurements requires both forward and aft looking antennas to obtain data at two azimuth angles for each resolution cell. An optimum implementation uses antenna beams, each oriented 45° relative to the subsatellite track, to provide observations which are separated in azimuth by 90° (Fig. 3). The time between illumination of a given resolution cell by the forward and aft beams depends on the cells position along the fan beam illumination. Thus the scatterometer must be designed in order to make the forward and aft beam cells cross at the same geographic site. Each 50-km resolution cell must have two footprints in it, (not required at the same time, however) giving σ° data at azimuth angles 90° apart.

The Doppler cells along the fan beam are adjacent so that the cross-track grid spacing (center-to-center) can be kept to 50 km and the along-track grid spacing is set at 50 km by the scatterometer digital controller. In modes 5–8, the Doppler cells give near contiguous coverage for either side of the subtrack to improve coverage in areas where strong wind gradients are expected.

The resolution cell size is larger than the Doppler cell size due to the smearing of the cell caused by satellite motion during the measurement period (t_p). The Doppler cell size is determined by the antenna beamwidth (1/2°) and Doppler bandwidth of the filters (Fig. 8). From antenna size considerations, antenna beamwidths smaller than 0.5° would be impractical.

Resolution cell size is also controlled by the orientation of the Doppler lines within the beam illumination which varies along the beam (Fig. 3). For the inner cells (low incidence angles) the Doppler line is oriented approximately 45° to the central beam axis. For the outer cells (high incidence angles), the orientation is about 13° with respect to the beam central axis. The Doppler bandwidths are designed so that the 50 × 50-km resolution cell size requirement is satisfied over the primary measurement zone (~25-~55°). At angles beyond 55°, Doppler bandwidths are held constant so the resolution cell size does increase slightly beyond the 50-km limit.

B. Improve Knowledge for Future Scatterometer Designs (0–65° Incidence Angle Range)

In addition to the 12 Doppler cells needed for wind determination, three more will be used for σ° measurements near nadir (0, 4, and 8° incidence angle). This completes the complement of angles required to develop a data library of σ° as a function of incidence angle (0-65°) for the full range of ocean surface conditions. From these data, one can determine whether geophysical parameters other than local winds

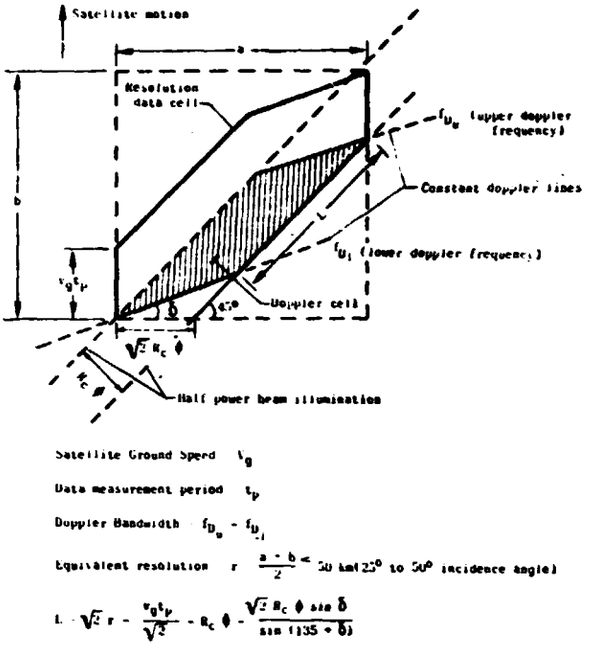

Fig. 8. *Geometry of one resolution cell at slant range R_c.*

affect the scatterometer measurements and as a result establish more definitive design boundaries (by optimizing incidence angle, polarization, wind speed measurement range, etc.) for future scatterometers.

During the early development phases of SeaSat, a fifth antenna was planned oriented parallel to the satellite subtrack so that these 0–65° data could be taken at the same geographic site. In this way, the surface conditions for any set of σ° versus angle data would be the same and thus reduce the possibility of data scatter caused by unknown geophysical effects. Although the fifth antenna is no longer part of the SeaSat scatterometer, a mode of operation is presently being considered which would allow the same sort of data to be taken. This would be accomplished by rotating the satellite 45° in azimuth so that two of the antenna footprints align with the satellite subtrack. The present scatterometer design would allow σ° measurements from 0 to 37° in small angular increments (15) and with higher resolutions (12 × 20 km).

IV. SENSOR VALIDATION AND DIAGNOSTICS

A. Hardware

One of the more important questions concerning every remote sensor is whether or not it is operating properly. Extensive in-flight housekeeping data are being provided routinely by the scatterometer in addition to planned subsystem level and system level performance validation and diagnostic activities.

An array of three land-based receivers is planned to verify transmitter performance as well as the antenna gain and pattern shape. This technique was used on the Skylab RAD-

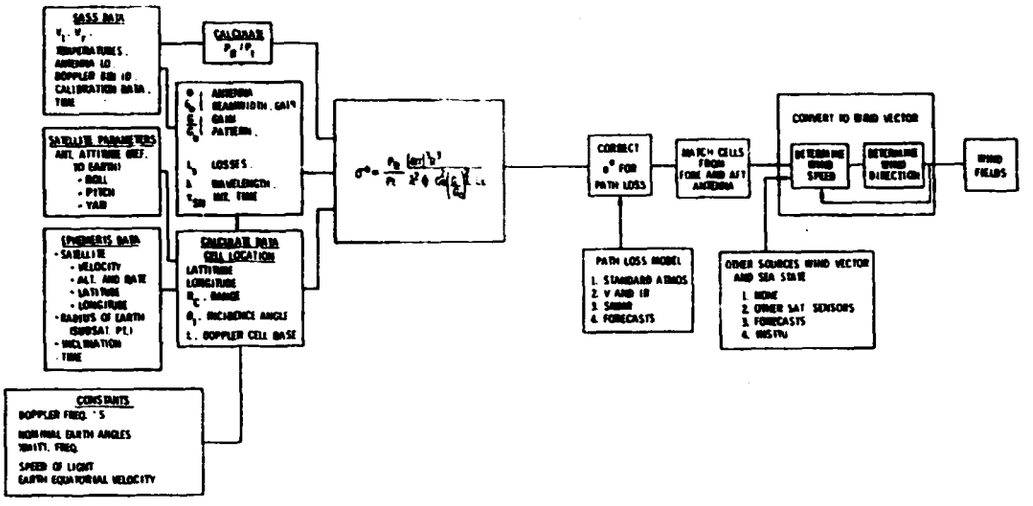

Fig. 9. Software flow diagram.

SCAT experiment [12] and it offers the only means of evaluating the transmitter and antenna on a subsystem basis. For diagnostic purposes, the SeaSat-A scatterometer can be operated in a radiometric mode (transmitter inhibited) in order to isolate the receiver for performance verification. Two test conditions are possible in this mode: 1) antenna not deployed and looking into deep space with a target brightness temperature ~5 K; 2) antennas deployed and looking at the ocean surface with a target brightness temperature ~125–175 K. A 5 K target offers high sensitivity for verification of antenna and receiver losses and VSWR. Receiver losses and noise temperature stability can be monitored throughout the mission, independent of the internal calibration source, by using the radiometric mode with the sea surface as a target. There are certain minimum requirements that must be met in order to certify the scatterometer as an operational instrument after it is placed in orbit. During the one-year period, aircraft underflights are required so that direct comparisons can be made between a well-calibrated (±0.5 dB) aircraft scatterometer and the satellite scatterometer. Direct comparison of aircraft and satellite σ° data will be used as an absolute calibration of the satellite scatterometer, thus removing any fixed biases from the data. Long-term instrument stability characteristics will be determined from periodic comparison of aircraft and satellite σ° values.

It has been demonstrated with extensive aircraft data that σ° measured at 8–12° incidence angle is relatively insensitive to ocean surface roughness and wind conditions. Consequently, long- and short-term stability information, independent of aircraft underflights, will be gathered routinely using data from the 8° near nadir Doppler cell.

The quality of the SeaSat-A scatterometer data can be further evaluated using measurement results from other sensors on the satellite. Altimeter σ° data, for example, can be compared with the scatterometer nadir data to reveal biases in either instrument and the time variation of these biases. Secondly, scanning multifrequency microwave radiometer data may be useful for correlation with scatterometer data during high wind speed measurements.

Techniques used in instrument validation and performance monitoring can in like fashion be used for diagnostic purposes in the event that malfunctions are indicated. The flexibility of the scatterometer will allow the isolation of a variety of possible component or subsystem malfunctions.

B. Computer Algorithms

The software for inverting raw scatterometer data to σ° and for converting σ° to wind vector must also be validated under all measurement conditions. Fig. 9 is a flow diagram showing the steps necessary in this process. This data processing is conveniently separable into the conversion of raw data to scattering coefficient and the conversion of σ° to geophysical units (wind vector), which allows each to be designed and evaluated independently.

Prior to launch, the scatterometer will be calibrated in terms of the ratio of received power to transmitted power P_R/P_T; thus the first step is to convert raw data to P_R/P_T using preflight calibration information. Satellite parameters such as attitude, ephemeris data, and various instrument and physical constants are used to determine cell locations on the earth, range, cell length (L), incidence angle, and antenna look angle. This information along with pertinent housekeeping data are used to determine antenna gain and are inputs for calculating σ° and rms error for use in the geophysical algorithm.

The first step in converting a σ° matrix to a wind vector map is to use both the visible/infrared and microwave radiometric data from other SeaSat-A sensors to make a path loss correction[4] to the values of σ°. Conversion to wind vector will be accomplished using algorithms that have been developed

[4] The use of microwave radiometer measurements to correct the scatterometer was first proposed by Moore and Pierson [13] and was successfully implemented during the Skylab S-193 experiment.

using several theoretical approaches with each algorithm being evaluated during the mission. These initial values will contain aliases caused by the multivalued relationship between σ° and wind speed and direction. Several methods for removal of these aliases and the generation of wind fields are being considered.

V. CONCLUSIONS

The microwave scatterometer design for SeaSat-A has been selected from a number of options, and detailed analyses show the design capable of satisfying user requirements of resolution cell size, grid spacing, swath width, and wind speed accuracy. Other instrument design characteristics have been included to resolve uncertainties about the effects of sea state on wind sensing ability and to verify instrument design boundaries such as optimum incidence angles and wind speed measurement range. With improved design boundaries, the scatterometer instrument can be optimized for future fully operational oceanographic satellites.

REFERENCES

[1] S. W. McCandless and V. J. Cardone, "Seasat-A oceanographic data system and users," presented at the I.A.F. 27th Congress, Anaheim, CA, Oct. 10–16, 1976.

[2] J. C. Daley, "Wind dependence of radar sea return," *J. Geophys. Res.*, vol. 78, pp. 7823–7833, Nov. 1973.

[3] K. Krishen, "Correlation of radar backscatter cross sections with ocean wave height and wind velocity," *J. Geophys. Res.*, vol. 76, pp. 6528–6539, Sept. 1971.

[4] J. P. Claassen, H. S. Fung, R. K. Moore, and W. J. Pierson, Jr., "Radar sea return and the RADSCAT satellite anemometer," presented at the 1972 IEEE Int. Conf. Engineering in the Ocean Environment, Newport, RI, Sept. 1972, IEEE Publ. 72 CHO 660-1 OCC.

[5] R. K. Moore *et al.*, "Simultaneous active and passive microwave response of the earth–The Skylab RADSCAT experiment," in *Proc. 9th Symp. Remote Sensing of the Environment*, Ann Arbor, MI, 1974.

[6] W. L. Jones, L. C. Schroeder, and J. L. Mitchell, "Aircraft measurements of the microwave scattering signature of the ocean," *IEEE Trans. Antennas Propagat./IEEE J. Oceanic Eng.* (Special Issue on Radio Oceanography), Jan. 1977.

[7] M. I. Skolnik, *Radar Handbook*. New York: McGraw Hill, 1970, ch. 25, pp. 25-16–25-24.

[8] G. T. Ruck, D. E. Barrick, W. D. Stuart, and C. K. Krichbaum, *Radar Cross Section Handbook*, vol. 2. New York: Plenum Press, 1970, Ch. 9.

[9] W. L. Grantham, E. M. Bracalente, W. L. Jones, J. H. Schrader, L. C. Schroeder, and J. L. Mitchel, "An operational satellite scatterometer for wind vector measurements over the oceans," NASA TMX 72672, Mar. 1975.

[10] R. E. Fischer, "Standard deviation of scatterometer measurements from space," *IEEE Trans. Geosci. Electron.*, vol. GE-10, pp. 106–113, Apr. 1972.

[11] W. J. Pierson, V. J. Cardone, and J. A. Greenwood, "The applications of Seasat-A to meteorology," City Univ. New York Tech. Report, Aug. 1974.

[12] A. C. Cook, D. L. Fayman, J. C. Holtzman, R. K. Moore, A. Sobti, and W. Spencer, "Measurement of microwave antenna patterns from an orbiting spacecraft," in *Proc. 1974 Int. IEEE/AP-S Symp. Digest*, Atlanta, GA, June 1974, IEEE Publ. 74 CHO-857-3 AP, pp. 51–53.

[13] R. K. Moore and W. J. Pierson, "Worldwide oceanic wind and wave predictions using a satellite radar-radiometer," *J. Hydronautics*, vol. 5, pp. 52–60, Apr. 1971.

APPENDIX B

Since Dr. Shemdin's presentation was principally concerned with SAR data processing and this has been included with JPL's data processing presentation provided by Mr. Edwin Pounder. Dr. Shemdin provided these two SAR papers for the general interest of the attendees.

DETECTION AND INTERPRETATION OF OCEAN ROUGHNESS VARIATIONS ACROSS THE GULF STREAM INFERRED FROM RADAR CROSS SECTION OBSERVATIONS

D. E. Weissman
Dept. of Engineering and
Computer Sciences
Hofstra University
Hempstead, New York 11550
and
Jet Propulsion Laboratory
Pasadena, Calif. 91103

T. W. Thompson
Planetary Science Institute
Science Applications, Inc.
Pasadena, Calif. 91101
and
Jet Propulsion Laboratory
Pasadena, Calif. 91103

Abstract

During the past several years, many radars have observed the distinct and interesting features associated with the Gulf Stream and its boundaries. Some of these Gulf Stream radar features have small scale, with dimensions comparable to and slightly greater than long gravity waves. Other features are larger, with dimensions much greater than the length of long gravity waves. This study describes radar cross section variations within the Gulf Stream and just outside, seen with a "scatterometer" type measurement.

The significant features of this radar cross section data were that the Gulf Stream always had a higher cross section per unit area (interpreted here as a greater roughness) than the water on the continental shelf. Also, a steep gradient in cross section was often seen at the expected location of the western boundary. There were also longer scale (10 to 20 km) gradual fluctuations within the stream of significant magnitude. These roughness variations are correlated with the surface shear stress that the local wind imposes on the sea. Using the available surface truth information regarding the wind speed and direction, an assumed Gulf Stream velocity profile, and high resolution ocean surface temperature data obtained by the Very High Resolution Radiometer onboard a NOAA-NESS polar-orbiting satellite (data provided by Dr. Richard Legeckis of NOAA-NESS), this study demonstrates that the computed surface stress variation bears a striking resemblence to the measured radar cross-section variations.

1. Introduction

The western boundary of the Gulf Stream has the unusual property of generating strong features (both small and large scale) in radar images. An imaging radar detection of the Gulf Stream in 1972 was reported by Moskowitz [1]. These showed large spatial scale and small-scale (narrow filaments) cross-section variations that are independent of the wave imaging characteristics. Also, radar altimetry (at 13.9 GHz) from aircraft and observations from the GEOS-3 and Skylab spacecraft have revealed definite differences in the radar cross section between the Gulf Stream and the continental shelf. Published data and quantitative analysis of these observations are very limited [2].

The Marineland Test [3], conducted during the first half of December 1975, provided new data on these Gulf Stream radar features. In particular, this test employed the JPL[1] and ERIM[2] airborne synthetic aperture imaging radars (SAR) and several surface instruments. All five flights of the JPL L-Band observed significant variations and oscillations of the surface radar cross section as detected by a "scatterometer" measurement mode. This scatterometer mode of measurement led to some unanticipated observations: the Gulf Stream often has a significantly higher radar cross-section (per unit area) than the water on the continental shelf between shore and the continental slope. These differences are often accompanied by large-scale (spatial) variations near the boundary. This report will concentrate on these variations. The primary data for this effect is the strip chart record of the received power history that was kept continuously on a selected flight line. Comparisons will often be made between the strip chart recording and the features observed simultaneously in the SAR images. Also, infrared satellite photographs (obtained by the very high resolution radiometer on the NOAA-NESS satellite), optical photos taken from the CV-990, and other sources of related information have been examined whenever available.

Much of the interpretation of our data is based on the concept of a Bragg scattering, where radar echo strength is determined by the number of ocean waves which have crests aligned with radar's line of sight and have crest-to-crest spacing which is equal to one-half of the peak-to-peak spacing of the electromagnetic radiation [4]. Thus, the L-band radar with 25-cm wavelength basically observes the population of ocean waves which have wavelengths of [12.5 cm/sin (angle of incidence)] and have directions directly toward or away from the aircraft. For simplicity, the ocean waves with these wavelehgths and directions will be called the "Bragg waves."

The Bragg surface wavelength is actually one value in a continuous spectrum of the randomly rough surface. The strength (radar cross section per unit area) of the signal backscattered by a small patch of the ocean (say a resolution cell of the SAR) will be proportional to the local number of short gravity waves of the proper length and directional alignment, and their maximum heights. The modulation of these shorter waves by the large gravity waves is the basis for the scattering differences observed as waves in a radar image. In the scatterometer mode described below, only the total cross section integrated across the large illuminated area (see Fig. 2) is being observed, at any instant. This provides an observation of the average "density" of Bragg wavelengths and is interpreted as the degree of roughness of the

[1] Jet Propulsion Laboratory

[2] Environmental Research Institute of Michigan

illuminated area. The physical quantity that controls these populations of Bragg waves is the wind stress.

The scatterometer measurements were also compared with the synthetic aperture radar images. The relationship between the effects seen on the strip chart and the image is generally complex. There are large differences between the spatial scales of cross-section variations observed with these two techniques. The strip chart measurement method is more sensitive to changes in cross-section magnitude as small as a few tenths of a dB, whereas the radar image gives very precise location, alignment, and finer spatial size information. Also, the separate flights will be analyzed separately because of the different character of the observed effects and because of the availability or lack of the infrared satellite data.

Observed radar cross sections were found to be correlated with an estimated surface stress. Surface stress estimates accounted for surface winds, differential modulation of the surface wind by the Gulf Stream, and air-sea temperature differences. Surface winds were measured by surface instruments at the Marineland Test sites, and we assumed that these were uniform everywhere in the test area. The Gulf Stream surface velocity was modelled, with a profile published earlier by Von Arx [5]. Sea temperatures were estimated from VHRR (Very High Resolution Radiometer) data provided by Dr. Richard Legeckis of NOAA-NESS. Air temperatures were given by the surface instruments. The sea temperatures given by the VHRR provided a substantial improvement over sea temperatures estimated in our earlier report [6].

These estimated surface stresses were compared with the radar backscatter data for December 4 and 15, 1975 (other days weren't studied, since the Marineland Test area was under clouds, preventing the acquisition of surface temperature information). These results show that both large scale trends (over a range of 250 km) and small scale features (on the order of tens of kilometers) in the radar data correlates extremely well with the square root of the computed surface stress.

The results presented here imply that the backscattered radar cross section measured by the radar is proportional to the surface stress which is seen to be a function of the local wind, the surface current, and the surface temperature. If the distribution of two of these quantities can be measured or estimated, then the third can be inferred, using the measurement technique and interpretation discussed in the following. Further evidence that sea-air temperature differences should be considered along with the wind and current interaction can be found in some recent cross-section measurements (from nadir) across the Gulf Stream made by the SKYLAB altimeter. This data shows that a variety of effects is observable, indicating a sensitivity to the meteorological conditions. The data analyzed by Parsons [2] cannot be fully explained by just considering the wind vector and the local current information. This implies that surface temperature influences the surface roughness.

2. Instruments and Flight Patterns

Imaging Radar

The radar data presented here was obtained in five flights of the JPL L-Band imaging radar onboard the NASA CV-990.[3] The data is basically scatterometry, where radar echo strength in terms of a backscatter radar cross section per unit area of the surface is measured. The variations of radar echo are monitored along a ground track parallel to the aircraft's line of flight. Also, radar echo strengths are provided by two different but simultaneous modes. The normal imaging mode records the full signal information on a signal film recorder on board the aircraft. After the flight, these signal films are converted to high-resolution images, using an optical correlator. The "scatterometer" mode simply records total received power returning from an area whose spatial width is determined by the azimuthal beamwidth of the antenna (usually 4.0 km) but whose range spread depends on the transmitted pulse width (usually 0.55 km). The incidence angle can be adjusted with the setting of a range gate. The echo strength recorded on a strip chart is real time on board the aircraft.

An overview of the JPL imaging radar, emphasizing both modes of scatterometry, is shown in Figure 1. Parameters are given in Table 1. Echoes from the surface are received and split into two nearly identical receiver chains and recorded on a signal film via the optical recorder. These signal films were developed, and processed in an optical correlator to provide the high-resolution images which can then be scanned by the densitometer to provide fine-scale scatterometry. Coarse-scale scatterometry was provided by a chain of electronics which sampled the echo at a specified delay, integrated the voltage, and then recorded the result on a strip chart. This provided a continuous record of the relative changes in the total received power from this particular incidence angle.

The geometry of the footprint for strip chart recordings is shown in Fig. 2. The JPL L-Band radar has a large beamwidth antenna (18 deg) which illuminated an area on the right side of the aircraft. This azimuthal beamwidth is aligned perpendicular to the aircraft fuselage. The elevation beamwidth of 90 deg is centered 45 deg above the vertical. A much smaller portion of this antenna footprint is observed by transmitting short pulses and sampling their echoes at a fixed time beyond nadir. Typical parameters for the scatterometer footprint are given in Table 2.

Flight Lines

Radar observations of the Gulf Stream were obtained on five flights in December 1975, when the NASA CV-990 operated out of Patrick AFB in support of the Marineland Test. An overview of these flights is given by Thompson [7]. The positions of some of these flight lines with respect to the Gulf Stream are shown in Fig. 3.

The western boundary of the Gulf Stream in the vicinity of Station III was observed often. The first leg of the Eight-Sided Pattern, was extended out to sea, started at the midpoint of the Gulf Stream and ran in toward shore. All five legs of the Five-Sided Pattern at Station III were centered on a position of 29° 57'N and 80° 17'W at a nominal location of the western boundary. The Gulf Stream Transit started east of the Stream, ran across it, past Station III, and into shore near Station I. The depth profile of the ocean just under the flight path is shown in Figure 4 [14].

Satellite Radiometer

As mentioned above, an important addition to our data base was the sea-surface temperature provided by

[3] The Galileo II, a four jet flying laboratory operated by the Medium Altitude Mission Branch, NASA Ames Research Center.

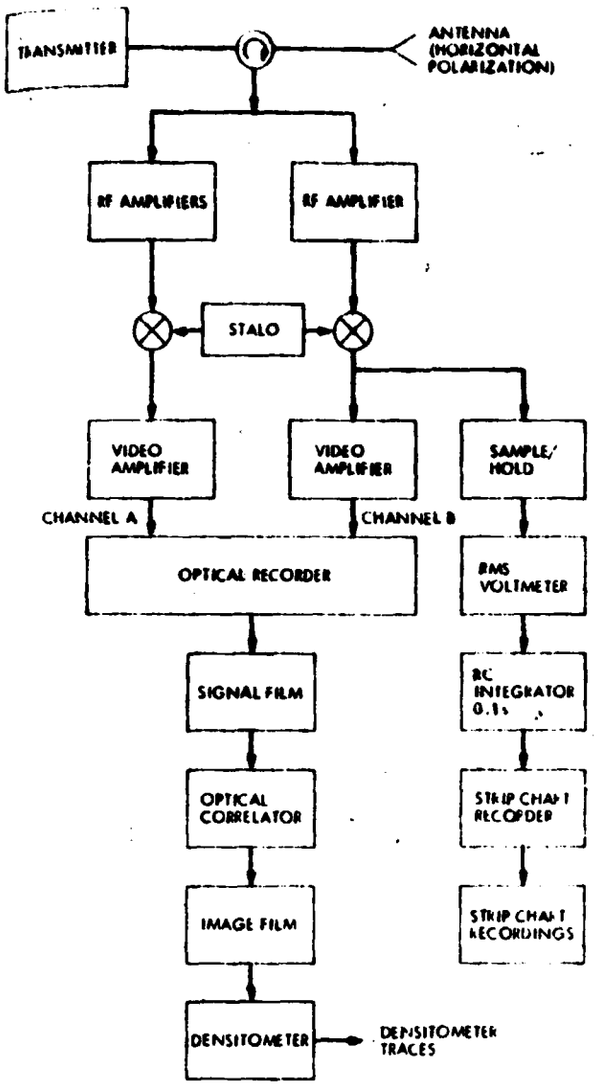

Fig. 1. JPL L-band Radar Block Diagram

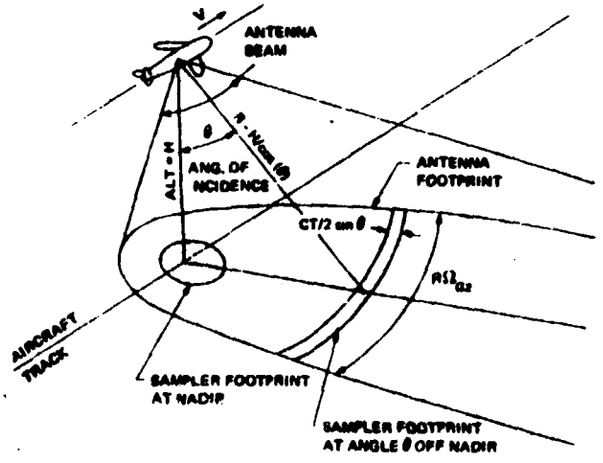

Fig. 2. Surface Illumination Geometry and Parameters

TABLE 1. OPERATING PARAMETERS FOR JPL L-BAND, TWT RADAR

Parameter	Value
Center frequency	1220 MHz
Wavelength	24.6 cm
Pulse length	1.25 μs
Bandwidth	10 MHz
Time-bandwidth product	12.5
Peak power	4 kW
Antenna azimuth beamwidth	18 deg
Antenna range beamwidth	90 deg
Antenna beam center gain	12 dB
Nominal altitude	3 to 12 km
Nominal ground speed	400-500 knots
Sweep time	55 μs
Sweep length	25 mm
Sweep speed	0.44 mm/μs
Range cells	1667
Nominal pulse repetition frequency	800 pps at 400 knots 1000 pps at 500 knots

TABLE 2. TYPICAL VALUES FOR THE STRIP CHART SCATTEROMETER

H	= altitude	= 12 km (40,000 ft)
θ	= angle of incidence	= 20 deg
R	= range	= 12.8 km
Ω_{az}	= azimuth beamwidth	= 18 deg
T_p	= transmitter pulse length	= 1.25 μs
C/2	= velocity of light/2	= 150 m/μs
$R\Omega_{az}$	= azimuth (along-track) footprint length	= 4.0 km
$C\,T_p/2 \sin(\theta)$	= range (cross-track) length	= 0.55 km
Nadir footprint area		= 14.1 km^2
Nadir footprint radius		= 2.1 km
Antenna gain at beam center (θ = 45 deg)		= 12.0 dB
Antenna gain at θ = 20 deg		= 10.5 dB
Antenna gain at nadir		= 7.5 dB

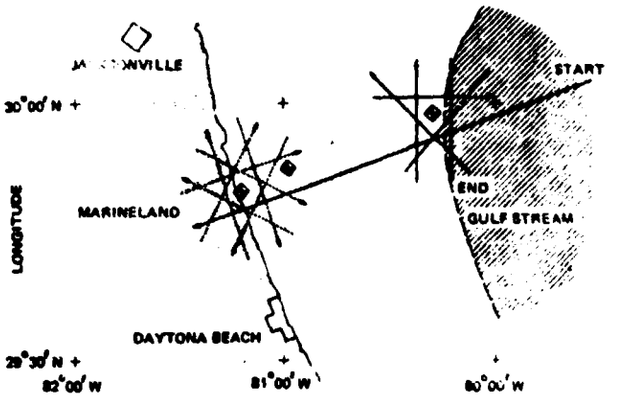

Fig. 3. Flight Paths for Eight-Sided Pattern at Station I and Five-Sided Pattern at Station III

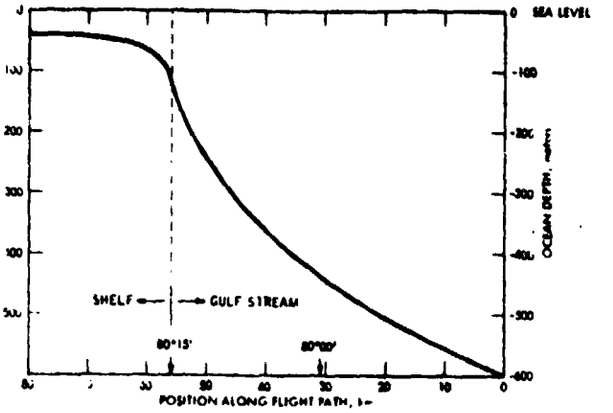

Fig. 4. Ocean Depth Along Flight Path near Gulf Stream Edge, Determined from a Topographic Map [14]

the Very High Resolution Radiometer (VHRR) onboard the NOAA-4 satellite. The VHRR has an instantaneous field of view of about 1 km, and measures radiation in the 0.6 - 0.7 μm (visible) and 10.5 - 12.5 μm (thermal IR) spectral bands. The NOAA-4 spacecraft provides complete day and night coverage of the globe every 24 hours, since it is in a polar orbit at an altitude of about 1500 km. Surface temperature images are constructed from successive scan lines, and the VHRR data can be displayed as gray scale images by using scale values appropriate to the measured radiances. The system sensitivity is about 0.5 to 1.0° C when viewing the ocean surface, and this represents the minimum temperature differential that can be resolved for two adjacent 1 km areas. For larger areas, temperature differences smaller than this can be resolved by suppressing some of the random noise effects by averaging.

The thermal data analyzed here was digitized from the analog transmissions and are presented in the form of quantized sea surface temperature levels (separated by approximately 1.1°), each level representing the temperature within a 2 km square cell. This resolution is comparable to that of the radar cross-section data from the strip chart.

3. Radar Observations During The December 4 Flight

As mentioned previously, the flights on December 4, 1975, provided the best day for correlation of estimated surface stress with radar backscatter from the strip-chart scatterometer. The sea-temperature estimates from the VHRR were acquired at 13:00 GMT, at four and seven hours before the radar data and at 02:00 GMT on December 5, 1977, at four and seven hours after the radar data was acquired. On this day, the strip chart recorder was monitoring the signal that arrived 5 μs after the leading edge, corresponding to a 20-deg incidence angle.

The differences in radar cross section between the Gulf Stream and the adjacent continental shelf waters were 1 to 2 dB. In addition, there were strong oscillations in the cross section near the edge of the stream. These oscillations can be seen in the strip chart data record (Figs. 5a and 6a), where the power levels are normalized such that unity is the minimum backscattered power (or 0 dB) on the continental shelf side of the boundary. The oscillations in the cross section have sizes between 10 and 20 km, which are larger than the resolution size inherent in this technique. These flight lines took place within three hours. Thus, the cross-section behavior with position shows that these 10 to 20 km features are not stationary over this time interval, but that the overall average higher cross section on the Gulf Stream is still evident. A cross correlation between the radar cross section and the computed stress (square root) variations (with means removed) shows a 0.52 correlation for the first Gulf Stream transit and 0.71 for the second. Thus, there is a close relationship between observed radar backscatter and estimated surface stress.

The one-dimensional nature of this strip chart data should be compared with the two-dimensional information in the SAR images. For example, Fig. 7 is the

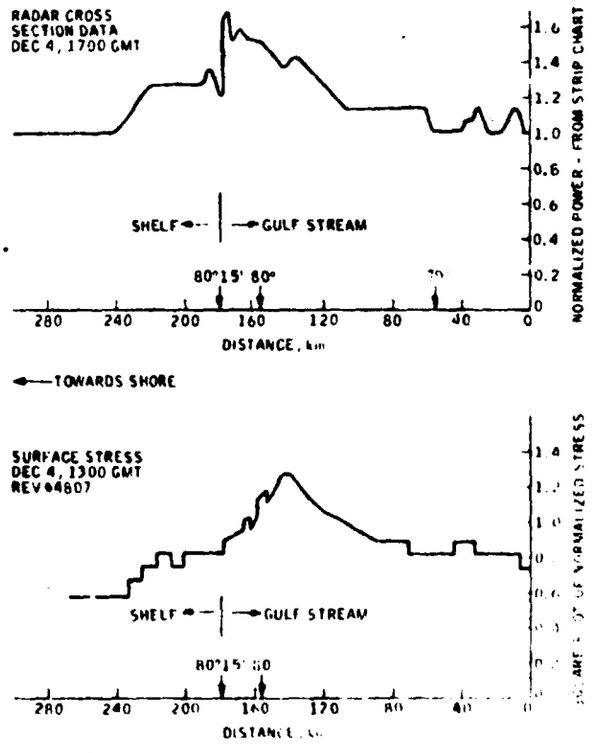

Fig. 5. Comparison between Radar Cross Section Variations and Surface Stress for First Gulf Stream Transit on December 4

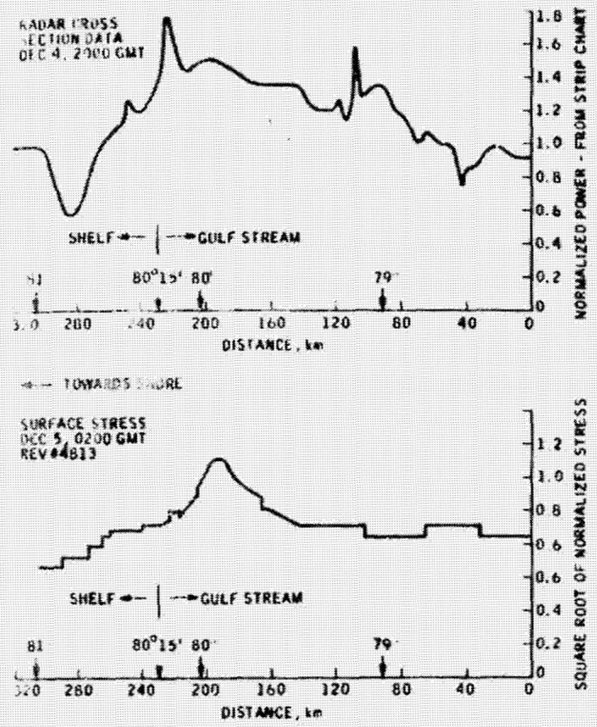

Fig. 6. Comparison between Radar Cross-Section Variations and Surface Stress for Second Gulf Stream Transit on December 4

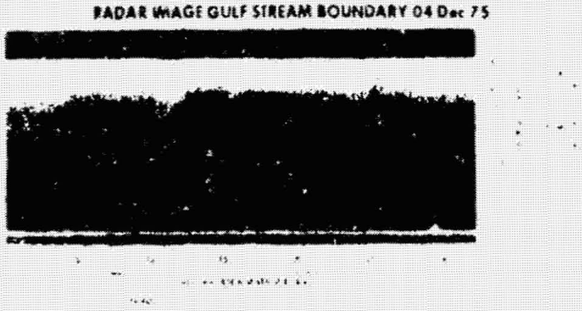

Fig. 7. Synthetic Aperture Radar Image, December 4, 1975 at 17:09:00 GMT

radar image corresponding to the strip chart records of Fig. 5. The linear features in the SAR image display neighboring dark and bright bands of intensity. These features in the image lie approximately parallel to the current flow direction (northerly direction) and to the edge of the Stream. Their positions agree closely with positions where strong changes in cross section were seen in the strip chart record. Moreover, later images of this area show that these linear features maintain their thin appearance for the several hours.

A study of a long record of the radar images (the second Gulf Stream transit) shows similar isolated features in the center of the Stream (for example at 28° 22' longitude, 100 km from western edge). This suggests that the phenomenon is not exclusively associated with the edge of the Stream or the continental slope. Similarly, on different days, other long flight paths will show multiple occurrences of these elongated features.

The features at the Gulf Stream boundary are typically one kilometer wide - too small to be accurately resolved by the scatterometer measurement. Thus, the actual cross-section changes in this thin filament are most likely stronger than those recorded on the strip chart. This record represents an average over a 4.0-km beamwidth. On the other hand, the longer scale undulations in cross section seen with the scatterometer cannot be observed visually from the SAR image, although they might be detectable with image processing.

4. Radar Observations During The December 15 Flight

This last flight of the Marineland Test was also examined in detail because the strip chart recording of cross section had the largest number of oscillations (about 5) and showed the largest maximum to minimum excursion, 2.8 dB for a two-cycle fluctuation extending over a 50-km span (Fig. 8). Once again, the strip chart recorder was operated for a 20-deg incidence angle. The waves over the continental shelf displayed a lower average cross section than the Gulf Stream. It was also noted in the strip chart record that the variations extended much closer to shore than had previously been the case (up to within about 50 km of shore). The extent of the area in which these cross-section variations occur can also be seen in the SAR images. These images indicate that the incidence angle chosen for the strip chart is not critical, and the 20-deg data cited above is a representative sample of similar behavior over a wide range of incidence angles from about 10° to 50° (Fig. 9).

The second Gulf Stream transit of this day yielded an image with a comparable dramatic feature at the edge. The incidence angle used for the accompanying strip

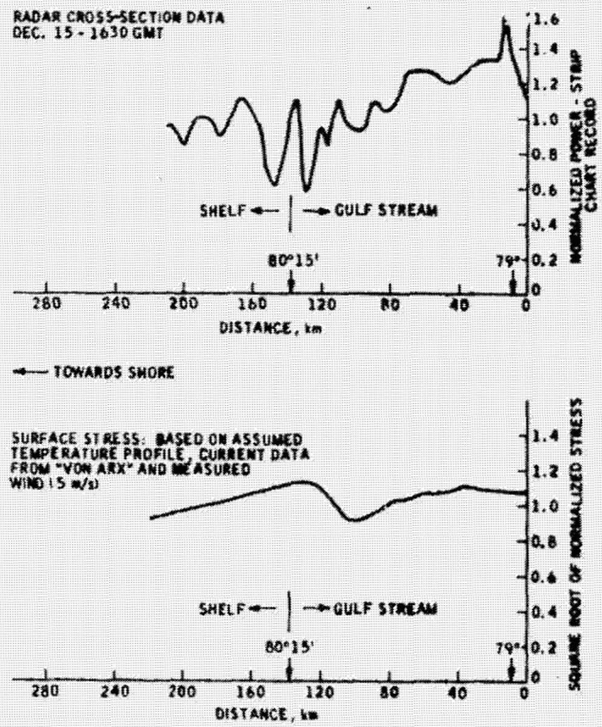

Fig. 8. Comparison between Radar Cross-Section Variations and Assumed Surface Stress for December 15

Fig. 9. Synthetic Aperture Radar Image on December 15, 1975 at 16:34:00 GMT

chart ... was 0°deg (nadir). Instead of the strong oscillations characteristic of the 20° angle of incidence observations, a much smoother history is seen. The radar observations only show a very gradual increase in cross section as the flight track passes from the Gulf Stream to the continental shelf, amounting to a net change of about 0.5 dB over a distance of about 75 km. This suggests that the ocean phenomena witnessed at off-nadir angles of incidence during the earlier pass with both the imagery and the strip chart record may be affecting the small-scale, Bragg wavelength gravity waves predominantly, and not having much of an effect on the RMS slope (which seems to be a bit higher on the Stream) that controls the nadir radar return.

5. Other Observed Radar Cross-Section Features

One puzzle in these Marineland Test observations is the nature of the thin linear features that are found at the edge of the Stream, and sometimes farther east (Fig. 9). These features probably have stronger cross-section excursions than those recorded on the strip chart. The SAR images show them to have a small width, relative to the width of the area illuminated by the antenna, so their strength would be diluted in the area integration that the antenna performs when the "scatterometer" type of cross-section measurements are made.

Their persistent north-south alignment and extremely narrow dimensions rule out an explanation based on purely temperature variation. It seems unlikely that steep gradients and differences in temperature in such a narrow region (less than 1 km) could be large enough to produce the large roughness difference implied by the observed variations. Based on a detailed optical scan of this feature in a radar image similar to Fig. 9, the temperature excursion would have to be 6°C in order to account for this effect. Also, one would expect some sharp temperature gradients to be aligned in other directions. One suggestion is that these features are related to internal waves generated by the tidal currents being deflected by the continental slope (as have been seen near the Southern California coast), and rising close to the surface because the thermocline becomes more shallow and often tilts upward in this region (Fig. 4). This view is mentioned because previous experimental studies have demonstrated the detectability of internal waves, due to the manner in which their currents affect the small-scale roughness [8]. Except for the December 14 flight, boundaries taken from the CV-990 were frequently obscured by cloud coverage. None of surface photographs showed any distinctive optical feature or foreign material at this location that might explain the radar observations. This negative photographic result would be consistent with the internal wave phenomena.

Another possibility is the presence of significant amounts of small-sized foreign material or debris which could be convected and aligned by the current. However, this condition might lead to a reduction in the local surface tension and roughness, which would then appear as a distinct depression in the radar cross section. Close examination of one image (accompanied by quantitative digital image scanning to infer a radar cross-section profile across this feature) reveals an oscillatory behavior, where the cross section ranged above and below the average value on the Gulf Stream. These features of the data, along with the absence of any visible (photographic) evidence, leave open the question of what type of phenomena is being detected here.

6. Interpretations Based on Surface Stress

The variety of observed cross-section effects suggests that several ocean phenomena may be responsible for the features seen on the strip chart record and the SAR images. It must be kept in mind that the modulation of radar echo is controlled primarily by the surface roughness, so that only those quantities that might influence this roughness must be examined. For example, the wave-wave interactions between long gravity and short gravity (and capillary) waves will produce effects with smaller spatial scales than are of interest in this analysis. The critical control of this surface roughness is the shear flow of winds close to the surface, to which the small Bragg-wavelength ocean waves are tightly coupled. This wind stress is known to be influenced by the mean wind several meters above the surface, any water current at the surface, and the air-sea temperature difference (especially under stable conditions). Aspects such as fetch and time scale for growth of waves of this size are believed to play a minor role in these cross-section measurements due to the time and spatial averaging inherent in this method. The discussion that follows will attempt to relate these quantities to the observed results, using known surface conditions and plausible ocean phenomena in this region.

The general question of why the Gulf Stream is always rougher than the water of the continental shelf water should be addressed in terms of the two most significant characteristics of this body: (1) it has a significant current distributed over a wide area that flows in a well-defined direction, and (2) its temperature is higher than the water on the continental shelf and is often higher than the overlying atmosphere.

The data shows that neglecting temperature and accounting only for the current magnitude and direction relative to the prevailing wind will not explain the observed cross-section changes. If the wind had a strong component antiparallel to the current, the friction velocity (and the radar cross section) on the Gulf Stream would be greater than it is on the stationary shelf water. Alternatively, for a wind component parallel to the current, the friction velocity on the Stream would be lower than on the shelf, implying that the shelf should have a larger cross section. Examination of the data shows that the shelf never had a greater cross section than the Gulf Stream. No changes in cross section can be correlated solely with wind direction changes for the five days described above. For example, on December 4, the winds were from the northeast, and on December 15 they were from the southeast, but larger cross sections on the Stream are clearly evident in the data for both days (Table 1). The conclusion here is that while the current velocity may influence the relative roughness between the Gulf Stream and the shelf, it cannot be assigned the dominant role.

TABLE 3. SURFACE INFORMATION AND TIMES OF OBSERVATION

Date	Time (GMT)	Station	Wind Speed, m/s	Wind Direction, deg	Air Temperature, °C	Sea Temperature in Gulf Stream, °C
Dec. 4	17:00:00	III	3	060	23.8	25.2
Dec. 4	20:00:00	III	4	080	25.3	25.2
Dec. 15	17:00:00	I	5	150	-	-

It seems fruitful to consider the state of knowledge of the dependence of wind stress on the air-sea temperature difference [9]. The emphasis in the literature on this subject is on the study of the growth of wind waves (large gravity) over large fetches, for long periods. The available evidence points conclusively to the importance of atmospheric stability, which depends on the vertical temperature gradient. Comprehensive field measurements indicate that when all other quantities are equal, a sea temperature larger than the air temperature (unstable conditions) causes the heights of waves generated to be greater, due to the higher drag coefficient of the surface.

Studies of experimental data carried out by Pleagle [9] lead him to conclude that the increase in wave height due to an air-sea temperature difference (unstable) is at the rate of 10% of the height per degree centigrade. Examination of our available surface-temperature information indicates that the sea temperature was never less then the local air (measured from the ship at Station III). On days such as December 4 and 6, moderate differences in temperature are evident (about 1 to 2 deg), consistent with the observation of larger cross sections on the Stream.

It should be emphasized that a nonneutral temperature condition alone cannot explain the cross-section variations, since a constant sea-surface temperature would yield the same cross section everywhere. If wind stress is the controlling factor, then it must be the temperature differences between the Gulf Stream and the shelf that account for the cross-section differences. Since surface temperature variations can be inferred from the satellite observations, some quantitative estimates of the variations of the drag (shear stress) coefficients, and the tangential stress of the wind on the sea due to thermal stratification can be made. Besides the temperature variations, the variation in the resultant velocity between the mean wind and local Gulf Stream current will also be considered in the surface stress calculation. These changes in wind stress can then be compared with the radar data.

It is customary to express the surface drag τ_0 of the wind at the surface in terms of the mean wind speed at a chosen reference height (10 m will be used in the following). This, then, defines the drag coefficient [10], C_{10}:

$$\tau_0 = (\text{air density}) \times C_{10} \times \bar{U}_{10}^2 \qquad (1)$$

$$C_{10} = (U^*/\bar{U}_{10})^2 \qquad (2)$$

U_{10} = mean wind speed at 10 m above the surface

U^* = friction velocity

For a fixed $\bar{U}_{10}$, any change in the vertical wind profile caused by temperature stratification will alter C_{10}. From these equations, it is evident that a change in C_{10} will also change the surface stress. Most data on C_{10} available in the literature is for neutral conditions. Approximate methods to take vertical gradients of temperature into account have been developed [11] and supported by experimental results.

This approximate theoretical development will be applied here to estimate the magnitude of the effects that were likely to occur during these Marineland Test flights. Since relative changes in wind stress are of interest (on and off the Gulf Stream) only the ratio of C_{10} at the measured air and sea temperatures relative to the value for a uniform temperature profile need be calculated. For the neutral condition, $(C_{10})_n$ depends primarily on the dynamic roughness, z_0, [10].

$$(C_{10})_n = \frac{k^2}{\left[\ln\left(\frac{10 + z_0}{z_0}\right)\right]^2} = \left[\frac{(U_*)_n}{\bar{U}_{10}}\right]^2 \qquad (3)$$

For a slightly stratified condition, the approximate similarity theory solution for the heat flux advanced by Monin and Obukhov [10] yields

$$\frac{U_{10}}{U_*} = \frac{1}{\left[(C_{10})_n\right]^{1/2}} + \frac{10\alpha\gamma}{kL} \qquad (4)$$

After some manipulation and insertion of the values for the constants α, k, and γ found in [10] and [11], the desired ratio is expressed as:

$$C_{10}/(C_{10})_n = \left[1 - 1.24\,\frac{\Delta\theta}{\bar{U}_{10}^2}\right]^2 \qquad (5)$$

where

$\Delta\theta$ = the air temperature minus the sea temperature, °C

$\bar{U}_{10}$ = wind speed at 10 m above the surface, in m/s

It is readily seen that for a warmer sea $\Delta\theta < 0$ and $C_{10} > (C_{10})_n$. Also, the effect becomes weaker for a higher wind condition, where the instability due to thermal stratification becomes subordinate to the dynamic turbulence.

A more sophisticated and critical appraisal of the state of knowledge of the factors that affect the drag coefficient can be found in a report on the marine boundary layer by Cardone [12].

1. Surface Stress Implications for 04 December, 1975

The prime data set for these surface stress/radar backscatter comparisons is 04 December 1976, since there are VHRR thermal images before and after two independent radar observations. In particular, the VHRR data was obtained at 1300 GMT on December 4, and 0200 GMT on December 5, and the radar data was obtained on "Gulf Stream transits" at 1700 GMT and 2000 GMT on this day.

This thermal data is in the form of quantized sea-surface temperature levels (separated by approximately 1.1°C), each level representing the temperature within a 2-km square cell. This resolution is comparable to that of the radar cross-section data. Figure 10 shows the two dimensional surface-temperature distribution at 1300 GMT, where the lines represent boundaries between the quantized temperature areas. The surface latitude and longitude coordinates are superimposed on this information to permit the construction of a temperature profile along the same ground path traversed by the radar for comparison with the radar cross-section variations, and for inclusion in a stress profile calculation. This profile is seen in Figure 11. Three interesting properties are evident:

(1) The temperature difference between the Gulf Stream and the shelf water is substantial, typically 4°C, with some small areas being 5°C warmer than the shelf. The temperature gradients in the shelf waters are by no means in the same direction, although the average behavior is for the temperature to decrease as one gets closer to shore. The substantial irregularities of the boundaries that separate the areas of uniform temperature are seen in Figure 24.

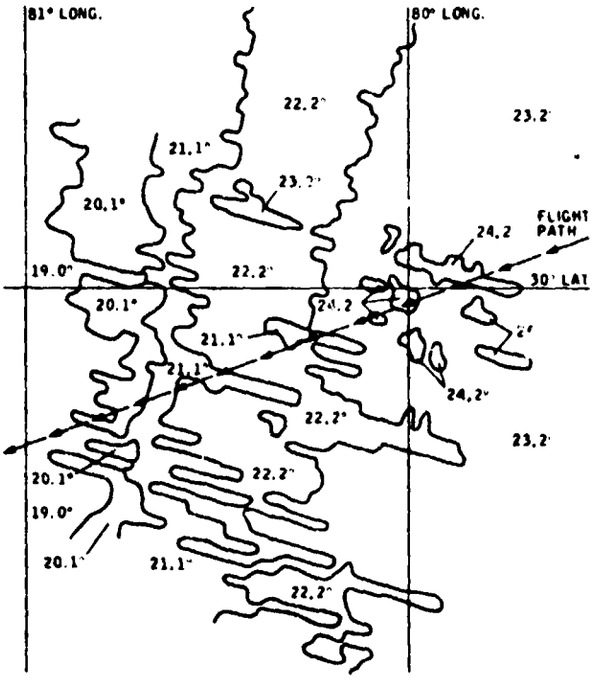

Fig. 10. Isotherms Inferred from Quantized Infrared Imagery December 4, 1975, 1300 GMT - Rev. No. 4807

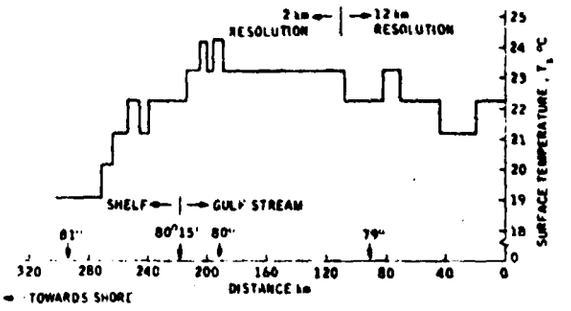

Fig. 11. Temperature Profile Along Gulf Stream Flight Path, December 4, 1975, 1300 GMT - Rev. No. 4807

In order to relate the radar cross section at this microwave frequency and incidence angle to the wind stress at the sea surface, this temperature information can be utilized in a theoretical calculation of the stress along the line of flight. As noted above, the magnitude of the drag coefficient is quite sensitive to any thermal stratification in the air, either stable or unstable. The wind speed (relative to the surface) also influences the drag coefficient, as well as being the dominant quantity in the total stress. Surface station instruments have recorded the wind speed and direction at the flight times of interest. The product of this drag coefficient and the square of the magnitude of the resultant vector velocity difference between the air and water surface (including the effect of the water current) equals the total stress. (See Appendix.)

This theoretical approach was followed, and a profile of sea-surface stress was calculated for comparison with the radar cross-section data. This included the temperature data of Figure 11, the known wind speed of 4 m/sec, and direction of 60° was combined with a northward Gulf Stream current. No timely observations of the Stream's structure or velocity were available for use in computing this surface stress. As an example of a "representative" shape, size, and current magnitude, the profile presented by Von Arx (Atlantis cruise No. 165, near latitude 38°, longitude 70° [5] was used in all the stress calculations presented herein. This embodies a width of 90 km, a maximum speed of 2.2 m/sec, and a western border at 60° 15', where the continental slope is steepest. The square root of the normalized stress is plotted in Figure 5(b), along with the radar cross-section profile that was measured about four hours later. The square root of the stress was plotted because previous aircraft measurements of the dependence of the cross section on the wind speed have shown it to be closer to a unity power law form (hence, square root of stress) than a square law dependence (linearly proportional to stress) [13].

The computed square root of surface stress and observed backscatter profiles have a striking similarity The magnitudes of both are higher on the Gulf Stream relative to the cold shelf. Also, both levels increase as one travels toward the western edge from the east. In addition, a steep decline occurs where the current gradient is believed to be in the greatest. Furthermore, in the region on the eastern edge of the continental shelf where the current is very small, the cross section is still relatively high and correlates well with the higher stress resulting from the relatively higher temperature in this region.

A second data set on December 4 showed similar features. The second Gulf Stream transit was conducted

at 2000 GMT, and a subsequent satellite photograph 6 hours later (at 0200 GMT, December 5) provided a sea temperature profile. These profiles are presented in Figure 6. Again, the length of the higher cross-section region extends twice as far as the width of the Gulf Stream, and with a steep decrease at the location where the current rapidly decays. Considering the six-hour time difference between these observations, the degree of agreement is considered satisfactory. Comparing the maximum and minimum magnitude levels reached by the measured cross section with the maximum and minimum levels of the square root of the stress, it appears that this value of the exponential power gives a good functional dependence for both data sets. A unity power law gives a poor fit.

2. Surface Stress Implications for 15 December, 1976

Further support for the preceding interpretation comes from the analysis of the data acquired during the first Gulf Stream transit on December 15 (Figure 8). This data was puzzling because the cross section on the western half of the Stream was (on the average) lower, as compared to the continental shelf, and to the eastern half of the Stream (which still had relatively higher roughness than the shelf). The radar cross section can be related to surface stress, only if one accounts for surface wind speed and sea-air temperature differences. The surface wind which was coming from the southeast produced a smaller relative velocity on the faster moving areas of the Stream, as compared to the slower current on the eastern half. Also, the higher temperature of the Stream increases the stress (and observed cross section) relative to the shelf. Unfortunately, cloud cover prevented the acquisition of satellite temperature information, but a crude model (based on the earlier temperature features seen on December 4) was assumed and combined with the Gulf Stream current velocity profile along with the measured wind information to compute a stress profile for comparison (Figure 8(b)). The general behavior of this theoretical curve agrees with the observed features noted above. The strong fluctuations in the radar data near the continental slope may be related to stronger temperature variations than those seen on December 4. This is suggested because a satellite infrared image taken on December 16 (24 hours later) shows a very intense, small eddy activity at this side of the Gulf Stream that may have existed at the time the radar observations were made.

7. Conclusions and Recommendations

The foregoing results demonstrate that the imaging radar measures an average radar cross section of the ocean surface that is related to surface stress. This relationship complements the Seasat-A SAR's primary objective of observing the directional spectrum of ocean waves. The directional alignment of the radar line-of-sight played an important role in the interpretation of the radar cross-section observations. When several different directions were examined the radar backscatter properties showed that the wind-driven, small gravity waves were aligned with the average wind direction. The observations of the Gulf Stream in this experiment provided an excellent opportunity to study the combined effects of wind magnitude and direction, of surface-current and of sea-air temperature differences on the surface roughness. The analysis carried out in this report, along with the radar and surface data presented, is in close qualitative agreement. While additional surface and related supporting information could be utilized (and would be welcome), the general behavior of the measured results can be explained with well-known phenomena that, heretofore, have been impossible to witness with as comprehensive and sensitive measurement as this. Prior to this experiment, very little experimental evidence existed to demonstrate the relationship and dependence of roughness on sea-surface temperature and air-temperature profiles. This fact could have implications for the interpretation of other microwave sensor systems, such as the radiometer and scatterometer.

Because of the ability of the microwave energy to penetrate clouds, the results described here could lead to a system for monitoring Gulf Stream current variations (given supporting satellite-temperature information) or they could be used for the detection of temperature variations (with a higher degree of spatial resolution than a satellite radiometer) in regions where current and other surface dynamic features are known to be sufficiently small.

References

1. Moskowitz, L.I., "The Feasibility of Ocean Current Mapping via Synthetic Aperture Radar Methods," Proceedings of the American Society of Photogrammetry, Part II, pp. 760-771, 1973.

2. Parsons, C.L., "An Observational Study of σ° variations in the Vicinity of the Gulf Stream," in SKYLAB S-193 RADAR ALTIMETER EXPERIMENT ANALYSIS AND RESULTS, G.S. Brown, Ed., CR-2763, Feb. 1977.

3. Shemdin, O.H., Blue, J.E., and Dunne, J.A., SEASAT-A Surface Truth Program: Marineland Test Plan, Memo 622-6, November 1975, (JPL internal document).

4. Wright, J.W., "A New Model for Sea Clutter," IEEE Trans. Antennas Prop., AP-16 (No. 2), 1968, pp. 217-223.

5. Von Arx, W., Introduction to Physical Oceanography, Addison-Wesley, 1974.

6. Weissman, D.E. and T.W. Thompson, "Preliminary Study of the Radar Cross-Section Variations at the Western Boundary of the Gulf Stream," SEASAT TN-7, August 4, 1976.

7. Thompson, T.W., JPL Radar Operations Report, Marineland/GASP Test Series, 25 November to 16 December 1975, Technical Memorandum 622-13, Jet Propulsion Laboratory, Pasadena, Calif., April 1, 1976, SEASAT TN-8.

8. Elachi, C., and J.R. Apel, "Internal Wave Observations made with an Airborne Synthetic Aperture Imaging Radar," Geophys. Res. Letts., Vol. 3, No. 11, 1976, P. 647.

9. Fleagle, R.S., "Note on the Effect of Air-Sea Temperature Difference on Wave Generation," Transactions of the American Geophysical Union, Vol. 37, No. 3, pp. 275-277, June 1956.

10. Roll, H.U., Physics of the Marine Atmosphere, Academic Press, New York, 1965.

11. Deacon, E.L., "Aerodynamic Roughness of the Sea," Journal of Geophysical Research, Vol. 67, No. 8, pp. 2167-3172, 1962.

12. Cardone, V.J., "Specification of the Wind Distribution in the Marine Boundary Layer for Wave Forecasting," Report TR-69-1, New York University School of Engineering and Science, March 1970 (Available as DDC no. AD702).

13. Daley, J.C., An Empirical Sea Clutter Model, Memorandum Report 2668, Naval Research Lab., Washington, D.C., October 1973.

14. Uchupi, E., Map Showing Relation of Land and Submarine Topography, De Soto Canyon to Great Bahama Bank, Department of Interior, United States Geological Survey, Miscellaneous Geologic Investigations Map I-475, 1966.

ACKNOWLEDGEMENT

The authors [illegible] all members of the Marineland Test Team for their support. The Medium Altitude Mission Branch, NASA Ames Research Center provided its usual invaluable assistance during the flight operations. Several members of the Space Science Division at the Jet Propulsion Laboratory provided many useful inputs to the analysis. And as mentioned in the text, a vital data set was the infrared surface temperatures provided by Dr. Richard Legeckis of NOAA-NESS.

Work performed at the Jet Propulsion Laboratory is one phase of the research carried out under Contract NAS 7-100 to the National Aeronautics and Space Administration.

Appendix - Surface Stress Calculation

Surface Stress = (Air Density) x (Drag Coefficient)

x (Magnitude of Relative Velocity at 10 Meters Above Surface)^2

$$\tau_o = \rho C_{10} U_{10}^2$$

$$C_{10} = (C_{10})_n \left[1 - \frac{1.24\ (T_a - T_s)}{\bar{U}_{10}^2}\right]^2$$

C_{10_n} = Drag coefficient under neutral (uniform) temperature conditions

T_a = Air Temperature - °C

T_s = Surface Temperature - °C

$\bar{U}_{10} = |\vec{U}_w - \vec{U}_c|$ = Magnitude of vector difference between wind and surface current

$\vec{U}_w$ = Wind Velocity Vector

$\vec{U}_c$ = Surface Current Velocity (Assumed to be in northerly direction at all points)

Square Root of Normalized Stress

$$= \sqrt{\frac{\tau_o}{\rho (C_{10})_n |U_w|^2}}$$

$$= \left[1 - \frac{1.24\ (T_a - T_s)}{U_{10}^2}\right] \times \frac{\bar{U}_{10}}{U_w}$$

= 1 when $\vec{U}_c = 0$ and $T_a = T_s$

COMPARISON OF *IN SITU* AND REMOTELY SENSED OCEAN WAVES OFF MARINELAND, FLORIDA

O. H. SHEMDIN, W. E. BROWN, JR., and F. G. STAUDHAMMER
Jet Propulsion Laboratory, California Institute of Technology, Pasadena, California, U.S.A.

R. SHUCHMAN, R. RAWSON, and J. ZELENKA[1]
Environmental Research Institute of Michigan, Ann Arbor, Michigan, U.S.A.

and

D. B. KOSS, W. McLEISH and R. A. BERLES
Sea-Air Interaction Laboratory - NOAA, Miami, Florida, U.S.A.

(Received 23 August, 1977)

Abstract. Some early results from an oceanographic experiment staged off Marineland, Florida, in December 1975 are presented, viz., intercomparisons between the X-band and L-band imagery obtained by the Environmental Research Institute of Michigan's (ERIM) dual-wavelength, dual-polarization multiplexed radar. This radar allows direct comparison since the images are produced simultaneously. The wave data obtained from the radar imagery are compared with surface measurements of waves obtained with a pitch-and-roll buoy. The conclusions are only applicable to medium and low wind and wave conditions encountered during the Marineland test. The results indicate that X-band images provide superior quality wave imagery and more useful Fourier Transforms compared to L-band under equivalent signal-to-noise ratios and resolution. Optimum wave imagery is seen when waves propagate in the range direction. Comparisons between *in situ* measurements and X-band imagery of the same area indicate that the dominant wave direction can be obtained from imagery to within a few degrees. A one-dimensional spectrum obtained from X-band imagery compares favorably with an equivalent wave frequency spectrum obtained from the pitch-and-roll buoy after suitable transformation using linear wave theory.

1. Introduction

A major collaborative oceanographic experiment was staged offshore of Marineland, Florida, in December 1975. The objectives and details of measurement systems were described by Shemdin *et al.* (1975). Briefly, the important objectives of the experiment are:

1. Determine the nature of synthetic-aperture-radar (SAR) image formation mechanisms by measuring the slope spectrum of short gravity and capillary waves and simultaneously imaging the same surface area with the ERIM X- and L-band SAR system.
2. Measure the modulation of short gravity and capillary waves by long ocean waves.
3. Determine the wave spectral transformation in shallow water.
4. Obtain SAR imagery in the vicinity and across the Gulf Stream to test SAR imaging capability of current boundaries.
5. Measure waves and currents in the surf zone.

[1] Now at Science Applications, Inc., Tucson, Arizona.

Boundary-Layer Meteorology **13** (1977) 225-234.

Three surface stations were instrumented in 10, 20, and 60 m depths along a line normal to shore. An attending ship was provided for each station. Three aircraft equipped with X and L, and K_u band radars were flown in patterns over the surface sites and across the Gulf Stream. The site was selected because there was a reasonable probability of encountering waves with lengths longer than 80 m and heights of the order of 2 m, and because of the availability of surface support facilities operated by the University of Florida. The locations of the instrumented surface-truth sites and the basic flight patterns are shown in Figure 1.

Much of the data analysis remains in progress and will be forthcoming in various technical papers. The results reported here are confined to inter-comparisons between the ERIM X- and L-band high resolution imagery and respective comparisons with *in situ* measurements obtained with the pitch-and-roll buoy.

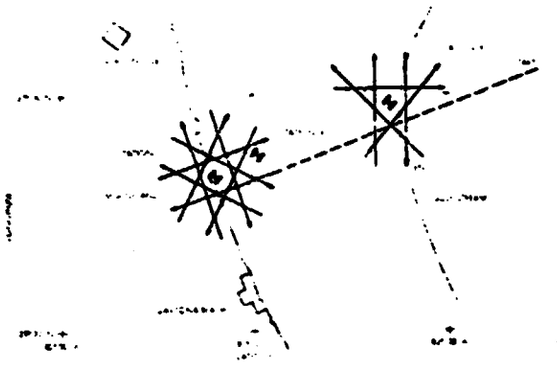

Fig. 1. Location of instrumented sites and flight paths for the Marineland Test. An eight-sided pattern is shown at station 1, and a five-sided pattern is shown at station 3.

2. The ERIM X-L band radar system

The ERIM X-L system described by Rawson *et al.* (1975) consists of a dual-wavelength and dual-polarization Synthetic-Aperture Radar that simultaneously images at X-band (3.2 cm) and L-band (23.5 cm). Alternate X- and L-band pulses (chosen to be either horizontally or vertically polarized) are transmitted, and reflections of both polarizations received; thus four channels of radar imagery are simultaneously obtained. Both polarizations of X-band are recorded on one film, both polarizations of L-band on the other. The Marineland data presented in this paper were obtained from the horizontal-transmit horizontal-receive channel (HH) of both the X and L-band receivers. Polarization effects have not been analyzed. The polarization of the electromagnetic radiation is defined by the direction of the electric field intensity, **E**, vector. For example, a horizontally polarized wave will have its **E** vector parallel to the local horizon.

The along-track or azimuth resolution on the ERIM system is obtained from the Synthetic-Aperture techniques given by Brown and Porcello (1969) and the cross-track or range resolution from the frequency-modulated pulse compression. During flight, the radar signals are recorded in their frequency-dispersed form and are later optically compressed in a ground-based processor. The latter has been extensively described by Kozma *et al.* (1972).

The SAR data were processed on the ERIM optical processor. The raw images were further processed at the Image Processing Laboratory of Jet Propulsion Laboratory to remove geometrical distortions and to enhance contrast. The Fourier transforms were obtained for segments of the enhanced images.

3. Surface Measurements—Pitch-and-Roll Buoy

A pitch-and-roll buoy developed by the National Institute of Oceanography (now called the Institute for Oceanographic Services), England, was operated by the Sea-Air Interaction Laboratory of NOAA during the Marineland Test. The characteristics of the system were described by Ewing (1969) and Tyler *et al.* (1974). The directional wave spectra are presented as one-dimensional frequency

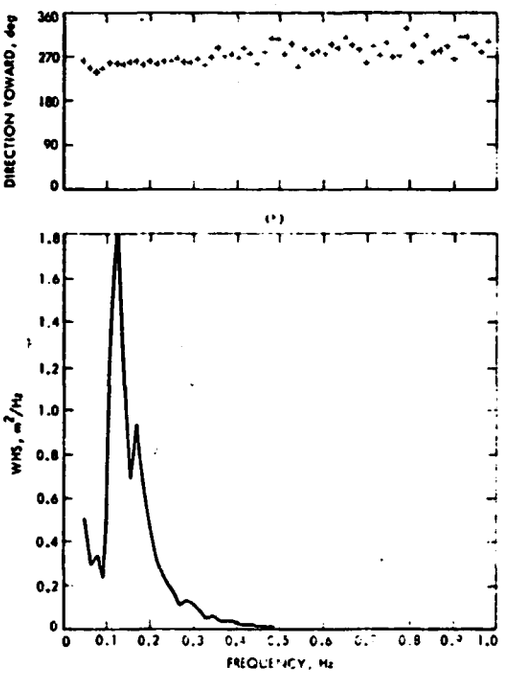

Fig. 2. A wave directional spectrum for December 14 1975, obtained with pitch-and-roll buoy: (a) centroid of wave directions as function of frequency, (b) frequency spectrum of wave energy.

spectra with directional characteristics at each frequency expressed in terms of the exponent of a cosine distribution centered on the mean wave direction. A typical spectrum measured on 14 December, 1975, is shown in the lower graph of Figure 2. The significant wave height was 1.56 m. The top graph in the same figure gives mean wave directions (centroid of the cosine distribution) as a function of frequency. On this day, the waves appear to be propagating uniformly towards 270° with respect to true north. The pitch-and-roll buoy was located at Station 1 (see Figure 1). The wind speed at the site was 3.0 ms^{-1} from the east, a direction of 90° with respect to true north. The wave system shown in Figure 2 is considered to be *swell*. The spectrum will be compared to a one-dimensional spectrum derived from radar imagery in section 4C2.

4. Results

A. X-BAND VS. L-BAND SAR WAVE IMAGERY

The Marineland test indicates that better wave images can be generated from the X-band radar with parallel polarization than from the L-band radar. Simultaneously-obtained, identical-resolution X-band (HH) ocean-wave images are compared with L-band (HH) images of the same area in Figure 3. Both X- and L-bands have approximately the same signal-to-noise ratio (SNR). Scans of image density in the direction perpendicular to the dominant crest direction indicate a higher crest-to-trough modulation for X-band than for L-band. Consequently, better definition is seen in wave-spectral peaks derived from X-band images than from L-band.

A possible explanation for the higher quality of X-band imagery was given by Shuchman and Zelenka (1978). They suggested that X-band data have a larger

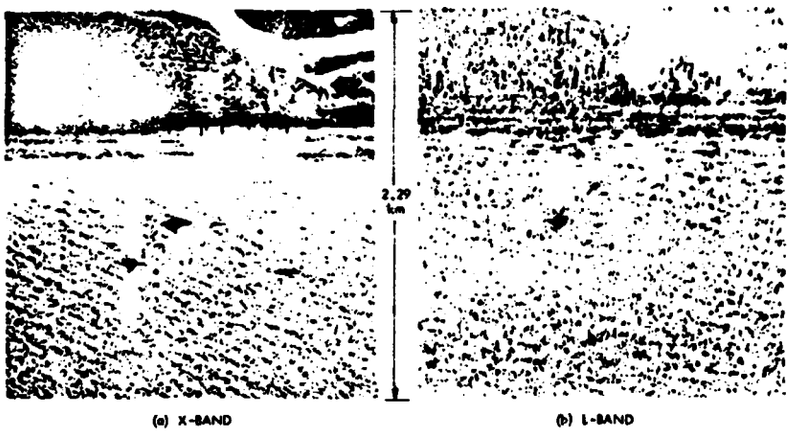

Fig. 3. Comparison of X-band and L-band images, 3 × 5 m resolution, at station 1 for 15 December 1975, with radar looking away from shore.

depth of focus than L-band, and therefore the azimuthally moving waves are not appreciably defocused as commonly occurs on L-band images of comparable resolution. The X-band also incorporates a shorter synthetic-aperture length or integration time than L-band. By using a shorter integration time, there are fewer motion errors which directly affect the azimuth or Doppler resolution.

The theoretical Rayleigh resolution of SAR is

$$\rho = \frac{\lambda}{2L}\frac{H}{\cos\theta}, \tag{1}$$

where λ = radar wavelength,
$L = VT$ = synthetic-aperture length,
V = velocity of aircraft,
T = flight time required to collect synthetic-aperture data,
H = altitude of radar, and
θ = angle from nadir.

For an estimated aircraft altitude of $H = 4.1$ km, a velocity of $V = 75$ m s^{-1} and off-nadir angle $\theta = 20°$ (depression angle = 70°), Equation (1) yields

$$\rho = 29.1\frac{\lambda}{T}. \tag{2}$$

For $\rho = 5$ m, the required time for the wave to be within the aperture for X-band is

$$T_X = \frac{29.1 \times 0.032}{5} = 0.19\ \text{s}, \tag{3}$$

and for the L-band, the wave must be in the aperture for

$$T_L = \frac{29.1 \times 0.235}{5} = 1.37\ \text{s}. \tag{4}$$

Thus for the same resolution, the angular beamwidth must be 7-8 times larger for L-band than for X-band.

Acceleration inherent in wave motion during these times causes degradation of resolution. In contrast, a constant horizontal velocity merely displaces the apparent position rather than degrading the resolution. The maximum allowable acceleration, A, as a function of H, V, and T can be found as follows. The apparent range, R, while generating a synthetic aperture is

$$R = R_0 + v_0 t + \tfrac{1}{2}a_0 t^2, \tag{5}$$

where R_0 is range to a typical cell at time zero, v_0 and a_0 are components of target velocity and acceleration in the range direction; v_0 is a constant which only displaces the wave in the image.

The error, ϵ_R, in the range which degrades resolution is

$$\epsilon_R = \tfrac{1}{2}a_0 t^2. \tag{6}$$

The corresponding phase error is given by

$$\phi_e = \epsilon_R \frac{4\pi}{\lambda} = \frac{2\pi a_{0t}^2}{\lambda} \leq \frac{2\pi}{\lambda} a_0 \left(\frac{T}{2}\right)^2 . \tag{7}$$

where the upperbound is realized at both ends of the synthetic aperture. The phase error should be kept within $\pi/2$ in order to achieve a properly focused image and to prevent resolution degradation, so that

$$\phi_e \leq \pi/2 . \tag{8}$$

The time, T, within the aperture is therefore restricted to

$$T \leq \left(\frac{\lambda}{A}\right)^{\frac{1}{2}} . \tag{9}$$

Using Equations (1) and (9), it follows that

$$A \leq [4V^2 \cos^2\theta \rho^2 / H^2 \lambda] . \tag{10}$$

Using known values of H, V, and θ, it can be shown that

$$A = 1.18 \times 10^{-3} \rho^2 / \lambda . \tag{11}$$

Figure 4 graphs the maximum tolerable acceleration, A, in $m\,s^{-2}$ vs. radar wavelength, λ, in cm; and is plotted for various resolutions, ρ, in meters. Thus one reason the X-band yields superior wave spectra is because it is less subject to wave velocity and acceleration effects than L-band.

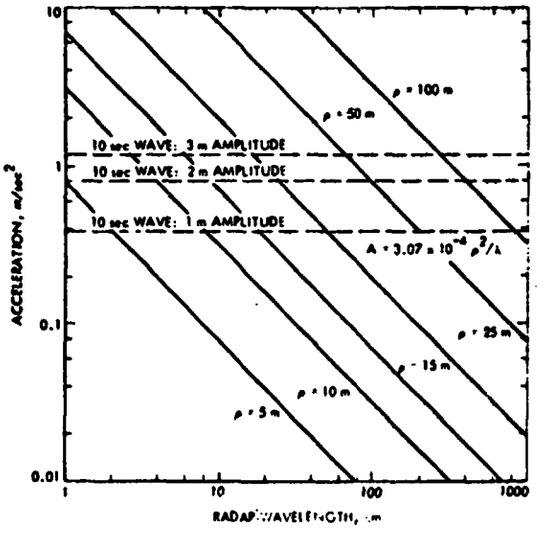

Fig. 4. Maximum wave acceleration tolerated by SAR as a function of radar wavelength and resolution ρ.

B. Wave Images as a Function of Radar Look Direction

Analysis of Marineland data also indicates that optimum wave images result when the radar is looking essentially up-wave or when waves propagate towards the aircraft in the range direction as shown in Figure 5. Shuchman and Zelenka (1978) indicate that waves traveling in the range direction yield images that are insensitive to defocusing effects. The lack of defocusing sensitivity in range becomes apparent when one considers that SAR employs in the range dimension a pulse train of very

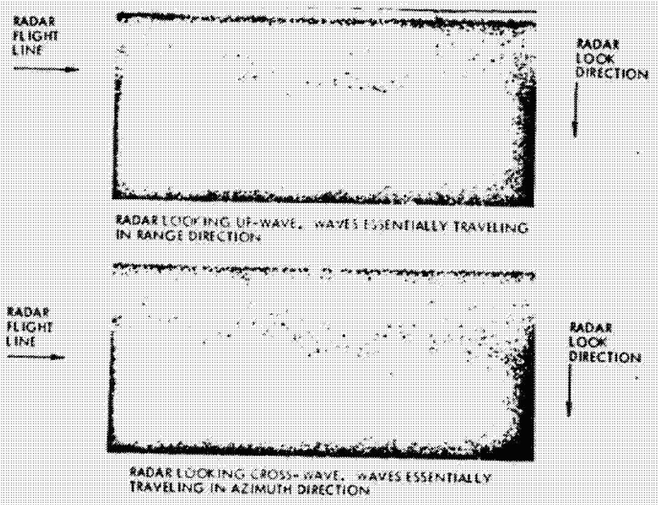

Fig. 5. Identical ocean area viewed with a different look direction, X-band 3 × 5 m resolution, on 14 December 1975, station 1.

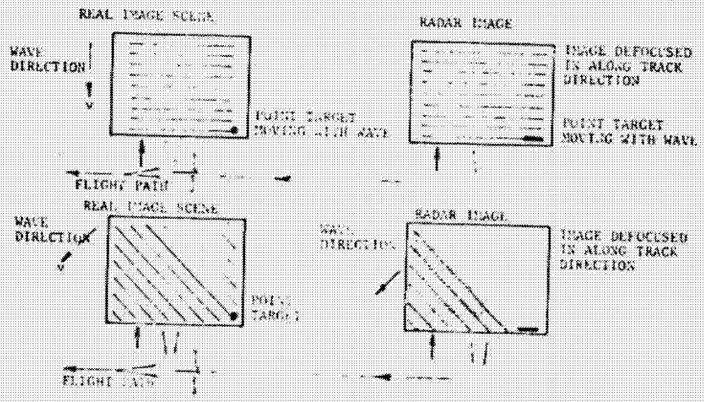

Fig. 6. Schematic representation of defocusing of waves as a function of propagation angle with respect to radar look direction.

short pulses or a coded pulse. Thus to the SAR the waves traveling in the range appear stationary over the short sampling time. Furthermore, when waves cause a displacement or defocusing, the displacement is in the along-track dimension (along wave crests) and therefore is not visible in the imagery. Figure 6 graphically demonstrates the displacement or defocusing of waves as a function of motion in the resulting image. From the figure it becomes apparent that range resolution controls only the quality of the wave imagery when waves travel in the range direction.

C. Comparison with Surface Measurements

1. *Wave Direction*

The directional properties of waves from the pitch-and-roll buoy are given in the top graph in Figure 2. The results suggest that the waves are predominantly unidirectional propagating towards 270°. The pitch-and-roll buoy location with respect to shore is shown in Figure 7, the X-band radar image of the area. The shoreline alignment with respect to true north is 340° at this location. The pitch-and-roll spectra then suggest that the waves are approaching the shore at a 20° angle.

An examination of the radar image in Figure 7 for wave-crest direction in the vicinity of the pitch-and-roll buoy yields 20° alignment of wave crest with respect to the shoreline. Alternatively, the direction of the peak energy in the Fourier transform of the image at Column 1, frame 4, also yields 20°. This comparison suggests

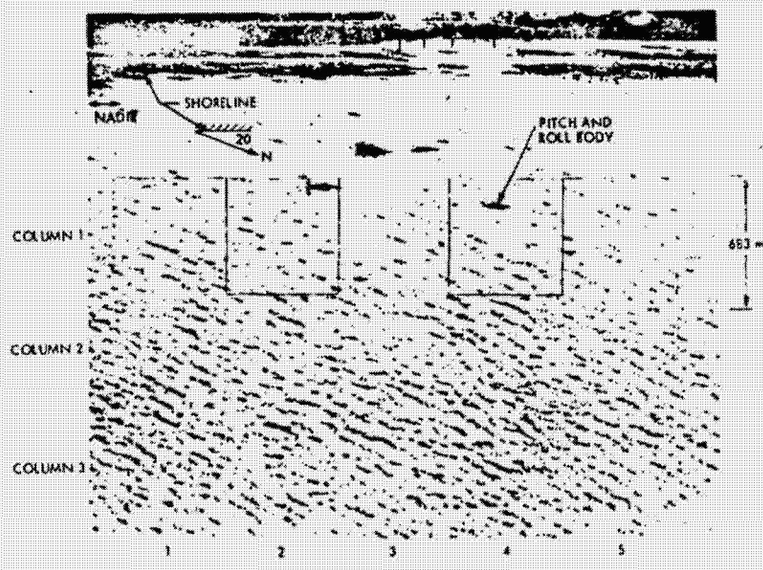

Fig. 7. Nearshore X-band image, 3 × 5 m resolution, on 14 December 1975.

that radar images, at least X-band images, provide information on wave direction to within a few degrees.

2. *Wave Spectral Shape*

A comparison between a surface wave spectrum obtained by a buoy with one derived from a radar image requires transformation of the spectrum from frequency to wave-number space. The one-dimensional wave-number spectrum derived from the two-dimensional Fourier transform of the image in the vicinity of the pitch-and-roll buoy was normalized in both coordinates using its peak energy value and the dominant wave number from the pitch-and-roll buoy spectrum. A comparison with the similarly normalized pitch-and-roll buoy spectrum is shown in Figure 8. The comparison is surprisingly good considering that little is known about wave imaging mechanisms for the SAR. The comparison provides encouragement for using imaging radars for wave studies. Certainly, more research is deserved and is in progress.

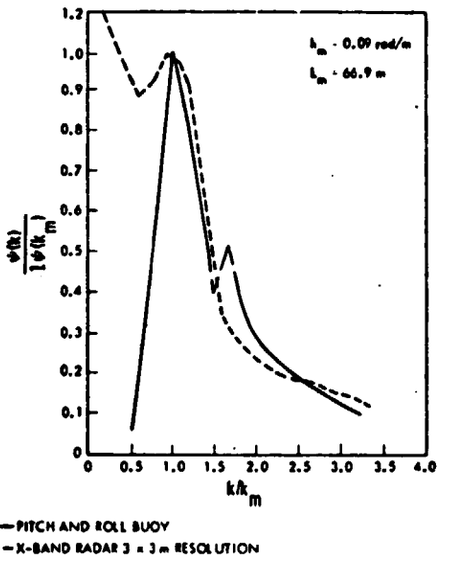

Fig. 8. Comparison of one-dimensional spectra derived from X-band radar image with that measured by the pitch-and-roll buoy at the same location on 14 December 1975. Both spectra are normalized by wave number (k_m) at peak of buoy spectrum, and by value of spectral energy density at peak of each spectrum. $L_m = 2\pi/k_m$.

5. Conclusion

The conclusions derived from early results of the Marineland Test are summarized below:

1. Under equivalent signal-to-noise ratio and synthetic-aperture resolution, superior wave imagery and more useful Fourier transforms are obtained with the X-band SAR compared to L-band.
2. Optimum wave imagery is obtained when waves propagate in the range direction under otherwise identical conditions.
3. A comparison between X-band wave images and *in situ* measurements with a pitch-and-roll buoy shows agreement in the dominant wave direction to within a few degrees. The normalized spectra show a surprising resemblance in the spectral shape. A better understanding of radar image-formation mechanisms is required to develop a sound basis for comparing radar-derived spectra with surface-truth spectra.

Acknowledgement

The organizations that participated in the experiment were: Coastal Engineering Research Center, Environmental Research Institute of Michigan, Fleet Numerical Weather Central, City University of New York, Jet Propulsion Laboratory, Sea-Air Interaction Laboratory of NOAA, and the University of Florida. The experiment was formulated by members of the Synthetic Aperture Radar Team and sponsored by the Surface Truth Program of SEASAT-A.

References

Brown, W. M. and Porcello, L. J.: 1969, 'An Introduction to Synthetic Aperture Radar', *IEEE Spectrum* **6**, 57–62.

Ewing, J. A.: 1969, 'Some Measurements of the Directional Wave Spectrum', *J. Mar. Res.* **27**, 163–171.

Kozma, A., Leith, E. N., and Massey, N. G.: 1972, 'Tilted Plane Optical Processor', *Appl. Optics* **11**, 1766.

Rawson, R., Smith, F., and Larson, R.: 1975, 'The ERIM Simultaneous X- and L-Band Dual Polarized Radar', IEEE 1975 International Radar Conference, New York, p. 505.

Shemdin, O. H., Blue, J. E., and Dunne, J. A.: 1975, 'Seasat-A Surface Truth Program—Marineland Test Plan', Jet Propulsion Laboratory Document No. 622-5, 86, Pasadena, California.

Shuchman, R. A. and Zelenka, J. S.: 1978, 'Processing of SAR Ocean Wave Data', *Boundary-Layer Meteorol* (this issue).

Tyler, G. L., Teague, C. C., Stewart, R. H., Peterson, A. M., Munk, W. H., and Joy, J. W.: 1974, 'Wave Directional Spectra from Synthetic Aperture Observations of Radio Scatter', *Deep-Sea Research* **21**, 989–1016.

GPO 927-101